Stellenbosch
UNIVERSITY
IYUNIVESITHI
UNIVERSITEIT

Design, build and testing of a 3D hologram-like RGB LED fan display

Mechatronic Project 478
Final Report

Author: Stefan Petrus Botes
25985116

Supervisor: Dr. Melody Neaves

24 October 2025

forward together
sonke siya phambili
saam vorentoe

Department of Mechanical and Mechatronic Engineering
Stellenbosch University
Tel: +27 21 808 4204 | www.eng.sun.ac.za
Private Bag X1, Matieland, 7602, South Africa

Plagiarism declaration

I have read and understand the Stellenbosch University Policy on Plagiarism and the definitions of plagiarism and self-plagiarism contained in the Policy [Plagiarism: The use of the ideas or material of others without acknowledgement, or the re-use of one's own previously evaluated or published material without acknowledgement or indication thereof (self-plagiarism or text-recycling)].

I also understand that direct translations are plagiarism, unless accompanied by an appropriate acknowledgement of the source. I also know that verbatim copy that has not been explicitly indicated as such, is plagiarism.

I know that plagiarism is a punishable offence and may be referred to the University's Central Disciplinary Committee (CDC) who has the authority to expel me for such an offence.

I know that plagiarism is harmful for the academic environment and that it has a negative impact on any profession.

Accordingly all quotations and contributions from any source whatsoever (including the internet) have been cited fully (acknowledged); further, all verbatim copies have been expressly indicated as such (e.g. through quotation marks) and the sources are cited fully.

I declare that, except where a source has been cited, the work contained in this assignment is my own work and that I have not previously (in its entirety or in part) submitted it for grading in this module/assignment or another module/assignment.

I declare that have not allowed, and will not allow, anyone to use my work (in paper, graphics, electronic, verbal or any other format) with the intention of passing it off as his/her own work.

I know that a mark of zero may be awarded to assignments with plagiarism and also that no opportunity be given to submit an improved assignment.

Signature: 

Name: Stefan Petrus Botes Student no: 25985116

Date: 24 October 2025

AI use declaration

1. I am convinced and can support my claim that my assessment product is an indication of my own learning, knowledge, skills, and understanding.
2. Where I have used AI tools for enhancing my own creation of ideas and words, I acknowledge that I have to declare it.
3. Where I have used AI tools for generating new ideas, words, code, image-prompts for other AI Image-generating tools, or structure and even presentations (or other AI tools that can be used as assistants to the knowledge building and representing process), I have declared and documented the use of such tools and I am prepared to talk about the process I used and what it contributed to my learning and insights.
4. I am aware that the lecturer can ask me to demonstrate my learning, for example through explaining the choices I made in terms of approach, content used, literature selected, conclusions drawn, etc. through an additional assessment like an oral (for example).
5. I understand that if I am not able to agree to the above points, there is a chance that my academic behaviour will be deemed unethical and might lead to a disciplinary case being brought against me on the grounds of cheating or plagiarism and that the standard procedures for such behaviour will be followed.
6. As per the Disciplinary Code of SU (par. 10.2.1 and 10.2.2), I understand that I take responsibility for the integrity of my work, which includes the obligation to ask for clarification from an academic member of staff if I am unsure of anything, and that I strictly adhered to all instructions received in the course of the academic assessment by relevant and authorized staff (whether the instruction is in oral or written format).
7. I understand that when I am not able to document and declare my use of AI tools, this behaviour will be deemed as cheating in examinations and assessments (Disciplinary Code 1.1 c.) as I referred to “unauthorized notes, books, electronic devices or other reference material”.

Signature: 

Name: Stefan Petrus Botes Student no: 25985116

Date: 24 October 2025

ECSA outcome self-assessment

GA1: Problem solving
Identified microcontroller PWM and DC speed controller incompatibility and implemented a solution using a low-pass filter circuit (section 5.8). Designed, simulated and implemented different rpm measurement circuits to improve the accuracy for rpm measurements (section 5.11). The wireless power transfer component was replaced with an alternative slip ring concept (section 5.10) which proved to be successful in power the rotating subassembly's components (section 5.17 and 7.2). A 6 MΩ resistor was placed in parallel with the low-pass filter circuits' output capacitor to drain the capacitor in the event of a power loss during fan operation, preventing the fan motor from spinning at high speed once power is restored (section 5.8). Magnet placement and slight design changes to parts helped make all parts 3D printable and allowed the entire fan to be assembled without the need for almost any adhesives (section 5.4 and 5.13).
GA 2. Application of scientific and engineering knowledge
The mass moment of inertia, centrifugal force calculations and DC motor torque requirements were calculated using knowledge from Machine Design A 314 and Electrical Drive Systems 324 (Appendix G and Appendix I). Power and temperature calculations of the power regulators, and simulations using NGSpice (sections 5.9 and 5.12, and Appendix H), using knowledge from Electronics 245 and Design E 314. Data transmission types, speeds and the amount of memory required were analysed to confirm compatibility between the microcontrollers and LEDs using knowledge from Computer Systems 245 and Design E 314, including hardware interrupts and timers (sections 5.1, 5.2 and 6.4).
GA 3. Engineering Design
Various designs of physical (blade) and electrical configurations were considered/synthesised, analysed and evaluated each concept using a qualitative approach, with alternatives mentioned, such as the type of motor and speed control (DC or BLDC) (section 4). Low-pass filter and voltage converter circuits, and custom slip rings were designed as solutions to problems encountered (sections 5.8, 5.10 and 75.11). Designed rpm measurement verification tests, such as using a stroboscope to confirm the fan speed (section 7.1). Designed/decided on different images to display to verify if the fans' performance requirements were met (section 7.2).
GA 5. Engineering methods, skills and tools, including Information Technology
Used embedded software skills and tools learned in the Design (E) 314 module to program, wire and select the ESP32 microcontrollers (section 5.2). Used

knowledge and skills learned in Machine Design A 314 for strength calculations (Appendix I). Used knowledge from both Electronics 315 and Design (E) 314 for calculating the power dissipation and heat generation of voltage regulators (sections 5.9 and 5.12). Learned new mobile application software tools, namely Flutter and VSCode, which are open-source, free-to-use software and are well-suited for web-based mobile applications with enough UI elements, which were used to create a user-friendly mobile application (section 6.3). Learned new Arduino IDE, PlatformIO and VSCode software tools for embedded programming of ESP32 microcontrollers (section 6.2). Used the NGSpice and LTSpice programs to simulate the low-pass and voltage converter circuits theoretically before building the circuit and testing it practically (section 5.11 and Appendix H). Used SMath solver for the strength and motor inertia calculations (Appendix G and Appendix I). Used Inventor Professional 2025 to create the required 3D CAD models and drawing files needed for 3D printing and laser cutting (sections 5.4 and 5.13). Used Creality Print 6.1 to 3D print the required parts.

GA 6. Professional and technical communication

Followed the "Guide for Writing Technical Reports" and lectures throughout the report to achieve effective written and oral communication. Kept meeting minutes for each of the scheduled individual and group meetings with my supervisor.

GA 8. Individual, Team and Multidisciplinary Working

Concept designs were evaluated with alternative approaches considered to ensure that the set objectives could be met (section 4.1 and 4.2). Worked strategically by first testing each system element separately before integrating and testing the entire system as a whole (section 5). Delivered all required documents and handed them in before the specified deadlines. Kept regular meeting minutes throughout the project for all individual and group meetings.

GA 9. Independent Learning Ability

Independent learning of the Arduino framework software and which relevant libraries to use in PlatformIO and VSCode IDE environments, used for embedded programming of the ESP32s (section 6). Independent research into the design of Schmitt triggers and comparator circuits used for the rpm measurement circuit design (section 5.11). Independent learning of front-end and back-end mobile application software using the Flutter framework to build standalone and downloadable mobile applications (section 6.3). The literature review section 2, includes independent learning on how WebSockets and wireless communication work. With independent learning on how to implement it. Learned how 3D printing and additive manufacturing can be used to design parts with the required strength based on the material type and orientation used (sections 5.16 and 5.17).

Executive summary

Title of Project
Design, build and testing of a 3D hologram-like RGB LED fan display
Objectives
Generate and evaluate concepts based on the specifications formulated for a 3D hologram-like RGB LED fan display. Select materials and components suitable for manufacturing the final design. Mobile application user interface/software development and integration. Testing of the unit using static/dynamic scenes.
What is current practice and what are its limitations?
Current similar products are expensive and need to be imported from overseas. These fans operate at very high speeds with limited safety measures to prevent injuries and limited control over the motor speed. Wires between multiple displays look messy and limit the distances between displays.
What is new in this project?
A more cost-effective solution is designed, built, and tested, which will make use of locally sourced off-the-shelf components. Wireless technology will be used to avoid the need for messy cables, and a new fan blade prototype, made using additive manufacturing techniques, will be tested to see if it can help increase fan safety. The fan motor speed will be controllable through the use of an accompanying mobile application.
Was the project successful? How will it make a difference?
The project was successful in designing a system with integrated safety features instead of needing to rely on separately bought components. A wireless communication interface using a user mobile application that can be downloaded as a standalone application, can be used to control the multiple fan displays independently. The user-mobile application also supports multiple different safety features some of which allow the fan displays to be switched of based on the mobile devices' movement.
What were the risks to the project being a success? How were these handled?"
Due to the wireless power transmitter not meeting the manufacturers listed requirements, a new cost-effective slip ring concept was designed and implemented, which proved to be successful in supplying the LEDs reliable power. The Hall-effect position sensor selected in the design phase proved to be noisy with a limited output voltage range, leading to inconsistent and inaccurate rpm measurements of the fan displays. This was remedied by designing and implementing a comparator circuit to make rpm measurements reliable between 495 rpm and 630 rpm.

What contributions have/will other students made/make?
Other students can further improve the project's display by determining the maximum refresh rate or resolution at which these displays can operate. Mobile application functionality can be enhanced either by making it more user-friendly or by adding new features. The slip ring design can be improved by making it more cost-effective, robust, or by using alternative materials or manufacturing methods.
Which aspects of the project will carry on after completion and why?
The 3D hologram-like RGB LED fan display can be used at open days to promote the Stellenbosch Engineering Faculty to first-years. The rpm sensor and balance of the system can be improved to show more complex and dynamic stable images. Custom images that can be uploaded to the device wirelessly via Wi-Fi or Bluetooth can be explored. Mesh Wi-Fi networks, such as Zigbee, which the ESP32 microcontrollers support, can be added to allow even more fans to be connected further apart. Other end-of-life strategies are discussed at the end of the report, e.g., recyclability and reusability.
What arrangements have been/will be made to expedite continuation?
The project's design, build, and testing will be defined and documented in sufficient detail so that future students can build on or improve this project by using Git repositories and README.md files documenting all potential designs considered during the project. All CAD models, drawing files and components considered will be given in the project file.

Acknowledgements

I'd firstly like to thank my supervisor, Dr. Melody Neaves, for guiding me during this project and believing in me despite the setbacks and challenges faced.

Secondly, I'd like to thank my parents, grandparents, and the rest of my family for supporting me throughout the project, who showed interest in it, and celebrated with me when things worked out. (And for sending some home-cooked meals to help get me through some of the long nights.)

Next, a thank you to my friends, (the Engénurs), Joshua, Daisy, Tian and Kyle, some of whom I've known since childhood and others whom I met in my first year during welcoming, where Daisy willingly stayed up with me a few late nights.

And lastly, a special thanks to some honourable mentions, Liam, Jop and Emmanuel (F1), who also showed interest in this project and helped me keep my sanity.

Table of contents

Page

Plagiarism declaration ..... **i**

AI use declaration ..... **ii**

ECSA outcome self-assessment ..... **iii**

Executive summary ..... **v**

Acknowledgements ..... **vii**

List of figures ..... **xi**

List of tables ..... **xiii**

1 Introduction **1**
- 1.1 Background 1
- 1.2 Objectives 2
- 1.3 Motivation 3
- 1.4 Use of generative AI 3

2 Literature review **4**
- 2.1 LUMINA L1 fan 4
- 2.2 USB clock fan 5
- 2.3 Persistence of vision effect 6
- 2.4 SPI communication standard 7
- 2.5 Motor speed controllers 7
- 2.6 Wireless communication 8
- 2.7 Hall-effect sensors 8

3 System specifications **9**
- 3.1 Stakeholder requirements 9
- 3.2 Engineering requirements 10

4 Concept designs **13**
- 4.1 Fan blade subsystem concept designs 13
  - 4.1.1 Concept 1: Pin-mounted 14
  - 4.1.2 Concept 2: Ball-and-socket joint with pinhole 14
  - 4.1.3 Final concept 3: Ball-and-socket joint with slits 15
- 4.2 Electronic hardware design concepts 16
  - 4.2.1 Concept 1: DC motor with wireless power transfer 17
  - 4.2.2 Concept 2: BLDC motor with slip ring 18

4.2.3 Final concept 3: DC motor with wireless power transfer and speed control 19

5 Detail design 21
5.1 LEDs 21
5.2 Position sensor and microcontroller selection 22
5.3 Wireless power transmitter 23
5.4 Final rotating fan subassembly CAD model 24
5.5 DC motor 26
5.6 Power supply 26
5.7 DC speed controller 27
5.8 Low-pass filter design 28
5.9 5 V, 1.5 A voltage regulator 29
5.10 Custom slip ring 31
5.11 Voltage converter circuit 32
5.12 5 V, 5 A voltage regulator 33
5.13 Stationary subassembly housing 34
5.14 Additive material selection 36
5.15 Fan blade design 36
5.16 3D printing orientation 37
5.17 Final built prototype 38

6 Software design and implementation 39
6.1 Start-up procedure 39
6.2 Overall functionality/communication 41
6.3 User-mobile application UI 43
6.4 Fan speed measurement and implementation 44
6.5 Displaying images 45

7 System testing and evaluation 46
7.1 Calibration and testing of the reported fan rpm 46
7.2 Performance requirements evaluation 46

8 Conclusion 50

Appendix A. Techno-economic analysis 51
A.1 Budget 51
A.2 Planning (time management) 55
A.3 Technical impact 56
A.4 Return on investment 57
A.5 Potential for commercialisation 57

Appendix B. Gantt chart 58

Appendix C. Risk analysis and safety procedures 59

Appendix D. Responsible use of resources and end-of-life strategy 62

Appendix E. Performance requirements 64

Appendix F. DotStars Testing 66

Appendix G. DC settling time and inertia calculations 68

Appendix H. Low-pass filter simulation and testing 71

Appendix I. Fan blade strength calculations 74

List of figures

Page

Figure 1: ABBA-hologram avatars tour (Voyage, 2022).....1

Figure 2: 3D hologram-like fan display (Jones, 2023).....2

Figure 3: LUMINA L1 logo image showcase (left) and acrylic case (right) (LUMINA, 2025c, 2025b).....5

Figure 4: USB LED clock holographic fan from Takealot (2025b).....6

Figure 5: Partial disassembly of a low-cost USB fan.....6

Figure 6: Low-cost USB fan display paper test.....6

Figure 7: Concept 1: Pin-mounted.....14

Figure 8: Concept 2: Ball-and-socket joint with pinhole.....15

Figure 9: Final concept 3: Ball-and-socket joint with slits.....15

Figure 10: Final concept and folding design operation.....16

Figure 11: Concept 1: DC motor with wireless power transfer.....17

Figure 12: Concept 2: BLDC motor with slip ring.....18

Figure 13: Final concept 3: DC motor with wireless power transfer and speed control.....20

Figure 14: Half-blue, half-red circle.....21

Figure 15: Rotating subassembly housing (wireless, front view).....24

Figure 16: Rotating subassembly housing (wireless, rear-view).....25

Figure 17: Final rotating subassembly housing (slip ring).....25

Figure 18: Low-pass filter circuit to generate an analogue voltage from a PWM signal.....28

Figure 19: Slip ring clip.....31

Figure 20: Comparator circuit practical testing.....33

Figure 21: Stationary subassembly housing (front view).....35

Figure 22: Stationary subassembly housing (front view).....36

Figure 23: Fan blade printing direction.....37

Figure 24: Fully built fan 1 (left), lab testing multi-display images “E” and “custom circle” (right).....38

Figure 25: Custom text "HOPE" at 630 rpm (left) and 850 rpm (right).....38

Figure 26: Software start-up procedure 40
Figure 27: WebSocket communication implementation.....42
Figure 28: User mobile application UI with dropdown (left), and advanced custom images (right) 44
Figure 29: Arc image, slight blur at 680 rpm 45
Figure 30: Fan system portability and weight measurement.....47
Figure 31: Noise measurement setup for residual noise level measurement 48
Figure 32: Project Gantt chart 58
Figure 33: Applicable warning symbols 60
Figure 34: Hand drawn rotating subassembly top view (left), side view (right) ...68
Figure 35: Smath calculations for DC motor inertia and settling time 70
Figure 36: Low-pass filter simulations, 100% duty cycle (left), 30% duty cycle (right) 71
Figure 37: Measurement of settling time difference at 80% duty cycle 73
Figure 38: Voltage output error of the low-pass filter circuit 73
Figure 39: Settling time difference of low-pass filter circuit 73
Figure 40: Weight of individual fan blade.....74
Figure 41: Fan blade centrifugal force calculations.....75

List of tables

Page

Table 1: Stakeholder requirements 9
Table 2: Engineering requirements 10
Table 3: Performance requirements.....11
Table 4: Planned project cost 52
Table 5: Actual project cost 52
Table 6: Planned consumable cost 53
Table 7: Actual consumable cost 53
Table 8: Activity-based risk assessment 60
Table 9: Responsible use of resources and end-of-life strategy.....62
Table 10: DotStars static test data.....67
Table 11: DotStars dynamic test data.....67
Table 12: Low-pass filter testing results 72

1 Introduction

1.1 Background

The term "hologram" originates from the Greek words "holos", meaning "whole" or "complete" and "gramma", meaning "letter" or "writing" (World, 2025). The terms "hologram", "holographic", and “hologram-like” are sometimes used interchangeably, though they generally refer to the same technology or visual effect. Holograms are three-dimensional (3D) images that appear to "float" in space and are often depicted in many science fiction and futuristic films like Star Wars and Star Trek. With the invention of the laser and extensive research over the years, these holograms have started to become a reality, or very close to it. Some of these 3D life-like holograms have been used by the music industry to perform concerts with singers and other artists who appear as life-like 3D holograms on stage (Kitcasthq, 2023). One such example is the ABBA Voyage concert (Figure 1), where none of the original performers were on stage, but appeared to be performing live by using these 3D life-like hologram displays (Kitcasthq, 2023).

Figure 1: ABBA-hologram avatars tour (Voyage, 2022)

However, these life-like holograms are complex, very expensive to manufacture and operate, and are therefore typically only used by commercial enterprises and/or companies (TomorrowDesk, 2025).

Therefore, a more cost-effective approach is to make use of hologram-like 3D LED fan-based displays (Figure 2). These displays are not true holograms like the ones mentioned previously and rely on the persistence of vision effect to make images/scenes appear 3D and floating. These displays work by placing LEDs on fan blades and by precisely flickering the LEDs on/off based on the rotation speed of the fan; a "floating" image and/or scene can be displayed. These displays are often used by companies to advertise products since they are much more cost-effective and easier to operate (Barnes, 2024b). Since these displays

can better convey 3D images than conventional displays, they are a prime candidate for use in classrooms where 3D concepts are sometimes difficult to grasp. For instance, it might be much easier for a biology/medical student to visualise the structure of a human heart and see it in the right proportions compared to viewing a flat 2D image from a picture or a textbook (Hypervision, 2023). They can also be used by those studying art or animation to view a 3D model to better visualise and understand how to draw/animate (Ali & Ramlie, 2021). The same is true for conveying new concepts or designs drawn up in CAD, where it is often difficult to tell how these components will look once manufactured or produced.

Figure 2: 3D hologram-like fan display (Jones, 2023)

This project focuses on the design, build and testing of a 3D LED hologram-like fan display and making it safer and more cost-effective by using local suppliers and designing all the required 3D printed components to fit onto a common 3D printing bed size of 250 mm x 200 mm x 250 mm (L x B x H), similar to those used by the University of Stellenbosch. The project further focuses on designing a user-friendly mobile application that can be used to control/interact with the 3D hologram-like fan display. The main design of the system was based on the L1 3D holographic fan from Lumina (2025a) and took place from February 10 to October 24, 2025, at the University of Stellenbosch, under the supervision of Dr. Melody Neaves, with an allocated budget of R5 000. All building and testing were conducted in the Mechatronics M3009 laboratory and the Electrical and Electronic laboratories E2029 and E4058.

1.2 Objectives

This project aims to design, build and test a safe, portable and cost-effective 3D holographic LED fan display, with an accompanying mobile application. Therefore, the following objectives are:

1. Generate and evaluate concepts based on the specifications formulated for a 3D hologram-like RGB LED fan display.
2. Select materials and components suitable for manufacturing the final design.
3. Mobile application user-interface/software development and integration.
4. Testing of the unit by using static/dynamic scenes.

1.3 Motivation

3D holographic LED fan displays are expensive and often lack integrated safety features, with clear protective enclosures for the blades or the entire unit often sold separately (3D HoloSPiN, 2025). Larger images typically require linking multiple fans together, which increases the cost and cabling requirements. To achieve a persistence of vision (POV) effect, the fans tend to operate at high rotational speeds, often exceeding 320 revolutions per minute (rpm) (Priya, Chithra, Sanjay et al., 2020), increasing the risk of damage to the display or injury if the blades are obstructed.

By designing these fan displays to be inherently safe, i.e. by using foldable fan blades, it will help circumvent the need to buy additional clear cases to keep the fans safe during operation, keeping costs down. By testing if these multiple fan displays can be reliably linked to one another without requiring cables, cable clutter can be reduced and allow fans to be spaced much further apart without being limited by cable length. Locally sourced components/suppliers available in South Africa will be used as much as possible to help keep costs down and to stay within the allocated R5 000 budget for this project. A user-friendly mobile application will be developed to interact with the displays, without relying on subscription-based models to operate. With the aid of additive manufacturing techniques, new types of fan blades can be prototyped and designed to help improve fan safety.

1.4 Use of generative AI

Generative AI tools were used in this project primarily for spelling and grammar checks via Grammarly. GPT-5 was experimented with later to optimise ESP32 code for reduced flash memory use and to design the Holo3D mobile app icon. However, the optimised code required thorough review and correction and did not succeed as well as expected. The AI also often made incorrect assumptions about embedded systems, most notably by assigning functions to pins unsupported by the microcontroller's datasheet. Google Translate was occasionally used to translate non-English sources.

2 Literature review

The literature review begins by examining existing market solutions, first, high-quality, expensive holographic fan from LUMINA (2025a) and secondly, a lower-cost USB clock fan available from Takealot (2025b). These holographic fans were analysed to adopt a bottom-up approach when establishing the system requirements in section 3.

Thereafter, the review outlines the key concepts required to understand how 3D holographic displays display images using the persistence of vision effect based on the existing designs examined (Barnes, 2024a; LUMINA, 2025a; Takealot, 2025b). Additional key concepts address the operation of components mentioned in the electronic design (in section 4.2) work, such as DC (Direct Current) and BLDC (Brushless Direct Current) motors, etc. The section concludes with a brief overview of wireless communication standards and why WebSockets are often the preferred choice for high-performance wireless applications.

2.1 LUMINA L1 fan

The L1 3D holographic fan from LUMINA (2025a) is the company's most affordable model, featuring a mobile application for wireless upload and display of 2D and 3D images. The fan is priced at $199.99, with ceiling and tripod mounts available separately for $34.99 and $89.99, respectively. An acrylic safety case, designed to prevent injury from the fan blades, is also sold separately for $49.99. Figure 3 shows a 3D logo displayed by the L1 holographic fan and a picture of the separately sold acrylic case.

A page on LUMINA 's website lists the key components for a 3D holographic fan display: a U18 Hall-effect sensor, a fan, LEDs, an Arduino Pro Mini, and an FTDI breakout. However, the provided instructions and components support only a basic display, lacking mobile application integration and multi-display functionality. The design given uses a battery to power the LEDs on the fan blade and standard green/red LEDs, limits the duration the fan display can remain on before the battery is drained and image complexity since no full colour images can be created. Several of the recommended components, such as the RGB LED beads, were described only with subjective criteria, without quantitative specifications for selection. Therefore, alternative components and hardware configurations will need to be designed and researched to ensure all the system requirements set in section 3 can be met, if these components listed are not sufficient or available from local suppliers.

A teardown of the L1 fan system, sourced from atomic14 (2022), revealed the use of full-colour LED beads, although the specific model number was not identified, with wireless power transfer coils to supply energy to the LEDs from a

stationary housing, eliminating the need for batteries or physical connections with low friction.

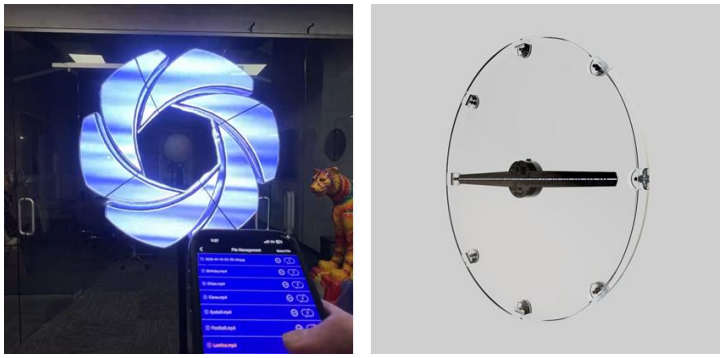

Figure 3: LUMINA L1 logo image showcase (left) and acrylic case (right) (LUMINA, 2025c, 2025b)

2.2 USB clock fan

The low-cost holographic fan examined was the USB LED clock fan from Takealot (2025b), shown in Figure 4. The fan displays a floating clock image when connected to a 5 V USB port and features a memory function to maintain the correct time during power loss.

Partial disassembly and inspection of the internal components (shown in Figure 5) revealed that the fan employs a small DC motor to rotate the fan blades at a fixed speed, with a 10 V, 100 µF capacitor to stabilise power delivery to the red and green LEDs mounted on the fan blades. Next to it a small battery beneath the fan blades was identified, presumably used to maintain the clock time when the device is disconnected from a power source. Further investigation revealed a small sensor beneath the fan blades which was discovered by manually rotating the fan blades slowly whilst the device was powered and monitoring LED changes. While rotating the LEDs would rapidly flicker upon passing a specific point. By using a phone camera aimed at the stationary trigger point, a light purple glow, invisible to the naked eye, was revealed suggesting that the sensor is an IR (Infrared) receiver triggered by a small, fixed IR LED (Sinoseen, 2024). This hypothesis was confirmed by placing a small piece of paper over the IR LED, which prevented the sensor from triggering and consequently stopped the red clock arms and green numbers from being displayed.

Unfortunately, further disassembly was hindered by the DC motor shaft being fixed to the blade assembly by a strong adhesive. However, since no physical connections could be identified underneath the fan blades, it was inferred that power is supplied wirelessly via a coil, similar to the LUMINA L1 fan, as indicated by the fan's low rotational friction.

Figure 4: USB LED clock holographic fan from Takealot (2025b)

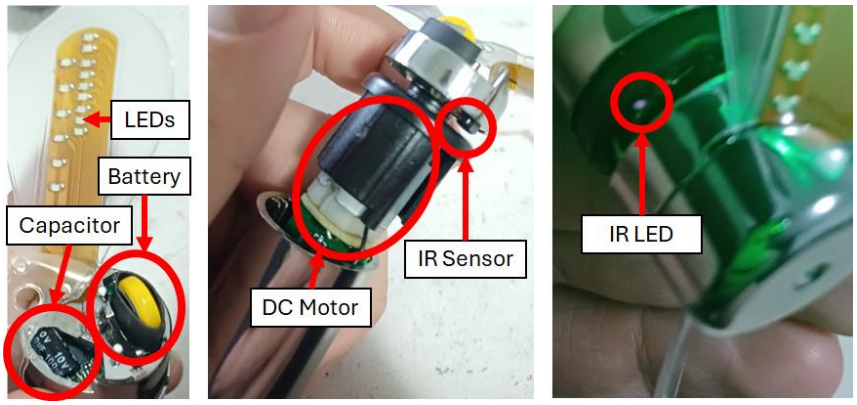

Figure 5: Partial disassembly of a low-cost USB fan

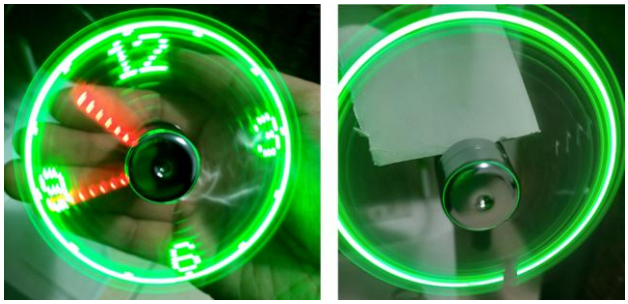

Figure 6: Low-cost USB fan display paper test

2.3 Persistence of vision effect

The POV effect is a type of optical illusion whereby multiple discrete images blend into a single image in the human mind (Priya et al., 2020). This effect is

used by television as well as animators who rely on flickering images to create the illusion of motion (Priya et al., 2020; Adobe, 2025).

For LED fan-based displays, the persistence of vision effect can occur at fan speeds as low as 320 rpm (5.33 Hz) (Priya et al., 2020). However, this might result in choppy images. Therefore, to smooth out the animations, animators tend to use at least 24 Hz (Adobe, 2025).

2.4 SPI communication standard

During the concept design phase (in section 4), a literature study was conducted on the various communication standards used by microcontrollers to communicate and control LEDs. One of these standards was the SPI (Serial Peripheral Interface), which is often used due to its high transmission speed compared to similar protocols (Chen & Huang, 2023). The protocol also boasts superior signal integrity with minimal hardware requirements (Patra & Saini, 2024). The SPI interface can be configured for full-duplex, half-duplex, or simplex configurations, with full-duplex allowing both the master and slave to communicate/send data to each another at the same time, with half-duplex only allowing one device to communicate at a time. However, since the LEDs are not capable of sending data to the microcontroller, the SPI could be set to a simplex configuration so that only the microcontroller is allowed to send data to the LEDs (FastBitLab, 2019).

2.5 Motor speed controllers

Speed control is essential for holographic fan displays, as it enables emergency shutdowns and limits the maximum operational speed of the fan. DC (Direct Current) speed controllers regulate delivery to DC motors from a constant power source, typically a DC power supply. These controllers modulate power delivery based on an analogue control voltage input using PWM (Pulse Width Modulation). PWM signals deliver power to devices based on the duty cycle of a digital signal. By varying the width/duty cycle of the PWM signal (the proportion of time the signal remains “high” in each cycle), the average power delivered to a device can be adjusted. DC speed controllers vary the PWM signal delivered to the DC motor from the constant power source proportionally to the analogue control signal supplied. This leads to precise speed control of a DC motor by adjusting the analogue control voltage supplied to the DC speed controller. (Mulindi, 2020).

However, PWM-capable microcontrollers are typically unable to meet the high current demands of DC motors despite possessing built-in PWM pins. Therefore, DC speed controllers are often used as intermediary devices between the DC motor and the microcontroller. (DIYElectronics, 2025a; Phipps Electronics, 2025).

For BLDC (Brushless Direct Current) motors, ESCs (Electronic Speed Controllers) are employed instead of DC speed controllers. ESCs operate similarly but differ in two key aspects: the power supplied is converted to three-phase before delivery to the motor, and a digital PWM signal from the microcontroller replaces the analogue control input. (RC Ratings, 2025).

2.6 Wireless communication

To enable wireless communication between a user's mobile application and the fan display, similar to the L1 fan from LUMINA (2025a), various wireless communication protocols and standards were researched and are discussed below.

WebSockets enable real-time communication between client and server devices, facilitating high-performance web applications. Unlike conventional websites that rely on HTTP polling and suffer from high latency, WebSockets maintain an open connection, enabling full-duplex data transmission (simultaneous server-to-client and client-to-server communication). Additionally, WebSockets permit the use of conventional web browsers rather than dedicated applications, allowing any device with Wi-Fi or internet connectivity on the same network to communicate. (Wang, Salim & Moskovits, 2013).

2.7 Hall-effect sensors

To accurately time the LED flashing of holographic fan displays, the position and speed of the fan blades must be determined.

One approach employs Hall-effect sensors, which are based on the Hall effect phenomenon discovered by Edwin Hall in 1879, nearly 20 years before Thomson’s discovery of the electron. The Hall effect describes the generation of voltage across certain materials in the presence of a magnetic field. (Ramsden, 2006; Walker, Resnick & Halliday, 2014).

By placing a magnet on a rotating fan blade that passes a stationary Hall-effect sensor perpendicularly, the generated voltage pulses can be counted over a known time period to determine accurate fan speed. This approach is commonly employed by industry-standard holographic 3D LED fans from suppliers such as LUMINA to determine precise rpm or fan blade position, which is required to create stable holographic images. (Barnes, 2024a).

3 System specifications

The stakeholder requirements for the 3D hologram-like RGB LED fan display are provided in Table 1. The primary stakeholders are staff and students, specifically those in the Department of Mechanical and Mechatronic Engineering at Stellenbosch University.

3.1 Stakeholder requirements

Table 1 summarises the stakeholder requirements and their respective rankings, where "*i*" indicates the highest priority. Fan safety was ranked highest, followed by project budget. To ensure project success, both static and dynamic image display were prioritised, as these are essential for a true 3D holographic fan display. The remaining requirements were ranked accordingly, with visual appeal rated lowest since it does not directly affect system functionality, unlike the mobile application, which adds greater value and feature potential.

Table 1: Stakeholder requirements

SR Number	Description	Ranking
SR1	The fan must still be safe when operating at high speeds	i
SR2	The system must be cost-effective	ii
SR3	Must be able to reproduce static and dynamic scenes	iii
SR4	Must contain at least some additively manufactured part	iv
SR5	The system must be able to interact with a mobile application	v
SR6	Must have multi-faceted design elements	vi
SR7	The system must be portable	vii
SR8	Mobile application must be user-friendly	viii
SR9	Must have low noise	ix
SR10	Must have a long lifespan with minimal maintenance required	x
SR11	Must be environmentally friendly	xi
SR12	Must be visually appealing	xii

3.2 Engineering requirements

The functional requirements listed in Table 2 list the functions which the system will need to perform to meet the relevant stakeholder requirements given in Table 1 from which they were derived. The performance requirements in Table 3 list the measurable target values and ranges that each of the related functions must meet to verify that the stakeholder requirements given are met. Information on how these performance requirement values were determined is provided in the relevant footnotes and Appendix E.

Table 2: Engineering requirements

FR Number	Description	Derived From
FR1	The system must have an emergency stop or power on/off switch	SR1
FR2	Fan blades and other moving parts must be adequately secured to ensure safety	SR1
FR3	The system must stay within the allocated budget given	SR2
FR4	Must be able to achieve a persistence of vision effect	SR3
FR5	Multiple fan displays can interact with each other to display static/dynamic scenes	SR3, SR6
FR6	The system must be made using at least one additively manufactured, or 3D printed part	SR4
FR7	The fan can be stopped and started using a mobile application	SR5
FR8	Fan display can be changed/updated using a mobile application	SR5
FR9	The mobile application must be able to "connect" to the fan wirelessly[1]	SR5
FR10	Fan must consist of modular components	SR6
FR11	The system must be small enough to be disassembled and reassembled to allow easy transportation of the system	SR6, SR7
FR12	The fan mobile application should be user-friendly/intuitive to use	SR8
FR13	Must comply with the Western Cape noise regulations	SR9

[1] Functional requirement set based on the L1 fan from LUMINA (2025a), where a user-friendly mobile application can wirelessly connect to the displays to upload images with some fan control.

FR Number	Description	Derived From
	for disturbing noises (Province of the Western Cape, 2013)	
FR14	The entire system must not require any maintenance/replacement parts for a set time	SR10, SR11
FR15	All parts used must be recyclable/reusable	SR11
FR16	All replaceable parts can be safely disposed of	SR11
FR17	Materials and components used to build the fan should be visually appealing	SR12
FR18	Fan's overall design must be aesthetically pleasing	SR12

Table 3: Performance requirements

PR Number	Description	Target	Range	Unit	Related SR
PR1	Can power on/off using a physical mechanism	Yes	Yes/No	NA	FR1
PR2	Can power on/off using the mobile application interface	Yes	Yes/No	NA	FR1, FR7
PR3	The fan is built with all components properly secured in place	Yes	Yes/No	NA	FR2
PR4	The system can be dismantled and reassembled	Yes	Yes/No	NA	FR2, FR11
PR5	Total system cost, including all fan displays and components	5 000	≤ 5 000	R	FR3
PR6	Display refresh rate	24	≥ 5	Hz	FR4
PR7	Static scenes can be displayed	Yes	Yes/No	NA	FR5
PR8	Dynamic scenes can be displayed	Yes	Yes/No	NA	FR5

PR Number	Description	Target	Range	Unit	Related SR
PR9	Number of fan displays onto which static/dynamic[2] scenes can be displayed	2	≥ 5	Number	FR5
PR10	Number of additively manufactured parts	2	≥ 2	Number	FR6
PR11	Scenes displayed can be controlled via a mobile application	Yes	Yes/No	NA	FR8
PR12	The mobile application has wireless connectivity to the system	Yes	Yes/No	NA	FR9
PR13	Number of interconnected subsystems	3	≥ 2	Number	FR10, FR11
PR14	Total weight per fan display	2	≤ 2	kg	FR11
PR15	Mobile application follows the applicable MAUX design features[3]	Yes	Yes/No	NA	FR12
PR16	System noise above the residual noise level	3	< 7	dB	FR13
PR17	Maximum fan noise level	60	≤ 60	dB	FR13
PR18	Minimum lifetime of any individual part used	12	≥ 12	Months	FR14
PR19	All parts can be disposed of in an environmentally friendly manner	Yes	Yes/No	NA	FR15, FR16
PR20	Aesthetic design and look, based on existing fan designs	Yes	Yes/No	NA	FR17, FR18

[2] Static images are images such as still/frames or snapshots of a video or a static circle image where no moving object or text is visible compared to dynamic images which can include the aforementioned or refer to scenes which can change based on user-interaction, etc.

[3] Based on previous research, key mobile application user experience (MAUX) design features are navigation bars, icons, low latency, etc. These all contribute to the user experience and should be incorporated when designing the mobile application. Table 5 (Lu, Qu & Chen, 2025:12).

4 Concept designs

Based on current 3D holographic fans, such as the L1 fan from LUMINA, the design of a 3D holographic fan can be split up into three main high-level subsystems. These subsystems are usually a spinning fan blade subsystem (where the LEDs and/or controller/s are housed), a fan base subsystem which supports the fan blade assembly (and usually contains the system's spinning motor and main power supply) and a stand/mount used to support the fan base. (LUMINA, 2025a).

Since each subsystem can have multiple different and/or complex designs, the scope of this project's design will be limited to the development of only the physical design of the fan blade subsystem, focusing primarily on the fan blades and the electronic hardware design of each fan. Different concept designs for fan mounts/stand subsystems were considered and made, although these only amounted to some basic hand drawings, since an affordable and stable tripod stand could be found from one of the local suppliers available (Takealot, 2025a). The following two sections 4.1 and 4.2, each start with an introductory paragraph which discusses the overall working/operation of the subsystem and highlights the similarities each of the following subsystem design concepts shares. Each design concept has a short description followed by a qualitative assessment, with the last concept for each section being the final concept chosen for the relevant subsystem.

4.1 Fan blade subsystem concept designs

All the fan blade designs discussed below were inspired by helicopter blades, which are sometimes attached with hinges to a central spinning hub and rotate about a fixed point, relying on centrifugal forces to "pull" the blades outwards so that they can be aligned/straightened (Fioretti, Di Maio, Ewins et al., 2010). Each of the fan blade designs has a small lip/space to provide a mounting location for the LEDs.

Using these rotating fan blades can improve the fan's portability by enabling disassembly and more compact storage, as required by SR7. Most injuries and damage from/to 3D holographic fans occur when users accidentally touch the spinning blades during operation, especially in public places where children may be present (SZLEDWORLD, 2025). Therefore, by allowing the blades to rotate freely, if the fan encounters an obstruction such as a hand or finger near the edge of the fan blade, the blades can rotate slightly out of the way or break off. This can help reduce damage to the fan blade and object, and can prevent or lessen injuries to users and the fan. Figure 10 shows a flow diagram of the final

fan blade subsystem chosen and how the blades can rotate to avoid a small obstruction near the edges of the fan.

4.1.1 Concept 1: Pin-mounted

The fan blade concept, shown in Figure 7, is similar to a conventional quadcopter blade with a pin hole, which can be used to secure the fan blade to the blade housing utilising a screw or other fastener.

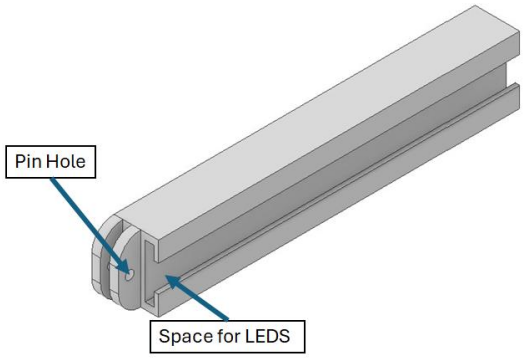

Figure 7: Concept 1: Pin-mounted

The simple design of the fan blade facilitates easier manufacturing compared to other fan blade concepts. However, since these fan blade concepts have a high likelihood of needing to be custom-made, as there is little to no availability of similar fan blades from local suppliers which are both foldable and/or capable of having LEDs mounted onto them, 3D printing or additive manufacturing techniques will be required. The strength of these fan blades might pose a concern, especially at the critical points near the pin holes. While this concept can be strengthened by increasing the amount of material around the pinholes, the other concepts below can provide a way to reduce the load on the pinholes.

4.1.2 Concept 2: Ball-and-socket joint with pinhole

The fan blade design, shown in Figure 8, uses a ball-and-socket joint while still allowing a pin hole, which can be used to secure the fan blade onto the blade housing using a screw or other fastener.

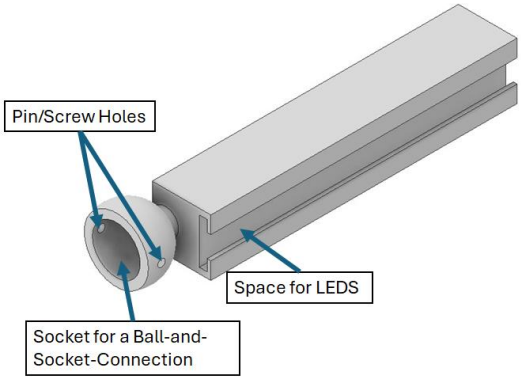

Figure 8: Concept 2: Ball-and-socket joint with pinhole

The ball-and-socket joint provides more contact points with the blade housing. This helps lessen the stress on the pin connection holes by allowing the ball-and-socket joint to bear some of the centrifugal and other forces generated by the spinning fan blades.

4.1.3 Final concept 3: Ball-and-socket joint with slits

The fan blade design shown in Figure 9 demonstrates a similar concept to the previous design shown in section 4.1.2, but includes an added slit in the ball-and-socket joint of the fan blade. The blade's shape has been slightly modified to enhance its aerodynamic performance and reduce noise during operation. The final adjustment involves adding a small lip underneath the blade to accommodate LED wiring if necessary.

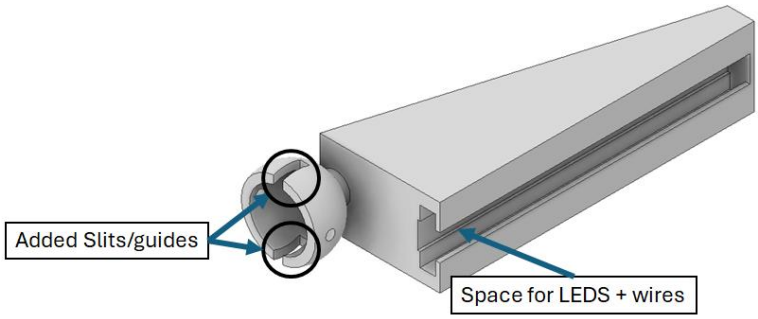

Figure 9: Final concept 3: Ball-and-socket joint with slits

One of the main benefits of adding slits to the fan blade design is that it enables the ball-and-socket joint to flex slightly outwards when inserting it over the ball joint of the fan blade housing, helping to reduce stress when fixing the fan blade to the housing. The second benefit is that the slits offer a way to limit the rotation of the fan blade to a specific angle by using a stopper, as shown in Figure 10, which can assist the blade in breaking off in the event of a significant impact.

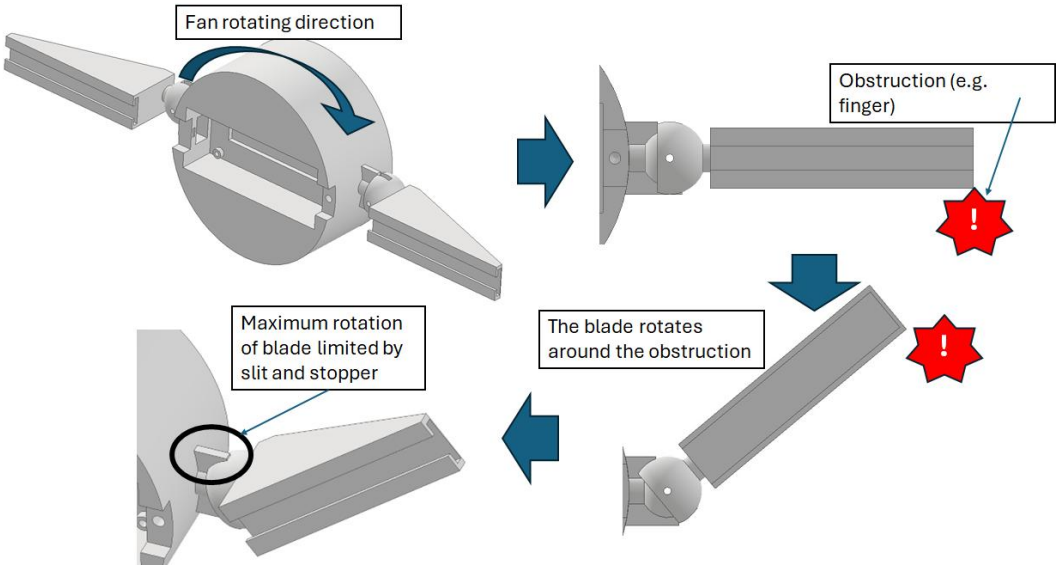

Figure 10: Final concept and folding design operation

4.2 Electronic hardware design concepts

Each design concept is illustrated by a flow diagram that shows the location of each component, either on the stationary fan base subsystem (stationary subsystem) or the rotating fan blade subsystem (rotating subsystem). Power and data flows between the components are indicated by solid and dashed arrows, respectively. Figure 24 of the fully built system can be used as reference on what parts are considered the rotating and stationary subsystems.

Typically, most LEDs and/or microcontrollers require 5 V power to operate, while most motors with higher speed and torque ratings might require 12 V or more (Communica South Africa, 2025c; DIYElectronics, 2025a; RS Components, 2025). Since there is limited research available on the components of 3D holographic fans, aside from broad listings without specific model numbers, as noted by Barnes (2024a), the electronic concepts in the design below use generic component names such as “microcontroller” instead of exact model numbers unless stated otherwise. These generic components will be further refined in the detail design phase (section 5), to ensure all system requirements outlined in section 3 are met.

The Hall-effect sensor on the rotating subsystem is used to detect a small magnet fixed to the stationary subsystem. Based on the signals the microcontroller receives from the Hall-effect sensor, the rpm of the fan can be determined. This allows the microcontroller to determine the position of each LED, enabling it to turn the correct LED/s on or off to create an image similar to the way done by Barnes (2024a).

4.2.1 Concept 1: DC motor with wireless power transfer

The following concept shown in Figure 11, was based on the low-cost 3D holographic USB clock fan examined in section 2.2. The design assumes that a 5 V main power supply is available to power a small 5 V rated DC motor similar to the low-cost USB clock fan. Further a wireless power transmitter is included in the design to allow power to be transferred to the rotating subassembly from the stationary subassembly.

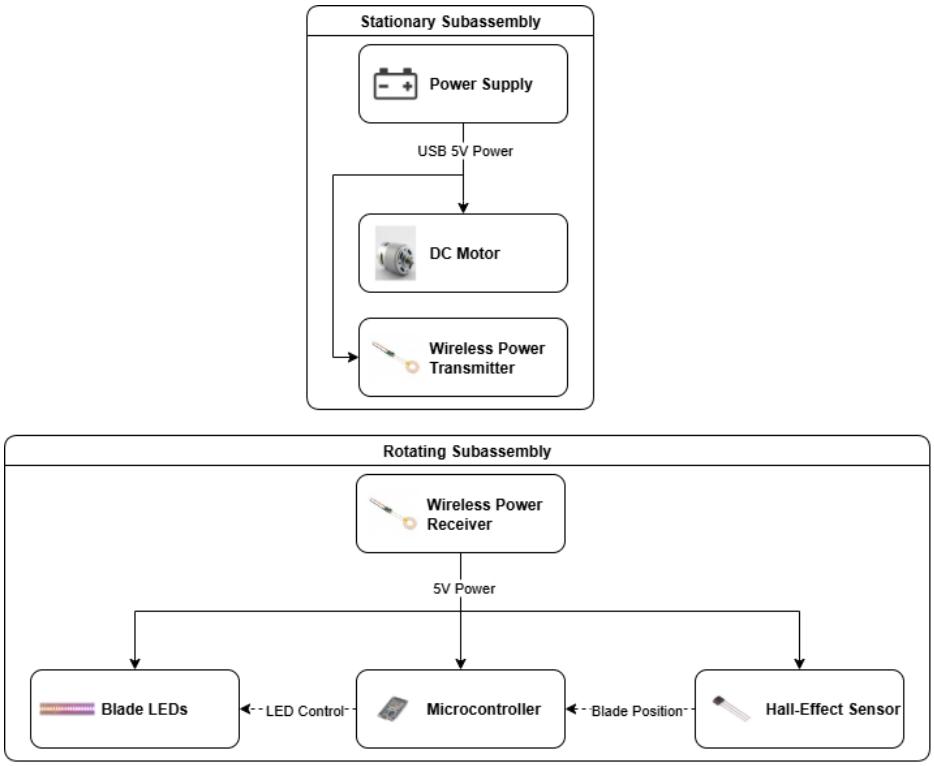

Figure 11: Concept 1: DC motor with wireless power transfer

While this design is simple, it does not allow any speed control of the motor. While speed control is not a requirement, being able to control the motor's speed allows for a more consistent rpm of the fan, which can result in a more stable image being created. Another advantage of using a speed control is that it allows the fan to be slowed down or switched off completely without needing to be near the fan.

The wireless power transmitter also requires no physical/sliding contact connectors, which can help to extend the lifespan of the device significantly. However, they can be less power efficient compared to physical wire or slip ring connections due to losses caused by heat during the power transfer process (Tidwell, 2025).

4.2.2 Concept 2: BLDC motor with slip ring

The design concept below uses a BLDC motor connected to an ESC to enable fan speed control as discussed in section 2.5. The wireless power transfer is replaced by an alternative slip ring design, enabling a physical connection for power and data transfer between the stationary and rotating subassemblies. This design also allows the microcontroller on the fan blade to control both the LEDs and motor speed through the ESC with minimal added complexity. Since the rated voltage of the power supply depends on the BLDC motor selected, a DC-to-DC converter is included to adjust the voltage to 5 V to power the components on the rotating subassembly.

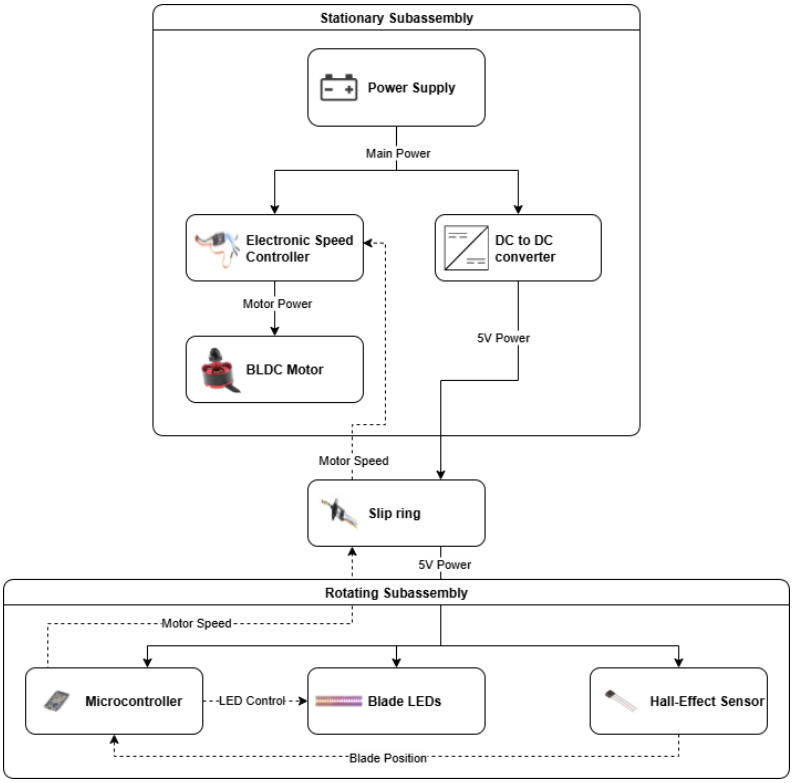

Figure 12: Concept 2: BLDC motor with slip ring

An advantage of using BLDC motors compared to DC motors is that BLDC motors are less prone to wear than DC motors due to BLDC motors not requiring carbon brushes, which can wear out over time. However, when conducting a feasibility analysis and looking at the motors available from local suppliers such as Communica and RS Components, the only cost-effective BLDC motors available were quadcopter motors (Communica South Africa, 2025a). These BLDC motors require high peak current draws up to 15 A or more based on testing videos from KendinYap (2024) and VR Tech Art (2025) as no openly available datasheets for these motors could be found. Compared to other DC motors, like

the HKD 795 Motor from Communica which only requires up to 3.34 A peak current (Communica South Africa, 2025c; Phipps Electronics, 2025). Therefore, while BLDC motors might have a higher lifetime, they would require much higher current-rated power supplies, which could drastically increase the cost of the project.

Since the slip ring will likely be required to fit over the motor axis, the feasibility of acquiring through-bore slip rings from local suppliers was conducted. However, no cost-effective through-bore slip rings from local suppliers could be found that are rated for speeds of 320 rpm or more, which is the minimum speed requirement to achieve a POV effect (section 2.3) (Micro Robotics, 2025b). While some slip rings do exist which can handle higher-speed data, they are typically only used in industrial applications due to their high cost. Slip rings are also more prone to wear out over time since they rely on a physical connection or sliding contact to work, compared to wireless power transfer (Dorsey & Daun, 2018; Tidwell, 2025).

4.2.3 Final concept 3: DC motor with wireless power transfer and speed control

The concept, shown in Figure 13, improves on the previous design concept by using a DC motor instead of a BLDC motor. This change avoids the need for an expensive, high-current-rated power supply. The design uses wireless power transfer, similar to that used in concept 1. It also includes two microcontrollers per fan: one for controlling the motor speed via a DC speed controller, and another for controlling the LEDs. Since the rated voltage of the DC motor is still unknown until final DC motor has been selected another DC-to-DC converter circuit has been included. This was done to ensure that 5 V power can be supplied to the 5 V rated components. This concept further assumes the wireless power receiver can output the 5 V needed for the rotating subassembly components, and that the transmitter includes a built-in converter circuit.

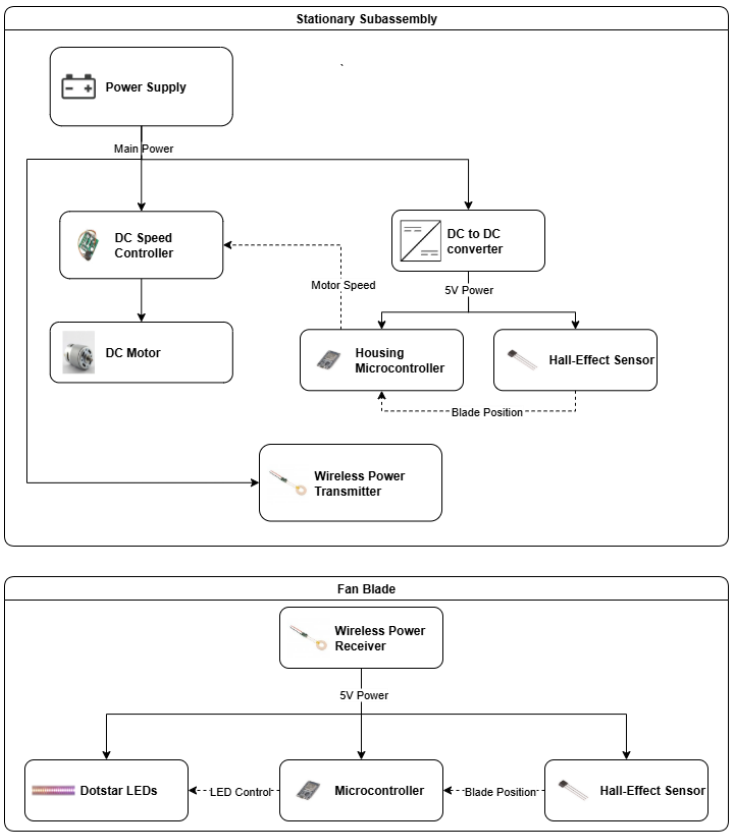

Figure 13: Final concept 3: DC motor with wireless power transfer and speed control

The wireless power transfer component supplies power to the fan blade assembly without the need for a physical connection, helping extend the system's lifespan. However, since no physical connection is present, two microcontrollers will be required so that both the LEDs and the DC speed controller can be controlled using the appropriate communication protocol/s (section 2.4). This design uses two Hall-effect sensors instead of one which allows both the microcontroller on the stationary and rotating subassembly to determine the fan speed independently. This increases the system safety by allowing the microcontroller controlling the motor speed to continually monitor the rpm of the motor, in the event the microcontroller on the rotating subassembly fails.

5 Detail design

The following section aims to show how the final design concepts chosen in the previous sections 4.1.3 and 4.2.3 were refined by starting with the most critical components, namely the LEDs and microcontrollers. These two components had the highest impact on the rest of the system, specifically on the power/interface requirements. Therefore, they needed to be chosen early in the design phase so that the other interfacing components could be chosen to ensure compatibility. After these components had been selected the rest of the components of the system were refined including the housings required for both the stationary and rotating subassembly. The section then concludes with the material selection of the additively manufactured parts required to build the system.

After each of the different components had been chosen, they were first tested individually to confirm that they met the requirements set before integrating them into the whole system with other components connected to them. This approach proved especially useful, as shown later in section 5.4.

5.1 LEDs

To create a POV effect as discussed in section 2.3, the refresh rate of the LEDs needed to be determined. 3D holographic fans generate a full image by spinning an LED strip/s to form a circular matrix of *n*-by-*n* LEDs. Since the physical design of this project uses a two-bladed approach, similar to the L1 fan from LUMINA from section 2.1, a simple half-blue, half-red static circle image can be created each time the blade has completed half a rotation (Figure 14), by switching a single LED once between blue and red during every full rotation of the fan blade.

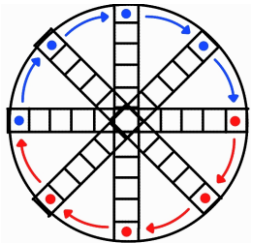

Figure 14: Half-blue, half-red circle

However, since the L1 fan from LUMINA, is capable of more complex static and dynamic images and able to change each individual LED of the *n*-by- circular matrix over the full-colour spectrum, each LED will need to refresh *n* times for every LED position during one complete rotation of the fan blade (LUMINA, 2025c). Therefore, the refresh rate of the LEDs will need to be at least the number of LED positions (*n*) multiplied by the target refresh rate of the display.

From local suppliers, the only LED light strips which allow each LED to be individually controlled were the DotStars and NeoPixels. Both LED light strips have a maximum density of 144 LEDs/m with the shortest length of 500 mm. According to FR5, which requires multiple fans to be built/tested, an LED light strip of 500 mm with 72 LEDs will allow two displays to be built, each with 36 LEDs. This will allow each of the two displays to display complex images using individually controllable LEDs by forming a 36-by-36 circular LED matrix.

Therefore, the required refresh rate of the LEDs will be 36 LEDs (n) multiplied by the target display refresh rate of 24 Hz, which gives an LED refresh rate required of 864 Hz. Therefore, the DotStars LEDs were selected since they can support up to 8 MHz to 32 MHz refresh rates, depending on the microcontroller being used, whereas the NeoPixels can only support up to 400 Hz (Burgess, 2024; RS Components, 2025).

Through testing, the capability and power requirements of the DotStars LEDs have been proven by using the microcontroller selected in the following section. The testing data and results, and links to videos are given in the Appendix F.

5.2 Position sensor and microcontroller selection

For position sensing a different digital Hall-effect sensor, like the OH44E unipolar Hall-effect sensor from DIYElectronics (DIYElectronics, 2025d), was considered. These digital sensors often allow hardware interrupts, which most microcontrollers support (like the PCNT (Pulse Counter) included in some ESP32 microcontrollers (Espressif Systems, 2025b)), to be used with edge detection, since these digital sensors can produce clean output signals due to Schmitt trigger often being integrated with them, with reduced noise. However, since this sensor was out of stock, the SS49E Linear Hall Effect Sensor was chosen since instead. This sensor produces a linear voltage analogue voltage in the presence of a magnetic field, with a high response time of 3 µs, and an output voltage range between 1 V and 4 V according to its datasheets depending on the strength of the magnet present (SEC Electronics inc., 2012; DIYElectronics, 2025b).

Therefore, the microcontroller requirements are as follows: An ADC interface to read the sensor's analogue output voltage, preferably with a measurable range of 1 V to 4 V. An SPI interface to communicate with the DotStars LEDs to achieve high refresh rates (Burgess, 2024). Since a 36-by-36 image at a refresh rate of 24 Hz (PR6) with each LED requiring 24-bits of data (iPixel LED, 2018), would require at least 746.496 kb[4] of memory per second of the displayed scenes' duration. A wireless interface is required to interact with the fan displays and images via the user-mobile application (required to achieve

[4] Memory required is equal to the number of LEDs times the image refresh rate times the number of bits of data required per LED.

PR12). Lastly, the size of the microcontroller needs to be as small as possible, since the microcontroller will likely need to fit onto the rotating subassembly, along with any other electrical components required.

Based on these criteria, different microcontrollers were considered, such as the Arduino Rev 2 (met all requirements, but larger than the other two), the Teensy 4.1 (met all requirements, was not available from local suppliers) and the final selected Firebeetle 2 ESP32-S3 microcontroller (Microchip Technology Inc, 2020a; Espressif Systems, 2025a; NXP, 2025). The Firebeetle 2 ESP32-S3 has an SPI interface with 16 MB of Flash (program memory) and 8 MB PSRAM (Psuedo-Static Random Access Memory), which can be used to store images in a frame buffer and will allow up to 85 s[5] of dynamic scene playback) and with a footprint of only 24.5 mm by 60 mm. Although the maximum ADC measurement range of the ADC is limited between 0 V – 3.3 V, a small voltage divider circuit can be built to reduce the 1 V – 4 V output of the sensor to 0.83 V and 3.3 V (Espressif Systems, 2025a).

For the second microcontroller used to control the DC motor, all the same requirements were applied except for program memory, as it does not need to update the DotStars LEDs. However, an additional requirement of a PWM or DAC (Digital-to-Analogue Converter) interface was set so that the microcontroller could interface with a DC speed controller. From this, the Firebeetle 2 ESP32-C6 was selected since it was the most cost-effective option from local suppliers that still met all requirements (DIYElectronics, 2025a).

However, during testing of the Hall-effect sensor, the maximum and minimum output voltage levels of the sensor with and without a magnet placed manually in front of the sensor, were measured to be between 3.3 V and 4.5 V, instead of the listed values from the datasheet (SEC Electronics inc., 2012). Therefore, a voltage converted circuit needed to be designed as discussed in section 5.11 below.

5.3 Wireless power transmitter

One of the main requirements for a wireless power transmitter is the amount of power it can transmit to the wireless receiver. Therefore, early in the design process, the first two components (DotStars LEDs and Firebeetle 2 ESP32-S3) were purchased and tested to determine the power consumption requirements.

From the tests conducted in the Appendix F, to operate the LEDs at 50% brightness, the wireless power transmitter will require a rated current of at least 1.2 A. The 50% brightness level was chosen since the LEDs were still clearly visible under the laboratory's indoor lighting conditions, and not much dimmer

[5] Calculated by dividing 8 MB by 746.496 kb, where 8 MB is equal to 64 Mb.

than the 100% brightness LEDs, as can be seen in this README.md file (Botes, 2025a).

From this, the wireless transmitter and receiver component from DIYElectronics was selected, since it can deliver 5 V, 2 A of power from a 12 V supply, which will allow the LEDs and microcontroller to be powered with a slight overhead (DIYElectronics, 2025e). This overhead will allow the LED's brightness to be slightly increased if necessary and keep the wireless power transmitter at a lower temperature during operation, which can help improve the lifespan of the device.

5.4 Final rotating fan subassembly CAD model

From the components selected, a 3D CAD model was created for the rotating subassembly, complete with mounting positions for each of the selected components. Fasteners and clever designs were employed to allow all components, including magnets, to be fixed without the need for adhesives while still allowing ease of assembly and disassembly. By using an LED clip with a peg and screw hole (inspired by the clip design of TV remotes) to cover the microcontroller and to secure the LEDs in place, cables could be hidden to improve the system's aesthetic. A USB hole was also added to enable programming the ESP32, without requiring disassembly. All cables and space allocations required to allow proper cable routing for the Hall-effect sensors with space for the PCB (Printed Circuit Board) of the wireless power receiver were also included in the design. The final design with allocation for the wireless transmitter coils is shown in Figure 15 and Figure 16[6].

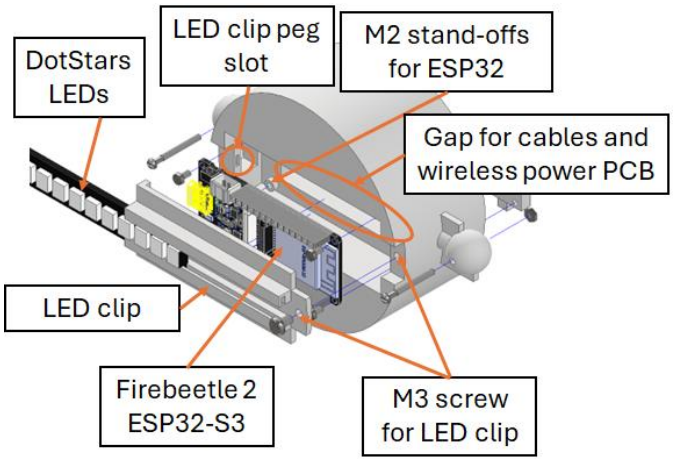

Figure 15: Rotating subassembly housing (wireless, front view)

[6] For visual clarity all shown CAD models are shown in grey. The final 3D printed design used black PLA to achieve a similar aesthetic to the L1 fan from LUMINA the design was based on.

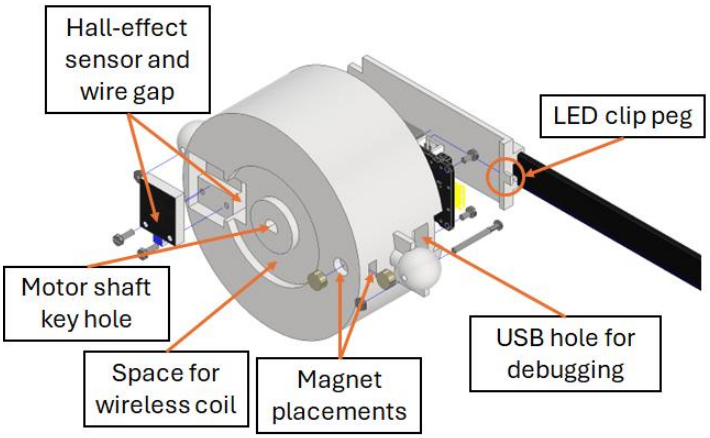

Figure 16: Rotating subassembly housing (wireless, rear-view)

However, when testing the wireless transmitter to confirm if it was indeed capable of delivering 2 A, by slowly increasing the load, the wireless transceiver burned up after delivering just over 600 mA of current. This was later confirmed after DIYElectronics page was updated with more technical specifications which were previously unavailable, where it stated the wireless power transmitter is only stable between 600 mA and 700 mA (DIYElectronics, 2025e).

Therefore, due to time constraints, a new custom wireless transmitter could not be designed and tested in time, since the PCBs and other difficult-to-source components would not arrive in time before the project deadline.

Therefore, an alternative new slip ring design and solution needed to be implemented (detail design in the later section 5.10) to replace the wireless power transmitter. The design change also required the addition of an additional 5 V, 2 A regulator circuit (detail design in the later section 5.12). Both of these components needed to be added and given appropriate mounting positions/space allocation which led to a final redesigned rotating subassembly. The redesigned housing is shown in Figure 17 with only the differences highlighted.

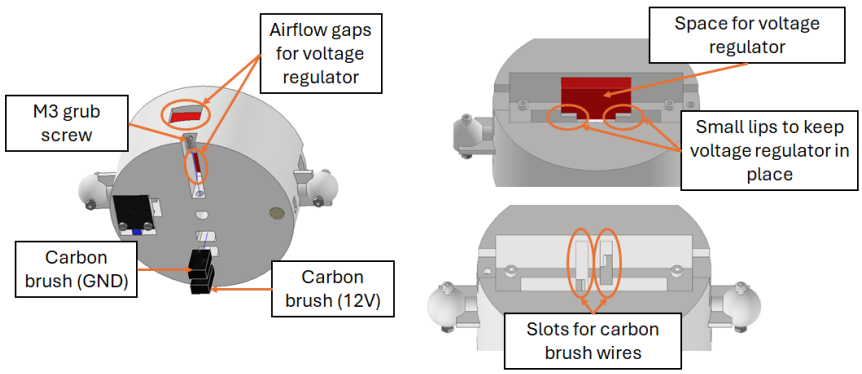

Figure 17: Final rotating subassembly housing (slip ring)

5.5 DC motor

The primary requirement for the DC motor was its rated RPM. Three options were identified from Communica South Africa: the HKD Coreless DC Motor, HKD Solar Cell DC Motor, and HKD 795 Motor. The HKD Solar Cell Motor was unsuitable due to its short 2 mm shaft (Communica South Africa, 2025e). Although the HKD Coreless DC Motor offered a longer shaft for better mounting and clearance, its high speed-to-voltage ratio of 10 540 rpm/V (Communica South Africa, 2025d) made precise speed control difficult, as a 10 mV voltage change could alter the speed by 150 rpm. The HKD 795 Motor was selected for its lower ratio of 833 rpm/V, providing more stable operation despite minor voltage fluctuations from the DC speed controller.

Using inertia and torque calculations (Appendix F), the motor's approximate settling time to reach the target 1 440 rpm—required for a 24 Hz refresh rate (section 2.3)—was determined to be 0.44 s, well below the 14 s deemed acceptable by Priya et al. (2020).

5.6 Power supply

The power supply rated voltage requirement was determined to be 12 V based on the DC motor's rated voltage. To determine the rated current requirement of the power supply, the peak current of all components must first be acquired and converted to a 12 V supply as needed the ratio 5 V/12 V. The peak current consumption of the DC motor at 12 V was determined to be 3.34 A[7] based on reseller data (Phipps Electronics, 2025). From the testing data in Appendix F, the DotStars and Firebeetle 2 ESP32-S3 require a peak current of approximately 1.2 A at 5 V, when converted give 500 mA. From the Hall-effect sensor datasheets, the maximum supply current is 5.5 mA at 5 V, after converting a combined 4.58 mA is required for both Hall-effect sensors. Since limited data is available on the power consumption of the microcontrollers, a maximum current draw of 500 mA was used based on the maximum input current to the microcontrollers given in Table 4-2 and Table 6-2 in the Firebeetle 2 C6 and S3's respective datasheets (Espressif Systems, 2023:54, 2025a:29). This value converts to 0.208 mA for a 12 V supply resulting in an estimated 0.416 mA required for both microcontrollers. By adding up the peak currents of all the components, a rated current requirement of 4.26 A was determined for the power supply.

[7] Since no datasheets for the generic DC motor model were available, only the suppliers' listings for the DC motor could be used. While Communica South Africa (2025c) listed the DC motor's rated current as 2.05 A, other suppliers listed the locked-rotor current closer to 3.34 A or 3.75 A (Phipps Electronics, 2025). This was confirmed to be more accurate during practical testing of the DC motor in the laboratory, where, through a partially-locked rotor test, the current draw exceeded 2.95 A.

From this the AC (Alternating Current) adapter 12 V, 5 A power supply from one of the local suppliers was selected, since it met both the rated voltage and current design requirements, while allowing some overhead (Micro Robotics, no date a). This overhead is used to ensure the power supply will not be overloaded by accident and allows more or higher power components to be added to the design in the future. The form factor of the AC adapter power supply also resembles a conventional laptop charger, which helps improve the overall aesthetic design of device compared to other less-aesthetic 12 V, 5 A switch power supplies (Communica Online, 2025).

5.7 DC speed controller

Based on the DC motor selected, the rated current and voltage of the DC speed controller need to be more than 3.34 A and 12 V or higher, respectively. The DC speed controller also needs to be controllable by a microcontroller typically through a PWM interface (as discussed in section 2.5).

From local suppliers, the 10 A PWM DC motor speed controller was selected because it was the most cost-effective while meeting the above requirements (Communica South Africa, 2025b). The DC speed controller can be controlled using an analogue voltage between 0 – 5 V. However, since the maximum output level of the Firebeetle 2 ESP32-C6 microcontroller at any GPIO (General-Purpose Input/Output) pin is only 3.3 V, the maximum no-load speed of the DC motor will be limited to 6600 rpm[8], which is still far above the target 1 440 rpm (based on Table 3, PR6). Since this DC speed controller cannot be directly controlled by a PWM input from a microcontroller, due to it requiring an analogue control signal as input (as discussed in section 2.5), a small low-pass filter was designed to convert the PWM signal to an analogue control voltage, as explained in the next section 5.8. This allowed for a more cost-effective solution, costing approximately R2 (Appendix A, Table 7), compared to buying a more expensive DC speed controller with built in PWM inputs.

To prevent accidental damage to both the selected power supply and DC motor a 5 A fuse was installed in place of the 15 A fuse the DC speed controller included. This will help limit the maximum allowable current through the DC motor and power supply in the event of an unexpected power failure or short-circuit. While a 4 A fuse would have been more ideal, being only slightly higher than the rated current of the DC motor, the 5 A fuse was selected since it was the only one available from one of the local suppliers Micro Robotics (2025a).

[8] Calculated by multiplying the rated 10 000 rpm of the HKD 795 DC motor by the voltage ratio of 3.3 V/5 V (microcontroller maximum GPIO output/maximum DC speed controller input voltage).

5.8 Low-pass filter design

Since the Firebeetle 2 ESP32-C6 microcontroller does not have a built-in DAC, the microcontroller is incapable of outputting an analogue voltage required to control the DC speed controller.

However, since the microcontroller supports 0 – 3.3 V PWM output with a configurable frequency, a cost-effective low-pass filter or RC (Resistor-Capacitor) circuit can be built to convert the digital PWM signal to an analogue control voltage. The low-pass circuit shown in Figure 18 shows the wiring configuration where the microcontroller supplies the *PWM_Input*, and a resistor *R* and capacitor *C* in parallel produce an analogue output voltage *V_Analogue_Output*.

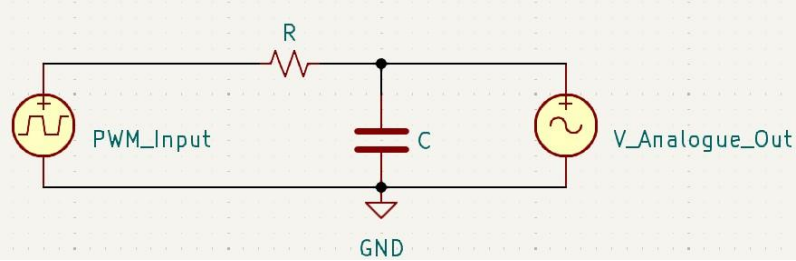

Figure 18: Low-pass filter circuit to generate an analogue voltage from a PWM signal

The frequency of the microcontroller's PWM signal can be configured by dividing the 80 MHz PLL (Phase-Locked Loop) clock by a 20-bit prescaler value (Espressif Systems, 2023:40). Therefore, the design decision was made, through some iteration, to set the PWM frequency to 8 kHz by using a prescaler value of 1000. This allowed the PLL clock to be divided without a remainder and enabled the use of laboratory components, including resistors and capacitors.

Based on previous research and documentation, the ideal attenuation of the low-pass filter should be designed to be less than -28 dB to produce a stable output signal (Microchip Technology Inc, 2020b). The attenuation in dB can be determined using the equation (5.1), where *f_PWM* is the PWM frequency of the microcontroller, and *R* and *C* are the resistor and capacitor values of the circuit, respectively.

$$\text{Attenuation (dB)} @ f_{\text{PWM}} = -10\log_{10}(1 + (2\pi \cdot f_{\text{PWM}} \cdot RC)^2) \qquad (5.1)$$

By setting *f_PWM* and the attenuation to 8 kHz and -30 dB, respectively, and solving for *RC*, a value of 628.8 µs was obtained for *RC*. From the laboratory's available capacitors, a 1 µF capacitor was chosen. From this, the required resistor value *R* could be determined as 628.8 Ω. From the laboratory, the closest chosen E12 10% tolerance resistor available was a 680 Ω resistor.

Before practically building and testing the circuit, it was first simulated using NGSpice (version 34) to ensure that the effect of the non-ideal resistor would be

negligible. Afterwards, the circuit was tested practically, which verified the design. For more information on the simulations and testing conducted, please refer to Appendix H.

After integrating the low-pass filter circuit into the system by connecting it to the DC speed controller and microcontroller a power cycling test was conducted. This was done to ensure the DC motor behaves as expected in the event of a sudden power loss, before the rotating subassembly is fixed to the DC motor. During testing of the system's response to sudden power loss and restoration, the motor would briefly shut off before switching on at near full speed once power was restored, without any input from the microcontroller via the DC speed controller. Using a multimeter to measure the output voltage of the low-pass filter during power loss while the motor was running revealed that the circuit's output voltage remained high, rather than being pulled to ground as expected. This was due to the 1 µF capacitor being unable to dissipate its built-up charge to ground. Therefore, a 6 MΩ resistor[9] was placed in parallel with the capacitor and ground to allow the capacitor to discharge to ground in the event of sudden power loss.

5.9 5 V, 1.5 A voltage regulator

To power the Firebeetle 2 ESP32-C6 and Hall-effect sensor at 5 V from a 12 V supply, a voltage regulator circuit was built. While a standard buck or step-down converter could be used from a local supplier, DIYElectronics (2025c), since a fixed 12 V supply is present, a much more cost-effective solution was to design and build a voltage regulator circuit which saved R72.49 per fan display (see the last paragraph of Appendix A.1 and Table 7). Voltage regulators are also capable of outputting precise voltages with minimal noise, which can help improve the Hall-effect sensor performance by helping to maintain a stable supply voltage (STMicroelectronics, 2004).

Since the microcontroller and Hall-effect sensor are unlikely to exceed more than 505.5 mA of current at 5 V (calculated in section 0), the LM7805CV 5 V regulator was chosen since it is capable of delivering 1.5 A of current. A slightly smaller input capacitor of 100 nF was used, compared to the 0.33 µF capacitor application circuit given in the component's datasheet (STMicroelectronics, 2004), since the AC 12 V, 5 A power supply was selected in section 0 should already be sufficient to produce a stable 12 V input with minimal high-frequency noise. For the output capacitor, since the Hall-effect sensor might induce low-frequency noise on the output side when the sensor is triggered at a 24 Hz interval by a passing magnet, a larger electrolytic output capacitor value of 220 µF was used to maintain a more stable output voltage.

[9] The high 6 MΩ parallel resistor value was chosen to prevent the attenuation of the low-pass filter from being influenced by influencing the *RC* time constant used in equation (5.1).

To determine if a heatsink will be required, the thermal characteristics of the regulator were calculated using the equation (5.2) below where T_J is the junction temperature, T_A is the ambient air temperature (assumed as 25 °C), P_D is the power dissipated through the regulator and θ_{JA} is the thermal resistance between the IC (Integrated Circuit) and the ambient temperature (Texas Instruments, 2024:20).

$$T_J = T_A + P_D\theta_{JA} \quad (5.2)$$

θ_{JA} can be calculated by using the equation (5.3), where θ_{JC} of is the junction-to-case thermal resistance of 5 °C/W and θ_{CA} is the case-to-ambient thermal resistance of 50 °C/W.

$$\theta_{JA} = \theta_{JC} + \theta_{CA} = 55\ °C/W \quad (5.3)$$

The power dissipation can be calculated based on the input currents using the equation (5.4) where V_{IN} is the input voltage to the regulator (12 V), V_{OUT} is the output voltage of the regulator (5 V), I_L is the load current the regulator supplies (505.5 mA) and I_G is the current sunk to ground from the regulator (assumed to be 0 A, due to the regulator being directly connected to ground) (Texas Instruments, 2024:20).

$$P_D = (V_{IN} - V_{OUT})I_L + V_{IN}I_G = 3.54\,W \quad (5.4)$$

Now, by using the equation (5.2) with the power dissipation as 3.54 W, the temperature of the regulator under operation was determined as 219.7 °C, which is far above the 150 °C maximum operating temperature of the regulator (STMicroelectrics, 2004:1).

Therefore, a heatsink was added to the regulator with a heatsink-to-ambient thermal resistance (θ_{HA}) of 20 °C/W (Micro Robotics, no date b), and a 0.2 °C/W case-to-heatsink (θ_{CH}) thermal resistance due to a thermal paste being used, the following equation (5.5) was used to calculate the new thermal resistance of the regulator as 5.25 °C/W.

$$\theta_{JA} = \theta_{JC} + \theta_{CH} + \theta_{HA} = 25.2\ °C/W \quad (5.5)$$

From this, the new operating temperature of the regulator was determined to be 114.21 °C, which is within the operating temperature range of the regulator. The circuit was tested afterwards practically, where it could successfully power both of the components for over 2 hours continuously.

5.10 Custom slip ring

Since the wireless power transmitter and receiver were determined unsuitable to supply 2 A of current (from section 5.4), and since no other 2 A or higher wireless power components were available from local suppliers, a custom slip ring was designed instead.

The design was inspired by a drill motor slip ring, where carbon brushes are used to contact rotating copper rings fixed to the rotating motor shaft. However, due to the limited space available on the selected DC motor shaft and rotating blade assembly, a pancake-style slip ring was designed instead to help reduce space requirements.

The copper plates were designed to fit over the shaft of the DC motor and fixed over it using a clip with a wall in between to prevent the carbon brushes from accidentally shorting. This wall also helped to maintain clearance between the rotating subassembly and the stationary subassembly housing by physically blocking the rotating subassembly from being pressed onto the motor shaft too far. The carbon brushes were spring-loaded and inserted into the rotating subassembly housing through gaps at the back of it. To ensure the carbon brushes maintain adequate pressure/contact with the copper plates, a grub screw was used, which can be screwed into the rotating subassembly housing and motor shaft. Figure 19 shows the clip designed and how the carbon brushes and copper plates make contact, with space for the 12 V and ground wires, indicated as well.

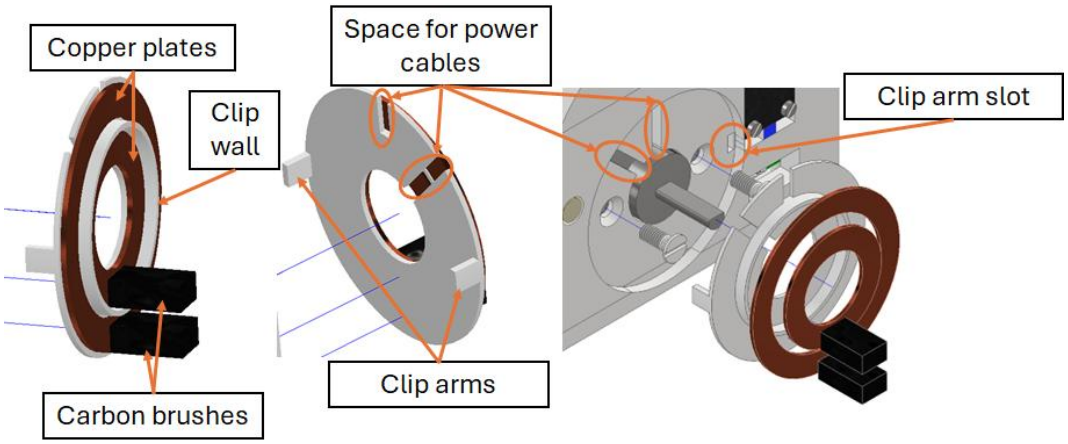

Figure 19: Slip ring clip

This allowed power to be transferred to the rotating subassembly to power the voltage regulator (designed in the following section 5.12) and connected LEDs, Hall-effect sensor and Firebeetle 2 ESP32-S3 microcontroller.

5.11 Voltage converter circuit

To convert the output range of the Hall-effect sensor discussed at the end of section 5.2, a voltage divider circuit was implemented to convert the 3.3 V to 4.5 V range to 2.42 V and 3.3 V. However, due to sensor noise and the small voltage difference/range of only 0.88 V, the ADC was unable to take accurate measurements determined during practical rpm testing by monitoring the reported rpms from the microcontrollers, using serial debugging.

Therefore, two other circuits were designed and simulated using LTSpice (version 24.1.10), before being practically implemented and tested. These circuits were a Schmitt trigger and a comparator circuit. The Schmitt trigger was first designed and implemented because these triggers are commonly used to produce a clean output signal even for noisy analogue signals (Dejan, 2015). Testing was conducted using a RIGOL DG1022 signal generator from the laboratory set to produce a sinusoidal wave at 25 Hz, with a DC offset and amplitude of 3.8 V and 0.5 V, respectively, to simulate the Hall-effect sensors' output voltage caused by a passing magnet between 3.3 V and 4.5 V. The input and output signals of the circuit was measured using a Tektroniks TDS 2001C oscilloscope and P6000 1X & 10X oscilloscope probes, where the measured practical circuit matched the theoretical simulations.

However, when tested with the Hall-effect sensor using a passing magnet fixed to the rotating subassembly instead of through manually placing/moving the magnets passed the sensor (which could only be completed after redesigning and building the new rotating subassembly in section 5.4), the circuit did not behave as expected. Upon further inspection, it was found that the Hall-effect sensor's minimum output voltage would slowly increase, while the maximum output voltage would slowly decrease at higher fan speeds. This prevented the Schmitt trigger's upper and lower threshold voltage from being triggered, preventing the circuit from producing consistent low and high output voltages. A simpler comparator circuit was designed was based on information from the LM339N comparators datasheet (STMicroelectronics, 2009). The first step was to create a suitable reference voltage at the midpoint of the sensors output at 3.8 V, since this should allow the sensor to trigger more reliably even if the maximum and minimum outputs of the sensor changes. This was done by dividing the stable 5 V output voltage of the regulator (designed in section 5.9) to achieve a reference voltage of 3.8 V, using a 3.16 kΩ and a variable 10 kΩ[10] resistor, which was connected to the non-inverting input of the LM339N comparator. A 3.3 kΩ current limiting resistor was added in series with the input signal and inverting input terminal of the comparator used, to ensure the

[10] The variable resistor chosen was based on availability which allowed tuning of the reference voltage to an exact value and allowed tuning to the reference voltage level to 3.42 V as shown in section 7.1.

absolute maximum input pin current rating won't be exceeded (STMicroelectronics, 2009). The VCC^+ and VCC^- pins of the comparator circuit were connected to the voltage regulators 5 V output and ground. By configuring the pin of the microcontroller to use a 3.3 V pull-up resistor connected to the comparator's output pin, the output will be pulled to ground whenever the sensor's input voltage is higher than the reference voltage of 3.8 V.

The output waveforms measured are shown in Figure 20 with the channels set to DC coupling with a 10X attenuation, where it can be seen that clean 0 and 3.28 V levels could be generated from a 3.3 V to 4.5 V sinusoidal input signal at 25 Hz.

When tested with the Hall-effect sensor, more consistent rpm measurements could be taken than with the Schmitt trigger implementation, however, the system was still prone to noise, as further testing revealed in section 6.4. However, unfortunately due to the late start in being able to properly test the circuit, as mentioned above, the circuit could only be added in the stationary subassembly.

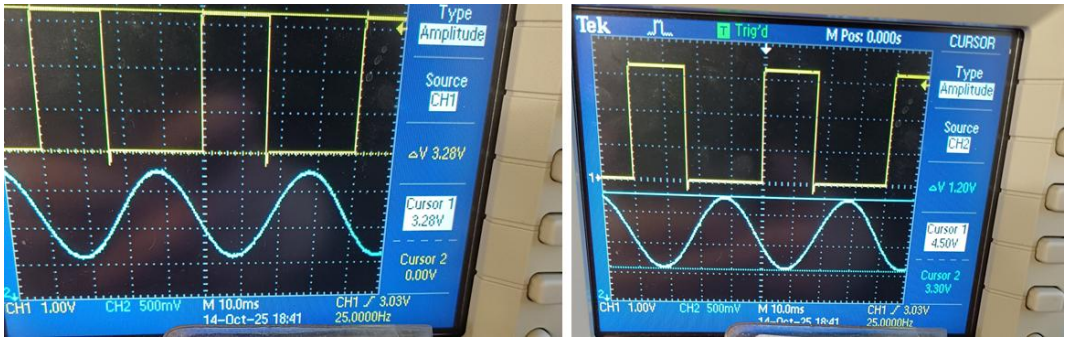

Figure 20: Comparator circuit practical testing

5.12 5 V, 5 A voltage regulator

To supply the rotating subassembly with 5 V power, another voltage regulator circuit needed to be designed. The placement of the voltage regulator could be placed either before or after the custom slip ring. Since the carbon brushes may introduce electrical noise or voltage drops due to poor contact or fan vibrations, causing intermittent loss of contact with the copper plates, the design decision was made to place the voltage regulator circuit on the rotating subassembly.

The current consumption on the rotating subassembly was estimated to be around 1.2 A of current at 5 V (Appendix F). Therefore, a voltage regulator capable of meeting this current demand needed to be chosen. From local suppliers, 2 A and 5 A, 5 V regulators were available, from which the LM1084IT-5.0, 5 V, 5 A voltage regulator was chosen (RS Components, no date). While the 2 A regulator might be sufficient for the 1.2 A current required, the theoretical peak current if all 36 LEDs were to be switched on is at least 2.16 A. Therefore, to

prevent accidental damage to the system, the higher current rated voltage regulator was chosen.

By using the same equations performed in section 5.9, the following was obtained. From equation (5.3) using θ_{JC} as 2.7 °C/W, θ_{CH} as 0.2 °C/W and θ_{CA} as 20 °C/W, 22.9 °C/W was obtained for θ_{JA}. From equation (5.4) P_D was determined as 8.4 W, using V_{IN} as 12 V, V_{OUT} as 5 V and I_L as 1.2 A. By assuming an ambient temperature of 25 °C (T_A) and using the values calculated for θ_{JA} and P_D, T_J was determined as 217.36 °C, which is above the thermal operating limit of the regulator. Therefore, a new maximum power dissipation had to be determined using the following two equations, taking into account both the control and output section temperatures (Texas Instruments, 2024:20).

$$P_{D_{Control}} = (125°C - T_A)/(\theta_{JC_{Control}} + \theta_{CH} + \theta_{HA}) \quad (5.6)$$

$$P_{D_{Output}} = (150°C - T_A)/(\theta_{JC_{Output}} + \theta_{CH} + \theta_{HA}) \quad (5.7)$$

By using the values 0.65 °C/W, 2.7 °C/W, 0.2 °C/W and 20 °C/W for $\theta_{JC_{Control}}$, $\theta_{JC_{Output}}$, θ_{CH} and θ_{HA} respectively all for an ambient temperature of 25 °C (T_A), $P_{D_{Control}}$ and $P_{D_{Output}}$ could be determined as 4.8 W and 5.5 W respectively.

Now by using equation (5.4), by setting the P_D equal to $P_{D_{Control}}$ and with V_{IN} and V_{out} equal to 12 V and 5 V respectively and I_G equal to 0 A (due to the regulator being directly connected to ground), the new maximum current I_L was determined to be 0.69 mA.

This limits the maximum brightness of the DotStars LEDs below the ideal 50% brightness originally designed for using a wireless 5 V, 2 A power transmitter, since the maximum load current of the voltage regulator I_L is less than the required 1.2 A current (Appendix F). To further improve and keep the ambient air temperature from rising during operation, the grub screw access slot was used to provide airflow to the regulator. An opening at the top of the rotating subassembly was also provided to allow the heatsink and voltage regulator to cool down using the moving air while the fan is spinning, which can be seen in Figure 17.

5.13 Stationary subassembly housing

After all of the components were selected, the stationary subassembly housing could be designed, as shown in Figure 21 and Figure 22. A CAD model of each part was created with accurate dimensions to ensure that all components would fit inside a compact housing, with USB access to flash the ESP32 without disassembly. The base, walls and cap of the housing were designed as separate parts to allow easier assembly and disassembly of the system following a

modular design approach. This allows the housing to be modified if a different stand or mount needs to be used in the future, by allowing only the relevant part to be modified and replaced. It also helped to decrease the time and complexity when 3D printing and prototyping the housing. All holes into which M3 and M2 screws needed to be screwed into were given exact diameters of 3 mm and 2 mm in the CAD model. This was done to ensure that the .STEP files generated from the CAD model could be used directly by the 3D printer slicer, to allow the machined screws to be inserted and screwed into the 3D printed holes securely without the need for brass inserts.

However, since the housing will be fixed and removed from the M6 screw of the tripod stand repeatedly, a brass insert was considered. But due to the limited availability of these inserts from local suppliers or requiring bags of 100 at a time to be bought, an exact 6 mm hole diameter was created on the CAD model to fix the housing onto the tripod stand securely. To secure the DC motor, two countersunk M4 boreholes with a clearance tolerance of 0.2 mm were added, to allow the clip for the slip ring copper plates to sit flush against the housing.

A housing cap was also designed with gaps for airflow to help mitigate rising ambient air temperatures, featuring a cut out to allow the heatsink of the LM7805CV voltage regulator to be monitored as well.

Furthermore, during the testing of the system's initial performance, and due to the clockwise rotation of the fan blade, a stopper was added to prevent the housing from rotating slightly while the fan is operating, and to aid in alignment when securing the housing to the tripod mounting screw.

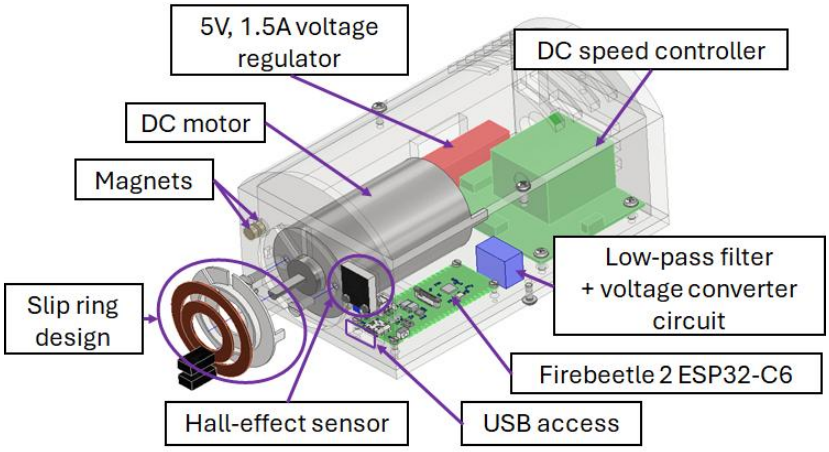

Figure 21: Stationary subassembly housing (front view)

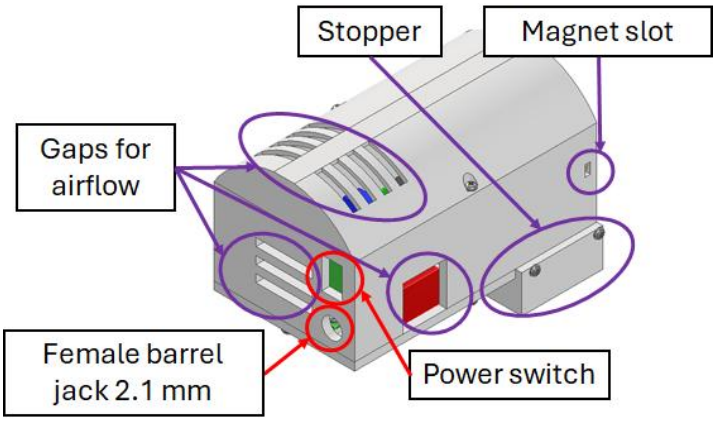

Figure 22: Stationary subassembly housing (front view)

5.14 Additive material selection

PLA and PETG are two of the most common types of 3D printing filaments used due to their low cost and ease of printing compared to other filaments, such as ABS and carbon fibre filaments. PLA is considered biodegradable/compostable, which makes it environmentally friendly (Ashby, 2023; Amador, Avendano, González et al., 2025). However, even just between these two common types of filaments, a large difference in their material properties exists. PLA is widely used due to its ultimate tensile strength and Young's modulus, which range between 46 MPa and 88 MPa, and 1.246 GPa and 4.409 GPa, respectively, at 100% infill density and 80 mm/s printing speed (Chacón, Caminero, García-Plaza et al., 2017). While PETG has lower ultimate tensile strengths and Young's moduli, between 39 MPa and 68 MPa and 1.22 GPa and 3.03 GPa, respectively. However, compared to PLA at 100% infill and printing speeds between 20 mm/s and 80 mm/s, PETG has an overall greater toughness, making it more suitable for repeated stresses or ductile stress applications (Valvez, Silva & Reis, 2022). PETG also offers superior chemical and UV resistance with higher toughness than PLA, making it more ideal for repetitive stresses and flexing/bending loads compared to PLA. PETG also performs better at higher temperatures than PLA, which can start to degrade at 50 °C (Amador et al., 2025).

Based on this PETG was selected for the rotating subassembly housing and fan blades since these parts will experience high temperatures and stresses.

5.15 Fan blade design

To refine the chosen fan blade design, the following steps were taken. The design decision was made to make the ball joint connection on the rotating subassembly 7 mm in diameter. From this, the inner ball-socket connection on

the fan blade was set to 7.5 mm, which enabled the blade to be fixed to the ball-joint with less force and bending stress compared to a zero-tolerance approach, while still allowing a secure fit. By designing the slit height to be 8 mm high from the base of the housing, the angle the fan blade is allowed to move could be restricted to 40°. This value was a design choice to test if the fan blade could be stopped or would break off, before hitting the rotating subassembly housing using the stopper. The outer socket diameter of the fan blade was set to 9 mm after iteration to achieve a balance between strength and flexibility, with all calculations given in Appendix I. From the calculations, a conservative safety factor of 31.21 and 1.54 was obtained at speeds of 320 and 1440 rpm, respectively, assuming the blade is only supported by the fasteners, with no additional mounting pressure from the ball-joint itself.

These safety factors were tested by using a 5 kg weight fixed to the blade using a fastener through the two holes of the fan blade, where it successfully held up more than the required 3.65 kg (35.78 N) of force the fan blade should experience due to centrifugal forces even at 1 440 rpm.

5.16 3D printing orientation

The orientation of the part on the printing bed can greatly influence the strength of 3D printed parts (Chacón et al., 2017). Depending on the orientation of the 3D printed parts on the printing bed, the tolerances and supports needed can vary greatly and add unnecessary material costs.

Therefore, when designing all of the parts, care was given to prioritise the printing direction which offered the most strength, specifically for the fan blades where the direction of the centrifugal forces the fan blade will experience is perpendicular with the build plate as shown in Figure 23, with some tree supports required. Random seams and an outer wall thickness of 5 was also used to further improve the strength of the fan blades.

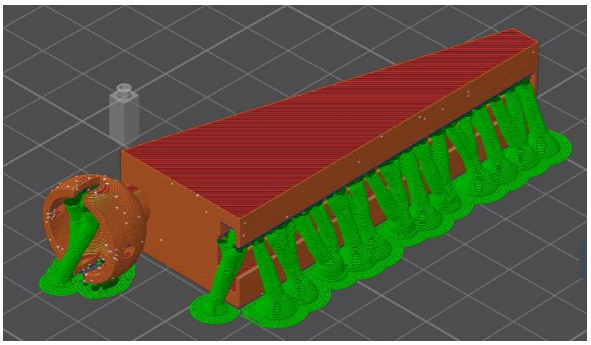

Figure 23: Fan blade printing direction

For the housings, supports for overhangs with no strict tolerance requirements (such as the USB holes), or where the aesthetic won't be

influenced due other components such as the Hall-effect sensor covering the bridged overhangs.

All parts were 3D printed using a K1SE 3D printer from Creality, using CR-PLA and CR-PETG filaments respectively. The time and cost of all the additively manufactured components are given in Appendix A.

5.17 Final built prototype

Below in Figure 24 the two fully built fan displays are shown with a close up of fan 1 on the right, with a picture of both fan displays 1 and 2, displaying an image E and a custom circle image respectively. With a test image when displaying custom test “HOPE” at 660 rpm and 850 rpm (right) in Figure 25. (Assembly instructions given in BUILD.md (LxttleSplat42U, 2025a))

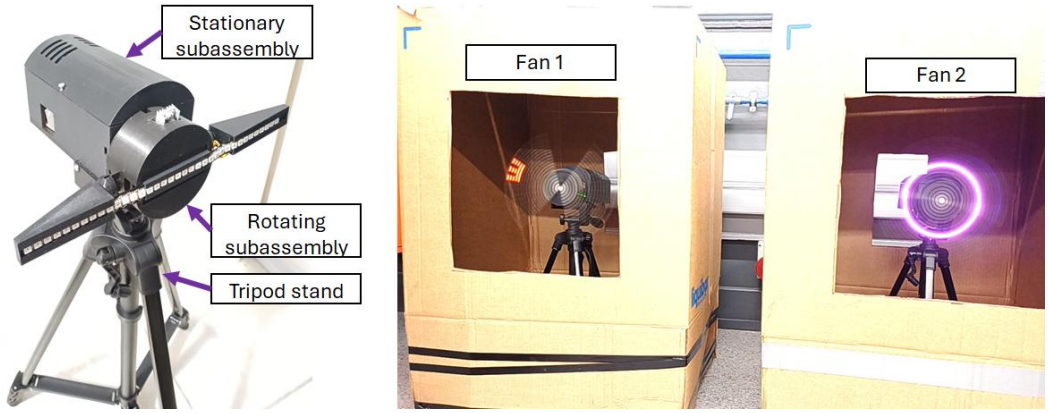

Figure 24: Fully built fan 1 (left), lab testing multi-display images “E” and “custom circle” (right)

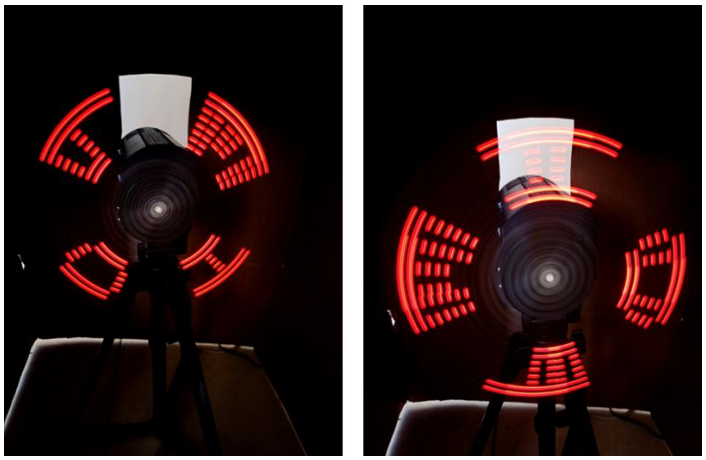

Figure 25: Custom text "HOPE" at 630 rpm (left) and 850 rpm (right)

6 Software design and implementation

The following section describes the software design and implementation of both the mobile application and the ESP32 microcontroller's software. All of the code and relevant and supplementary information can be found on my GitHub page as follows, for the mobile application (Holo3D) (Botes, 2025c), main server ESP32 (Base_ESP32) (Botes, 2025d), other motor control ESP32 clients (Base_Client) (Botes, 2025e) and fan blade ESP32s (Fan_Blade) (Botes, 2025b). The Base_ESP32 refers to the Firebeetle 2 ESP32 C6 microcontroller located on the stationary subassembly in fan 1. The Base_ESP32 is responsible for controlling the fan one speed, taking rpm measurements of the fan display and hosting the WebSocket server. The Base_Client is the other fan displays' Firebeetle 2 ESP32 C6 microcontroller, which has the same responsibilities as the Base_ESP32, but acting as a WebSocket client instead of a server and is located on the stationary subassembly of fan 2. The Fan_Blade's are the Firebeetle 2 ESP32 S3 microcontrollers situated on the rotating subassemblies of the fan displays. They are responsible for receiving rpm fan measurement data and commands sent from the user's mobile application to update the images/scenes to display using the connected DotStars LEDs. Each of the Fan_Blade, Base_Client and Base_ESP32 source code folders include a "HardwareSoftwareConfig" file, which can be used and edited if other hardware or software configurations are required, with instructions given on how to use it in their respective README.md files. For example, if the Hall-effect sensors are connected to another pin other than pin 1 for the Base_ESP32, the RPM_SENSOR variable in this file can be changed to another pin, without requiring any changes to the rest of the software (this can also be seen by following the link here at the end of the README.md file (Botes, 2025d). To speed up development and compile time PlatformIO was used in VSCode using the Arduino framework to program the Fan_Blade microcontrollers. However, since the Base_Client and Base_ESP32 microcontrollers were unsupported using PlatformIO, the Arduino IDE 2.3.3 was used instead also using the Arduino framework. For the mobile application VSCode was used with Flutter as the mobile application development framework, chosen due to it being well documented, with a wide open-source library of UI elements, and could be used to create user-friendly, standalone applications (end of section 6.3).

6.1 Start-up procedure

The following describes the start-up procedure of the system, where Figure 26 can be used as a reference. Upon each of the microcontrollers receiving power, the following occurs. Each fan immediately pulls all of its pins to low, to ensure

the DotStars LEDs and DC motor are switched off entirely. Thereafter, the Base_ESP32 creates a Wi-Fi network AP (Access Point) called “Holo3D” with a WebSocket server at the IP address “192.168.4.1” as soon as it receives power. After the AP is set up, all other Fan_Blade and Base_Client microcontrollers (acting as WebSocket clients) connect to the network by using a unique IP address in the format “192.168.4.ID”[11] to prevent IP address conflicts. Thereafter, each client sends a “REGISTER:ID” command to the server, where “ID” is the globally assigned unique ID variable number of each microcontroller assigned in its respective configuration file. The format for each ID of the Fan_Blades and Base_Clients is in the format X1 and X0 respectively, where X is the fan number. Therefore, for a third fan display the respective IDs will be 31 and 30 for the Fan_Blade and Base_Client respectively. When the WebSocket server on Base_ESP32 receives the message, it generates a unique WebSocket address for each of the clients based on the value of the “ID” received. Thereafter, it sends a message back to the client in the form “REGISTERED:ID”, which the client uses to confirm if a successful connection has been established. The same is done by the user-mobile application, where, after the user connects to the AP, the message “REGISTER:255[12]” is sent to the server, with the server responding with the command “REGISTERED:255”, to inform the user’s mobile application that a successful connection has been established.

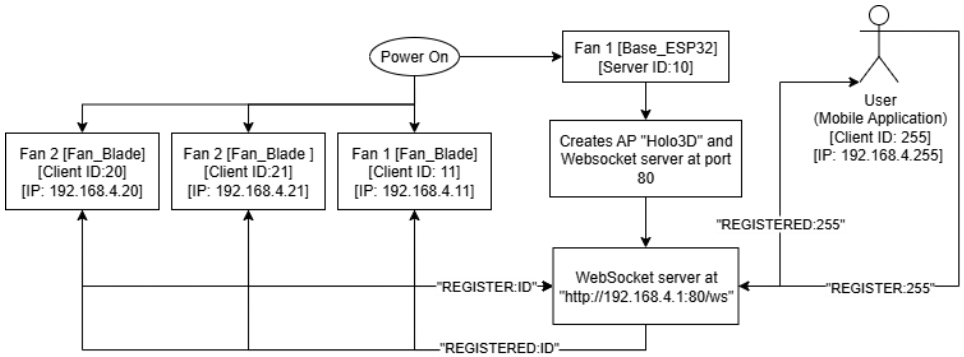

Figure 26: Software start-up procedure

[11] This “ID” is configurable using the ”HardwareSoftwareConfig” source file found on their respective .git repositories and variable “ESP_ID”. Instructions are given on the expected format shown in the README.md files and comments in the source code (links for the Fan_Blade: README.md, “HardwareSoftwareConfig.cpp” (Botes, 2025b)).

[12] “255” is the “ID” of the “REGISTER:ID” message the server expects and is configurable in the software of the mobile application by changing the global variable “USER_WS_ID” at the top of the main.dart source file (LxttleSplat42U, 2025b).

6.2 Overall functionality/communication

The flow diagram (Figure 27) serves as a reference to illustrate how the WebSocket server and client communication have been implemented, and how each microcontroller interacts with the others and the mobile application. All commands from the mobile application are sent in packets to the Base_ESP32, which hosts the WebSocket server in the format “ID:COMMAND:VALUE:”, where “ID” is the client the user-application want to control, “COMMAND” is the type of action the client must perform, and “VALUE” is the required additional information the client needs to execute the command. For example, suppose the user wants to display the second image, selected from a dropdown box of available preloaded images/scenes on the first fan display. In that case, the command sent from the user-mobile application to the Base_ESP32 will be “11:DISPLAY:1[13]”. This message is then forwarded to the respective Fan_Blade with the registered ID 11. Upon receiving a command from the server, the Fan_Blade will first confirm if the message is in the expected format “ID:COMMAND:VALUE:” and that “ID” matches its globally defined ID number. This was done to ensure that if by accident the message is sent to the wrong client or in the wrong format, the system will reject the invalid message. After the Fan_Blade has finished validating the message, if the “COMMAND” part of the message is equal to “DISPLAY”, a switch statement is used to set the display of the ESP32 to the desired image based on the “VALUE” received. Since “VALUE” is “1” in this case, the second image preloaded on the ESP32 will be displayed. Therefore, if the second display’s image needs to be updated to the second image in the dropdown as well, only the “ID” number in the message sent from the user-mobile application needs to be changed to 21.

To control the speed of the motors, the user can send commands to the server in the format “MOTOR_SPEED:VALUE”. The “VALUE” sent is determined based on a slider value 0 - 100 from the mobile application's UI which is scaled linearly to the range 0 – 150[14] before sending the message to the server. Therefore, if the server receives the “MOTOR_SPEED:20” based on the slider value from the mobile application, the message is forwarded to all clients with a trailing 0 in their registered ID, which are the Base_Clients. Upon receiving the command the Base_Client sets the PWM output frequency duty cycle to the received value. This changes the analogue control signal to the DC speed

[13] “ID:DISPLAY:INDEX:”, where the “INDEX” is the array index of the dropdown item selected (with 0 being the first element in the array)

[14] The “VALUE” will be used by the Base_ESP32 and Base_Client microcontrollers to update the PWM duty cycle, which requires an input value between 0 – 255 (Espressif Systems, 2023). However, the fan range has been limited to 0 – 150 to limit the maximum no-load speed of the DC motor as an added safety measure.

controller, as explained in sections 2.5 and 5.7, which sets the no-load speed of the motor to 784 rpm[15].

The rpm measurements taken by the Base_Client and Base_ESP32 microcontrollers are sent to the server in the format “ID:RPM:VALUE” which it forwards to the respective clients based on the “ID” received and the user-mobile application.

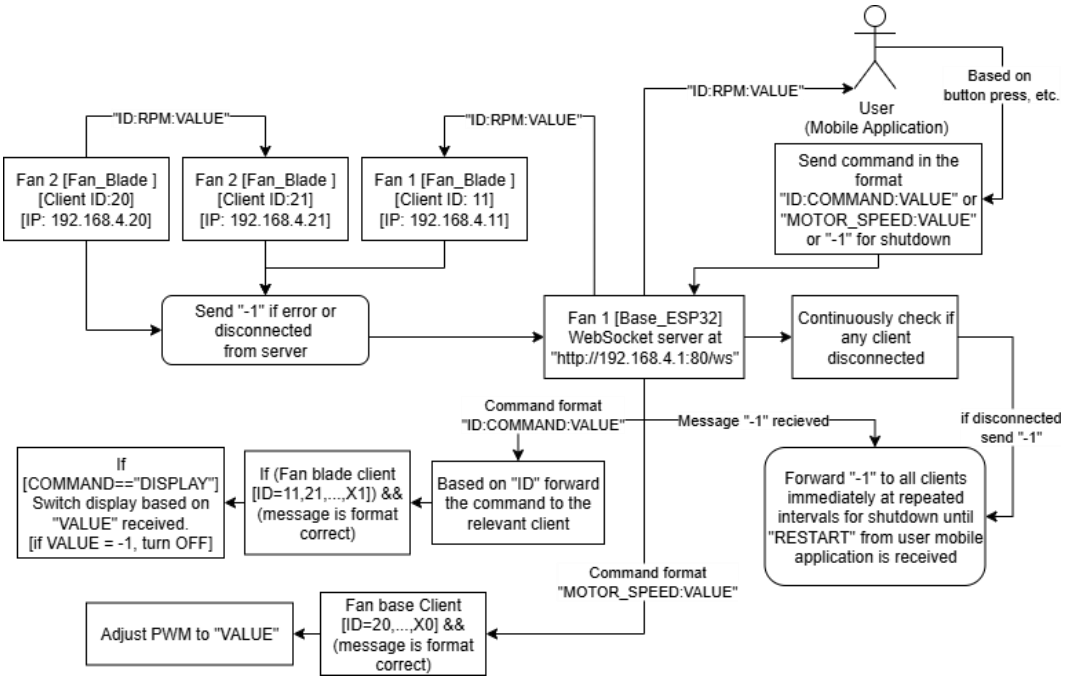

Figure 27: WebSocket communication implementation

The software implementation also supports safety features such as sending and receiving a shutdown “-1” command to all devices in the network. The “-1” shutdown command can be sent from the client devices whenever they experience an error or are disconnected. Upon the server Base_ESP32 receiving the message, the message is forwarded to all of the connected client devices repeatedly at 500 ms intervals (which is configurable using the “tshutDownRepeatInterval” variable in the respective the configuration file, link), until a “RESTART” command from the user-mobile application is received, after which the shutdown “-1” command being forwarded ceases. Whenever a client device receives the “-1” command, a shutdown procedure is immediately executed, which turns off all fan motors and displays, and informs the user through the mobile application that an error has occurred by closing the fan

[15] 784 rpm determined by using the ratio of 20/255 and multiplying it by the rated 10 000 rpm speed of the DC motor at 12 V, where 255 is the maximum input range of the ledcWrite() function used.

controls and displaying a “Restart Fan System” button, which can be pressed to restart the system by sending the “RESTART” command.

6.3 User-mobile application UI

The mobile application was developed using Flutter, which allowed an intuitive UI to be created with support for different mobile device screen aspect ratios (some showcase videos of the features available, like the self-adjusting aspect ratio given in the README.md file (LxttleSplat42U, 2025b)). A global colour and font scheme was designed to ensure visual consistency and a cohesive look for the mobile applications’ UI. The mobile application features a welcome page and a navigation rail on the left, allowing users to access fan controls by tapping the fan controls icon “✇”. Once the mobile device connects to an AP (Access Point) “Holo3D” created by the Base_ESP32, the fan controls for both fans are displayed after pressing the “Connect” button. Both of the respective fan rpms, reported from the WebSocket server Base_ESP32, can be seen just above the respective image dropdown box. The application allows both fan images to be selected independently by selecting an image from the dropdown box of the respective fan. The buttons “Turn On” and “Turn Off” can be used to turn the displayed image of the fans on or off, respectively. The speed of both fans can be changed by moving the slider at the bottom of the display. Figure 28 shows screenshots of the UI of the user-mobile application.

The application supports Bluetooth remote functionality, utilising the included Bluetooth remote that came with the selected tripod stands. This allows both fan displays to be switched on or off remotely after pairing the remote with the user’s mobile device. For safety, an emergency “Enable Fan E-Stop” button was added, which allows a shut-off command to be sent to the Base_ESP32 based on the absolute acceleration measured by the user’s mobile device’s accelerometer. This value, which needs to be exceeded, can be changed by using the global variable “accelThreshold” (currently set to $2\ m/s^2$ of absolute acceleration) in the main.dart source code file (LxttleSplat42U, 2025b). The application was exported to an .apk file, allowing it to be downloaded and installed as a standalone application on Android devices without requiring source code to be downloaded or used.

Since the mobile application “Holo3D” used in testing in section 7 cannot be used to showcase the mobile application UI without being connected to the “Holo3D” AP, a demo version of the application “Holo3D Demo” was created, on repositories “Demo-mode branch”. The application has all of the same features as the main “Holo3D” application, but with an added “Enter Demo Mode” button, which can be used to showcase and experiment with the UI, without needing to be connected to the “Holo3D” access point. For a more detailed list of the app features, including installation instructions for Android devices using the .apk files, with some video showcases, please refer to the main and demo user

application's README.md and installation files, *MainREADME* and *MainAPK*, and *DemoREADME* and *DemoAPK*, respectively.

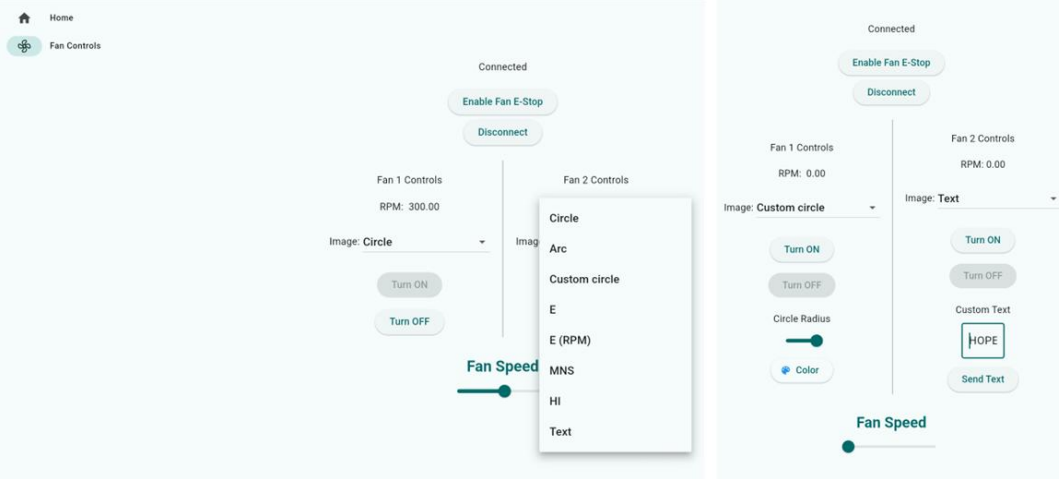

Figure 28: User mobile application UI with dropdown (left), and advanced custom images (right)

6.4 Fan speed measurement and implementation

Due to the circuit designed in section 5.11 only being completed after the rotating subassembly was fully built, the circuit could only be implemented in the stationary subassembly and connected to the Firebeetle 2 ESP32 C6 microcontrollers for rpm testing. Therefore, to measure the rpm of the fans a "RPM_Measurement" header and source file was created for the Base_Client and Base_ESP32 microcontrollers. By using the voltage converter circuit in section 5.11, the Base_ESP32 and Base_Client microcontrollers were configured to have a 3.3 V pull-up resistor, with a hardware interrupt set to falling edge detection, to count the number of blade passes. The default priority of 0 was taken to prevent the rpm measurements, from interfering with the WebSockets interrupts, which might cause the microcontroller to potentially miss an emergency shutdown command from the server. A small debounce time of 1 ms was also implemented to prevent multiple interrupts to trigger, when the sensor voltage crosses the reference voltage of the voltage comparator circuit.

To achieve accurate rpm measurement, the number of blade passes was calculated at precise 1 Hz intervals[16] by setting up a system timer as follows. The timer frequency was configured to 1 MHz by using a prescaler value of 80 to divide the 80 MHz PLL clock of the microcontroller, with the ARR (Auto Reload

[16] "HardwareSoftwareConfig.ino" files of both the Base_ESP32 and Base_Client microcontrollers by changing only the integer value of the "RPM_MEASUREMENT_TIME" variable to the desired timer frequency in Hz (1 for a 1 Hz timer). This variable determines the ARR value calculated in "RPM_MEASUREMENTS.ino" (clickable links provided in this footnote for the Base_ESP32).

Register) set to 1 000 000 (Espressif Systems, 2023). The rpm could then be calculated using a conversion factor[17] which is multiplied by the number of blade passes to estimate the rpm of the fan blade. For increased accuracy, after each rpm calculation the number of calculations that have occurred in a 2 s[18] period is stored so that an average can be taken over a 2 s period, which is sent to the respective Fan_Blades at the 2 s intervals, as shown in Figure 27 and explained in section 6.2. The accuracy of the rpm values was tested in section 7.1 and determined to be accurate within 50 rpm between 495 rpm and 630 rpm.

6.5 Displaying images

The Fan_Blade microcontroller display can display preloaded images, where each image is stored in a 36-by-36 array with 1's representing LEDs which will need to be switched on and 0's indicating off LEDs of the image. The arrays are compiled at run-time and stored into the Flash memory of the microcontroller. The microcontroller then reads and displays each row of the array at a time interval calculated by dividing the average reported rpm[19] of the fan (received from the respective Base_ESP32 and Base_Client) by the number of rows in the array (36) (Priya et al., 2020). Each row of the array is multiplied by a hexadecimal (0x0F0000 for 50% brightness red) value to convert all the 1's in a row to the required hexadecimal value. This value is used by the "strip.setPixelColor()" function to set the LEDs at the corresponding index positions to display one line of the image at a time. Some showcase videos can be seen in the README.md file of the Base_ESP32 (Botes, 2025d). Figure 29 shows a picture of the "Arc" image selected with slightly blurry lines due to the rpm inconsistency as explained section 7, with a more complex image display text shown in Figure 24.

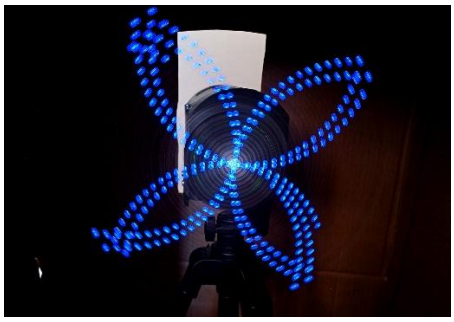

Figure 29: Arc image, slight blur at 680 rpm

[17] The conversion factor is calculated based on the "RPM_MEASUREMENT_TIME" variable explained in the footnote above as (RPM_MEASUREMENT_TIME) multiplied by 60.
[18] Variable also configurable by changing the "tReportInterval" variable in the configuration files.
[19] Average reported rpm calculated using the previous two rpm values from the respective Base_Client or Base_ESP32 microcontrollers.

7 System testing and evaluation

7.1 Calibration and testing of the reported fan rpm

To tune the comparator circuits' reference voltage (designed in section 5.11) so that more accurate rpms could be measured, stroboscopic aliasing was performed as follows. The fan speeds were set to a low fixed speed using the mobile application's fan speed slider. A stroboscope[20] was then set near the reported rpm value of the fan and adjusted until mode 1 of the fan could be observed. The reference voltage was then adjusted until the reported rpm of the fan closely matched the frequency of the stroboscope. The stroboscope frequency was then doubled and adjusted until mode 2 of the fan could be observed, after which the reference voltage was again adjusted until the reported rpm of the fan closely matched half of the currently set stroboscope frequency. This was repeated a third time for mode 3. After this the test was repeated for higher rpms. After tuning it was found that the most accurate measurements could be obtained using a reference voltage for the comparator of 3.42 V. However, the this still only allowed accurate reported rpms of $\pm$50 rpm between fan speeds of 495 rpm and 630 rpm. This inaccuracy might be due to the non-ideal stroboscope that was used, in combination with the increasing minimum and decreasing maximum output voltages of the Hall-effect sensors as noted in section 5.11. The slip rings built also created friction making it difficult to have both displays at the same speed, due to the minor frictional differences,

This led to a difficulty in being able to display more dynamic and stable images across a wide range of fan rpms, where Figure 24 shows how a almost completely stable text "HOPE" can be displayed at 630 rpm, but becomes blurry at 850 rpm.

7.2 Performance requirements evaluation

To evaluate the system, the system was compared to the set performance requirements' target values set in Table 3, some of which could be evaluated after building the system such as PR3 which required all components to be properly secured in place. While this is true for all of the components in the rotating subassembly, delayed and unplanned added circuit designed in section 5.11, the circuit could not be properly fixed in place in the stationary subassembly. Therefore, PR3 could only be partially met. PR4 however, was

[20] Due to delays and setback faced which prevented a stroboscope to be acquired in time, a mobile application "Stroboscope Engineer" version 11.6 was used (GyokovSolutions, 2025).

determined to be satisfied due to all components of the system being able to be disassembled into multiple individual parts repeatedly. The only parts that could not be fully dismantled are the some of the circuits, which were soldered onto the device's pins, however by using a soldering pump or wick, even these circuits can be disconnected and allow the microcontrollers and voltage regulator components to be reused. PR10 was determined to be satisfied since each fan made use of seven different additively manufactured parts, namely the base, walls and cap of the rotating subassembly, the slip ring and LED clips, the rotating subassembly housing and fan blades. PR13's target value was achieved, since all three subsystems, namely the tripod (stand), rotating and stationary subassemblies are all interconnected and resemble the L1 holographic fan's subsystems (Appendix E). The target weight of system PR14 was achieved, since the combined weight of the entire system was measured 3.634 kg as shown in Figure 30 which is be below the 2 kg target value per fan display. PR15 was achieved by including intuitive fan speed controls, by using dropdowns and using a consistent style and colour theme for the UI interface. An aesthetic design PR20 of the fan system could be achieved by using black filaments for all of the additively manufactured parts and using a housing cap and LED clip on the stationary and rotating subsystem housings to hide cable clutter (Figure 24).

Figure 30: Fan system portability and weight measurement

The remainder of performance requirements were evaluating during testing as follows: Both fans were able to be powered on using the physical switch at the back of each fan display (confirming PR1). Thereafter, the user's mobile application was opened, and after connecting to the "Holo3D" AP created by the Base_ESP32, the "Connect" button could be pressed to open the fan controls. Using the fan speed slider, the speed of both fans could be changed successfully, and a static circle image could be displayed on both fans successfully using a POV effect, which satisfies the target values of PR7, PR9, PR11 and PR12 (Figure 24).

Due to the system not being properly balanced even with some counter weights added to the tips of the fan blades, the fan still became unstable near 1 000 rpm, however since the POV effect could be achieved at lower rpms (Figure 25), PR6 was still within the acceptable range of more than 5 Hz.

With the difficulty and time constraints faced, and the rpm measurement of the fan not consistent enough for moving images, since even a small blur in the image led to an unrecognisable image to be created, therefore PR8 was determined to be unsatisfied.

By using either the movement based “Enable Fan E-Stop” button, the fan speed slider by pressing the disconnect button on the mobile application, a shutdown command can be sent to the fan systems, which allows the system to be switched off. The fans can also be restarted by pressing the “Restart fan system” button or by reconnecting to the fan system. PR2 was determined to be achieved since the fan displays could be used to power the displays on/off.

The residual noise level of the system could only be estimated using a mobile application sound meter. Although the original plan was to acquire a class 1 instrument from the department, setbacks and late testing, resulting from the redesign mentioned in sections 5.4 and 5.11, which caused balancing issues, a class 1 sound meter could not be acquired in time before the project deadline. Therefore, an alternative approach was used as an estimate of the system's residual noise level by using a mobile Samsung SM-A346E/DSN phone and the “Sound Meter” application version 10.8 was used (KTW Apps, 2025). Which allowed 10 min readings to be taken using an S-time weighting (slow) and dB-A frequency weighting according to the requirements set in the SANS 10103 (2008) standard for indoor occupancies. Figure 31 shows the residual noise measurement setup using the “Sound Meter” application, where the device was placed away from any sound reflective surfaces used (KTW Apps, 2025).

Figure 31: Noise measurement setup for residual noise level measurement

The background noise level of the system was recorded for 10 minutes and 27 seconds, where the minimum, average and maximum sound levels were measured to be 36.4 dB, 43.7 dB and 87 dB, respectively. Thereafter, the fans were powered on and set to their maximum allowable speed, just below the speed at which the fans start to become unstable. After powering on the fans, both fans were set to display a randomly chosen image. New minimum, average and maximum sound levels of 46.2 dB, 50.7 dB and 64.1 dB were measured over a time span of 11 minutes and 17 seconds. From this the estimated fan noise

above the fan noise level. Based on this the noise increases for the minimum, average and maximum sound levels were calculated as 2.5 dB, 7 dB and 22.9 dB. This indicates that the target 3 dB might have been met at the minimum noise level measured, however since both the average and maximum noise levels are higher than the target 3 dB value and 7 dB allowable ranges, leading to PR16 being determined as unsatisfied. However, since the average noise measured was below the 60 dB requirement for PR17, PR17 was determined to be satisfied, since the maximum noise values of 64.1 dB and 87 dB occurred due to other students in the laboratory, opening and closing one of the laboratory's doors.

Based on the techno-economic analysis's project cost breakdown given in Table 7 (Appendix A.1), the total project cost was determined to be R6 158.09. Due to the redesigns needed leading additive manufacturing costs being higher than expected, and difficulty in sourcing components from the same local supplier which led to an unforeseen amount of shipping costs of R611 and overrun of R1 550.09 for the budget allocated budget of R5 000. Even if only the final built system's cost is considered, by neglecting the initial unused additively manufactured parts (R92.42 from Table 7, for the reprinted parts which costed the same as the initially printed parts), the system still exceeded the R5 000 target by R6 065.67. Therefore, PR5 was determined to be unsatisfied.

To estimate the system's lifetime for PR18, most components were covered by warranties exceeding 12 months. However, the slip ring's lifespan remained uncertain due to its custom design and lack of manufacturer data, particularly for the carbon brushes. By assuming negligible wear on the copper plates during operation, the carbon brushes the carbon brushes lengths of both fans were measured three times each before and after the stress test of 2 hours. The observed wear was approximately 0.05 mm and 0.06 mm for the ground and 12 V brushes after two hours of continuous testing. By assuming brushes are unusable once they have reduced from their original length of 13.55 mm to 3 mm, the estimated lifetimes are estimated to be 542 and 452 hours for the ground and 12 V brushes, respectively. With fan operation expected from 8 a.m. to 9 p.m., five days per week (based on the typical working hours in South Africa I the fans are used for marketing purposes) the 12 V brush minimum lifespan equates to roughly 50 weeks, slightly below the PR18 12-month requirement. Therefore, PR18 was determined to be unsatisfied.

As shown in Table 9 in Appendix D, nearly all of the parts and materials used can be disposed of in an environmentally safe manner, except for the magnets and PETG additively manufactured parts used, since these are often not widely recyclable. However, if PETG can be granulated and given to Trade Avail 346 cc according to Plastics SA (2016) the environmental impact of the components can be reduced. However, since the magnets remain difficult the PR19 was determined to be nearly achieved.

8 Conclusion

The main objective of the project was to design, build and test a 3D holographic fan display, with a focus on integrated safety, cost-effectiveness and additive manufacturing.

To achieve these goals research into a low-cost and more feature-rich 3D holographic fan display was conducted in sections 2.1 and 2.2. Based on these and the stakeholder requirements defined in Table 1, the system specifications in section 3 were used to generate the different fan blade and electronic design concepts required, focusing on safety features such as breakaway/foldable fan blade designs, and fan speed control, respectively. After the final concepts were selected the detail design phase in section 5 was used to select the most suitable components. Testing was conducted of each component individually before implementing them into the rest of the system where problems with the selected wireless power transmitter and Hall-effect sensor were encountered.

Due to limited availability from local suppliers, a new extremely cost-effective slip ring design component (compared to commercial options) needed to be designed in section 5.10, which could reliably supply power to the LEDs of the holographic fan display. These setbacks also caused the system to exceed the allocated budget despite many cost-effective circuits, being designed such as the voltage regulator circuits designed in sections 5.9 and 5.12.

However, due to the setback of the redesign the rpm measurement of the fan proved to be unreliable and only accurate to $\pm$50 rpm between fan speeds of 495 and 630 rpm, which limited the display to mostly static images with no recognisable dynamic images that could be displayed. This was mainly due to the type of Hall-effect sensor used in the final system due to local supplier availability. However, despite the setbacks faced the software implementation proved successful in proving the feasibility of using WebSockets to control multiple fan displays wirelessly using a user-mobile application. The mobile application allowed multiple safety features to be implemented including shutting of the fan system if too much movement is detected by the users' mobile device. This wireless integrated safety implementation can be integrated into existing 3D holographic fan displays, without requiring items to be bought separately, which current implementations use. For more information on the technical impact of the project, please refer to Appendix A.3.

To further improve the system, a different rpm measurement implementation will be required by using the originally planned digital Hall-effect sensor or an IR LED and sensor which the low-cost existing solution in section 2.2 uses. An alternative to the slip ring will need to be considered or a more reliable one will need to be designed to improve the system lifetime. For more recommendations and the potential for commercialisation, please refer to Appendix A.5.

Appendix A. Techno-economic analysis

The appendix below outlines the project's technical and economic impact, covering its budget, planning and time management, technical impact, return on investment, and potential for commercialisation.

A.1 Budget

According to information from the Mechatronics Project 478 module page, the engineering costs are based on a nominal tariff of R500/hr for junior engineers. The 450 engineering hours allocated to the project were based on the Mechatronics Project 478, which is worth 45 credits, with 10 hours of work per credit.

Facility use costs include provisions for the depreciation and maintenance of previously purchased equipment and/or infrastructure used. This project only used a few resistors and capacitors from the laboratories, which amounted to R28.32.

Capital costs are expenses incurred when buying equipment needed solely for the completion of this project, provided that the equipment can still be used for other purposes after the project is finished. At the University of Stellenbosch, only items exceeding R2000 are included in this breakdown, of which this project had none.

Mechanical and Mechatronic Workshop (MMW) labour refers to the total hours technicians from MMW were required to spend, calculated at an hourly rate of R300. MMW material includes any direct running expenses, which typically include incurred material costs.

The project's running costs include the goods and services used and/or consumed during the project, which were not included elsewhere in the budget.

Table 4 and Table 5 show all of the above mentioned costs of the project with a full breakdown of all the projects planned and actual running costs incurred, shown in Table 6 and Table 7.

Table 4: Planned project cost

Activity/tasks	Engineering time		Running costs	Facility use	Capital costs	MMW		TOTAL
	hr	R	R	R	R	Labour R	Material R	
Research components	15	7500						7500
Concept design and evaluation	25	12500						12500
Develop a basic mobile application user interface	15	7500						7500
Find and order initial components required	5	2500	620					3120
Display static and dynamic light sequences on a single LED light strip	25	12500						12500
Display static and dynamic light sequences on a multiple LED light strips	25	12500						12500
Find and order the final components required	30	15000	1540					16540
Design and manufacture additively manufacturing parts	20	10000				906	318	11224
Build and balance the first display prototype	30	15000						15000
Finalise additively manufactured parts	15	7500				906	318	8724
Display and test static and dynamicimages on a single final prototype	50	25000						25000
Display and test static and dynamicimages on multiple final prototypes	50	25000						25000
Improve the user mobile application	15	7500						7500
Literature study	30	15000						15000
Finalise report	100	50000						50000
TOTAL	450	225000	2160	0	0	1812	636	229608

Table 5: Actual project cost

Activity/tasks	Engineering time		Running costs	Facility use	Capital costs	MMW		TOTAL
	hr	R	R	R	R	Labour R	Material R	
Research components	25	12500						12500
Concept design and evaluation	35	17500						17500
Develop a basic mobile application user interface	15	7500						7500
Find and order initial components required	5	2500	1815.10					4315.1
Display static and dynamic light sequences on a single LED light strip	15	7500						7500
Display static and dynamic light sequences on a multiple LED light strips	0	0						0
Find and order the final components required	45	22500	3330.95	28.32				25859.27
Design and manufacture additively manufacturing parts	25	12500				523.90	205.60	13229.5
Build and balance the first display prototype	40	20000						20000
Finalise additively manufactured parts	25	12500				161.80	92.42	12754.22
Display and test static and dynamicimages on a single final prototype	55	27500						27500
Display and test static and dynamicimages on multiple final prototypes	55	27500						27500
Improve the user mobile application	25	12500						12500
System redesign (slip ring)	10	5000						5000
Literature study	35	17500						17500
Finalise report	100	50000						50000
TOTAL	510	255000	5146.05	28.32	0	685.7	298.02	261158.09

The running costs, or consumables budget, for the project were specified as R5 000, with the initial planned costs shown in Table 6, estimated at R4 608. The costs were based on the prices of generic off-the-shelf components, where two of each component would be required to build at least two fan displays. The 3D printing costs were estimated according to the M&M department's 3D printing procedures cost breakdown, which lists the costs as follows: For FDM and resin prints, R15 and R18 per hour of printing, R370/kg (with a density of 1.3g/cm3 for PLA (MakeItFrom.com, 2025)) and R1/ml of material, with a setup fee of R50 and R200 per build plate, respectively. The part dimensions estimated were based on

preliminary concepts of the existing design of the L1 fan from LUMINA (2025a) with an acrylic case, but with a smaller fan blade size. This was done to ensure that, if only the smallest available resin printer (Creality Halot Sky (Creality, 2025)) could be used, all parts could still be manufactured without requiring redesigns.

Table 6: Planned consumable cost

Activity/task	Estimated components required for two fan displays	Cost [R]
Initial components	Microcontrollers (based on ESP32s)	350
	LED light strips (Based on generic RGB light strips)	150
	SD card storage if required (16 GB)	120
Final components	High-speed DC motors with encoders (Communica South Africa)	1 100
	Hall effect sensors (DIYElectronics + overhead for shipping)	40
	AC to DC power supply (Communica South Africa)	400
Initial additive parts	Clear resin 3D prints for the fan cases (Ø120 x 200 mm part dimension with a 2 mm wall thickness)	658
	FDM 3D prints for the fan stand, etc. (based on part dimensions Ø200 x 100 mm with 5mm thickness [0.418g])	423
	FDM LED strip mount (based on part dimensions Ø200 x 100 mm with 5 mm thickness [0.418g])	143
Final additive parts	Overhead for 3D prints (allow all parts to be reprinted if a redesign is required)	1 224
Total		4 608

The following Table 7 lists the actual running costs of the project. All 3D printing was done using a Creality K1 SE FDM 3D printer at home, which helped to make up some of the time lost during the system redesign (mentioned in section 5.4). The CR-PLA and CR-PETG were acquired from a local supplier, Wootware (2025), for R300/kg earlier in the year. However, to allow comparison against the planned initial budget in Table 6, consumable costs were calculated according to the M&M department's 3D printing procedures, mentioned above.

Table 7: Actual consumable cost

Activity/task	Component	Supplier	QTY	Unit cost [R]	Total [R]
Initial components	FireBeetle 2 ESP32-S3 with Camera	DIYElectronics	2	424.00	848.00
	Adafruit LEDs 5V DC 144/m	RS Components	1	967.10	967.10

Activity/task	Component	Supplier	QTY	Unit cost [R]	Total [R]
Final components	Wireless Charging Module - 5V 2A	DIYElectronics	2	200.00	400.00
	Hall Effect Sensor Module - Analogue	DIYElectronics	4	17.00	68.00
	FireBeetle 2 ESP32-C6	DIYElectronics	2	139.00	278.00
	HKD 795 MOTOR 12-24V HI SPD/TORQ	Communica	2	210.00	420.00
	MGT DISC MAGNET 6X3MM 10/PK	Communica	1	18.40	18.40
	BDD PWM DC MOTOR CONTR 10A 6-90V	Communica	2	75.00	150.00
	AC Adapter 12V 5A - 2155 Standard	Micro Robotics	2	167.90	335.80
	Koosda Extendable Stable Tripod Stand	TakeAlot	2	397.00	794.00
	ST Micro 7805 Linear Voltage Regulator	Micro Robotics	1	10.35	10.35
	100 nF Capacitor	E&E Laboratory	2	0.16	0.32
	1 µF Capacitor	E&E Laboratory	2	0.90	1.80
	220 µF Capacitors	E&E Laboratory	6	1.00	6.00
	680 Ω Resistors	E&E Laboratory	2	4.90	9.80
	6 MΩ	E&E Laboratory	2	5.20	10.40
	LM1084IT-5.0/NOPB Voltage Regulator	RS Components	2	50.44	100.88
	Ryobi Carbon Brush Set HG-650	BUCO	2	55.00	110.00
	Coper Plates	Fabrinox	4	8.63	34.52
	Total shipping costs from all suppliers	-	1	611.00	611.00
Initial additive parts	Stationary subassembly 3D prints (4 parts)[21]	-	2	54.67	109.34
	Rotating subassembly 3D prints (2 parts)[22]	-	2	35.41	70.82

[21] The number of individual parts required. The stationary subassembly's parts are the base (floor), walls, cap, slip ring clip and the redesigned wall for the slip ring concept.
[22] The rotating subassembly's parts are the main housing and the LED clip, of which the main housing had to be reprinted for the slip ring design.

Activity/task	Component	Supplier	QTY	Unit cost [R]	Total [R]
	Fan blade (1 part)	-	4	6.36	25.44
	Number of Printing hours	-	18.26	15.00	273.90
	Number of printing requests/build plates[23]	-	5	50	250.00
Final additive parts	Redesigned wall and housing	-	2	46.21	92.42
	Number of Printing hours	-	4.12	15.00	61.80
	Number of printing requests/build plates	-	2	50.00	100.00
Total					6158.09

The expected budget for the project was R4 608. However, this amount was exceeded by R1 550.09, as shown in Table 6 and Table 7.

Several factors contributed to the project being over-budget, primarily due to the unplanned system redesign and higher-than-expected shipping costs. This was due to the inability to qualify for free shipping at most suppliers, as the components could not all be sourced from the same supplier. However, the overhead allocated in the planning phase for finalising the additively manufactured parts helped lessen the cost impact of the redesign. However, some costs could be saved by designing 1.5 A and 5 A power regulator circuits, which cost R11.51 and R52.44 per circuit, respectively, instead of using more expensive off-the-shelf power converters of R84 and R254 (DIYElectronics, 2025c; Micro Robotics, 2025c). The custom slip ring designed in section 5.10, allowed major cost savings, by costing just R72.26 per slip ring, compared to the alternative $645 cost per slip ring with $70 (values from one of the sales representatives contacted at MOFLON).

A.2 Planning (time management)

The Figure 32 shows the Gantt chart, which displays the planned and actual timeline of the project for each activity, with each project deadline listed at the bottom. The actual number of hours spent on the project exceeded the initial

[23] The number of build plates required for all components was calculated as follows. Four fan blades and two slip ring clips could be placed on a single build plate. The two rotating housings required a single build plate. Both LED clips were printed together with the two stationary subassembly walls on a single build plate. The remaining two caps and two floors of the stationary subassembly each required one build plate per pair, and lastly, two more build plates for the redesigned two walls of the stationary subassembly and the rotating subassembly's two housings.

planned amount (shown in Table 4 and Table 5) by 60 hours, resulting in R30 000 of engineering costs, more than the initially planned amount. This was mainly due to some project activities, such as the “Research components” (activity 1) and “Concept design and evaluation” (activity 2), which took much longer than expected due to the need to consider all of the various components, for which a feasibility and cost analysis needed to be performed to ensure the project stays within the allocated R5 000 running cost budget. Other modules also attributed to this by taking up more time than expected.

However, after completing activity 1, activity 7, which involved purchasing the final components, could be completed sooner based on the research conducted at that point. This helped allow activity 10, “Finalising the additive manufactured parts”, and testing of individual components before integration to start sooner than initially planned. This proved to be crucial since the slightly earlier start in testing the final selected components helped give more time for the unplanned system redesign to take place. Unfortunately, this still had a firm knock-on effect on the other activities, mainly activity 9, where the first prototype display could not be tested until the new redesigned system and components could be acquired. This limited the number of tests and system improvements that could be conducted/made, preventing the system from meeting all of the set performance requirements in Table 3 due to insufficient time. Activity 6 was also omitted, since testing the LED light sequence with multiple displays would have required cutting the LEDs (since one light strip needs to be used for both of the fan displays), and the final concept design and fan diameter still needed to be determined. Therefore, an alternative test was conducted to determine if the two microcontrollers purchased at that point could communicate with each other using a wireless mobile application interface. The test demonstrated that two microcontrollers’ built-in LEDs could be reliably switched on and off using a mobile application, thereby validating the feasibility of the electronic design concepts under consideration. The rest of the tasks were completed close to the planned amount, with a slightly earlier start date for finalising the report. This allowed the report to be started during the university recess, while also waiting for the new redesigned components to arrive.

A.3 Technical impact

The constructed 3D holographic RGB fan display, along with its software, demonstrated the feasibility of utilising wireless technology and WebSockets to communicate and to control multiple fan displays (section 7.2). It was further demonstrated that these displays can be built using components from local suppliers. They helped show how the fan displays could be designed for inherent safety by utilising both passive and active safety measures, such as breakaway or foldable fan blade designs and motion-activated system shut-off (section 6.2).

The project also demonstrated how additive manufacturing enables the creation of complex and modular designs, with materials such as PLA can be widely recycled or composted since it's a bio-plastic, whereas PETG however will need to be disposed of safely using a landfill (Appendix D).

A.4 Return on investment

While not all of the set performance requirements in Table 3 could be met, given the time constraints and the maximum allowable power for the LEDs, the research presented in this report can serve as a foundation for developing a more feature-rich system.

The alternative components/concepts mentioned in the report, along with other interesting concepts that could not be fully explored or included in this report, will be added to the project file for future research. Since the software design was made to be as modular as possible, it can help accommodate different hardware configurations by changing the "HardwareAndSoftware" files as explained in each of the README.md files on my GitHub page for each of the respective programs. The modular software approach should also enable the construction and testing of more than two fan displays by using the software for the Fan_Blade and Base_Client, but configured with a different fan ID number, as explained in their respective README.md files. All of the software resources can be used by future students, researchers and the general public by accessing the pages on my GitHub, which will stay public.

A.5 Potential for commercialisation

While the current prototype system cannot be directly commercialised due to the slight system imbalance at high fan speeds and the limited image complexity, the fan can be improved in the following ways to make it more commercially viable. Such as by expanding on the standalone user mobile application developed in section 6.3.

The slip ring can be improved by using a better way to fix the rotating subassembly to the motor shaft, compared to a grub screw, which has the risk of potentially sliding off after long-term/repeated use. Alternatively, a wireless transmitter and receiver could be built instead of using an off-the-shelf solution. The system balance can also be improved since the system started to become unstable at fan speeds near 1 000 rpm. The 5 V, 5 A voltage regulator designed in section 5.12 can also be redesigned or replaced with an off-the-shelf component with a higher continuous power output, which will allow more of the LEDs to be powered at once or at a higher brightness level.

Appendix B. Gantt chart

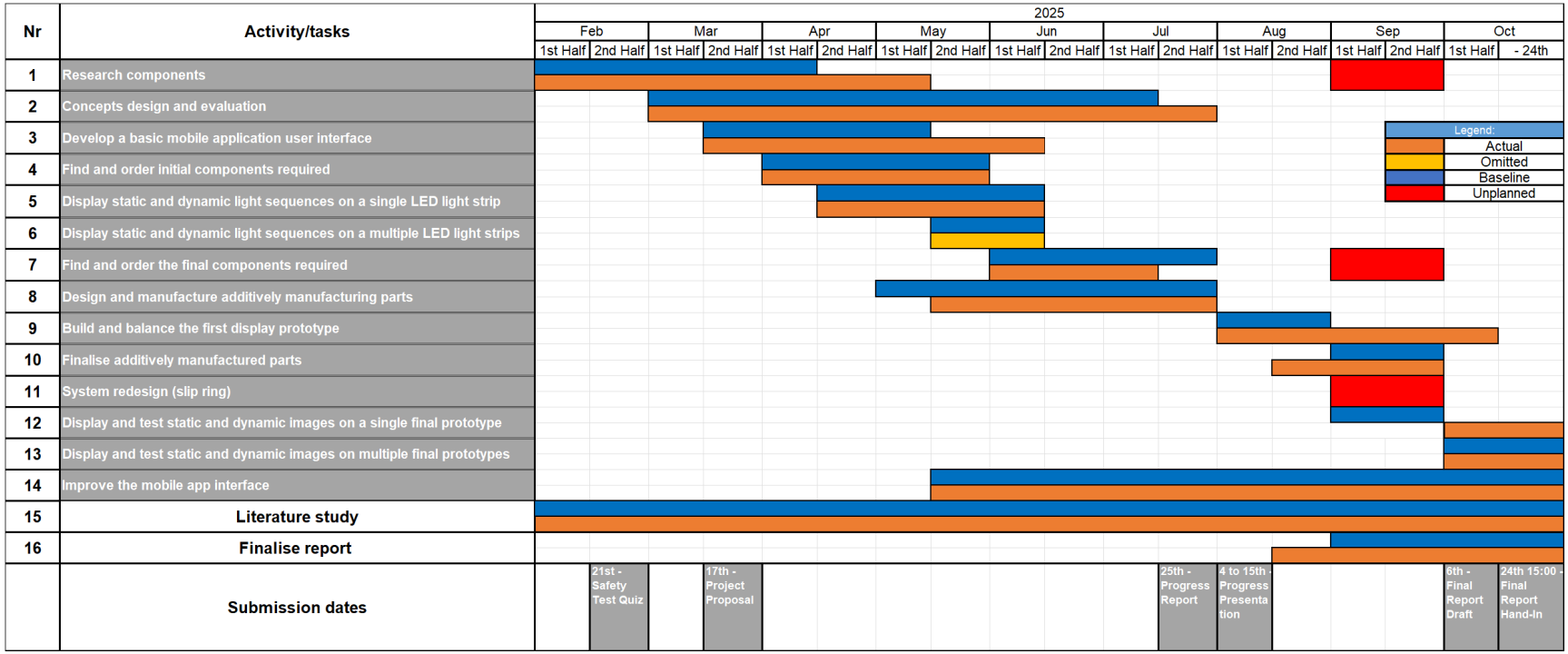

Figure 32: Project Gantt chart

Appendix C. Risk analysis and safety procedures

The order of steps that were taken when operating/testing the fan:

1. The fan will be assembled without the fan blades attached and connected to the laboratory DC power supply set to 12 V and current limited to 3 A.

2. A box will be put around the fan with a small opening to look through at the front of the fan.

3. Safety glasses will be put on before starting the fan and enabling output from the DC power supply.

4. Before starting the fan for the first time, either Mr Kevin Neaves or Mr C. Zietsman will need to be present to ensure that the fan is safe and stable enough to start.

5. The fan will be started slowly at low speeds at first (100 rpm approximately) by using a potentiometer, without any fan blades attached.

6. After it has been confirmed that the fan operates safely without any major vibrations or safety concerns, the speed will be slowly increased up to the target 1 440 rpm.

7. Once it has been confirmed that the fan can operate safely at this condition, the fan will be stopped, and the blades will be attached/screwed on as well.

8. Steps 3 to 5 will be repeated with the fan blades attached to confirm that the fan blades do not add risk or instability to the fan when it's operating.

9. Afterwards, the LEDs and other electrical components will be added to the spinning fan blade assembly, and steps 3 to 5 will again be repeated.

10. Thereafter, the different images/scenes displayed by the fan will be recorded/monitored.

11. Once all testing has been completed and the fan has stopped completely, it will be disassembled safely, ensuring all electrical connections and power sources are entirely disconnected.

(a) Flying debris

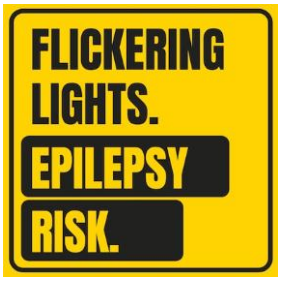

(b) Spinning fan blades

(c) Flashing lights

(d) Soldering

Figure 33: Applicable warning symbols

Table 8: Activity-based risk assessment

Activity	Risk	Risk Type* (P/E)	Mitigating Steps	Classification of Risk Severity
Assembling the fan (soldering)	Burns	P/E	Care was taken to only solder at open and clean work benches, with no other laboratory equipment nearby. Turning off the power to the soldering iron after use to prevent accidental burns.	Very unlikely, with a risk of minor burns or damage to laboratory equipment.
	Smoke inhalation	P	Solder in a well-ventilated area.	Likely, with minor risk when working in well-ventilated areas.

Activity	Risk	Risk Type* (P/E)	Mitigating Steps	Classification of Risk Severity
Starting the fan blade	Fan blades might fly or break off	P/E	The fan will be started slowly and monitored at low speeds for any safety concerns. Safety glasses will be worn, and a box and screens will be set up around the fan until it is proven to be sufficiently safe by either of the two laboratory managers. Nearby laboratory users will be warned before starting the fan. All people nearby will be warned about the dangers/risks and be asked to move away if possible.	Unusual but quite possible, risk is minor first aid.
Turning on and off the DC power supply	Electric shock	P/E	Check all connections thoroughly before enabling the DC power supply.	Very unlikely, only four connections need to be checked, which can be done using a conventional multi-meter continuity test. Severity is moderate.
Monitoring the images/scenes displayed by the fan	Fan blades might fly or break off	P/E	The fan will be started slowly and monitored at low speeds for any safety concerns. Safety glasses will be worn, and protective screens will be set up.	Unusual but quite possible, risk is minor first aid.
Data management	Loss of data	P	Save any software files to a git repository.	Very unlikely, and the severity is low.

*P – personal, E – equipment

Appendix D. Responsible use of resources and end-of-life strategy

This appendix outlines how the resources used during the project were obtained, with an end-of-life strategies on how the components can be disposed safely by the respective services as follows. For E-waste and non-ferrous metals Reproc Metals (2024) in Cape Town can be used. For composting Gordon's Bay Drop-off (2025) can be used and for other general, non-hazardous waste, the Stellenbosch landfill can be used. The end-of-life strategies follow a sustainable approach where reusability is prioritised the most, followed by recycling and lastly safe disposal. Priority was given to components that could be bought from the same local supplier, to help minimise transport costs and emissions.

Table 9: Responsible use of resources and end-of-life strategy

Category	Obtaining the resources	End-of-life strategies
Electronic components	All electronic components used were acquired from local suppliers or the laboratory, if/when available, to minimise the transport cost and emissions compared to using suppliers from overseas.	All electronic components, such as the DC motors, DC speed controller, microcontrollers, switches, barrel jack, power supply, DotStars LEDs and Hall-effect sensors, can be reused in future projects after disassembling the project. The other electrical components (resistors, capacitors and voltage regulators) can be disposed of safely through e-waste services or desoldered to reuse in other projects. One of the two damaged wireless power transmitters must be disposed of safely using e-waste services, while the other, undamaged transmitter can still be reused in future projects. All electrical wires can be disposed of safely or stored in a drawer in the Mechatronics laboratory for use in any future projects or given to Reproc Metals (2024).
Magnets	The magnets were bought	Since the design allowed magnets to be mounted to the respective housings

	from a local supplier, Communica South Africa	without the need for adhesives, the magnets are fully reusable and can be reused in future projects. Otherwise, the magnets will need to be disposed of in separate bins before being sent to landfills.
Fasteners	All fasteners were obtained from local suppliers	All of the fasteners can be removed with a screwdriver and reused in future projects or sent to non-ferrous recycling services.
Tripod	The tripod stand was acquired from Takealot	The tripod can be reused by future projects as needed, including the Bluetooth remote which came with the stand, since the tripod stand has little to no wear. Otherwise, it can be disposed of safely in a landfill.
Additively manufactured parts	All parts were 3D printed using PLA, except for the final rotating subassembly housing and fan blades which were made using PETG	All 3D printed PLA parts are considered bio-plastics with a recycle fraction percentage of 33% according to Appendix B8 in Ashby (2023:509). However, in South Africa these materials are usually disposed of at a composting facility's. Since PETG is not widely recyclable in South Africa, it will need to be sent to a landfill, if it cannot be granulated or accepted by Trade Avail 346 cc according to Plastics SA (2016).
Slip rings	The copper plates were laser cut from a 2 mm copper sheet, and the carbon brushes were acquired from a local supplier, BUCO Hardware and Buildware (2025)	The copper plates can be reused or disposed of safely at non-ferrous recycling centres. Otherwise, other projects can also reuse the carbon brushes if the wires are cut from the 5 V, 5 A voltage regulator circuit. However, since the carbon brushes have a limited lifespan, they will eventually need to be disposed of safely once they have completely worn out. This can be done in a landfill if they are partially worn out, or by recycling the copper wires if they are completely worn out, by giving them to non-ferrous recycling centres.

Appendix E. Performance requirements

The following describes how the values for the targets and/or ranges in Table 3 were determined.

- PR5 Total system cost, including all fan displays and components: Values based on the allocated running cost of R5 000 for the project (given in the Appendix A.1), where the total system cost may not exceed this amount.
- PR6 Display refresh rate: Values determined from the literature review in section 2.3, where 5 Hz is the minimum required refresh rate to achieve the POV effect, with 24 Hz or higher resulting in smooth images (Adobe, 2025).
- PR9 Number of fan displays onto which static/dynamic scenes can be displayed: To prove that multiple fan displays can interact with each other, at least two fan displays will be required.
- PR10 Number of additively manufactured parts: Since multiple additively manufactured parts are required according to the functional and stakeholder requirements, at least 2 parts will be made using additively manufactured processes.
- PR13 Number of interconnected subsystems: To allow easier transportation of the system and to comply with the functional requirement of using modular components, at least two interfacing subsystems will need to be used. The target value of three is based on existing designs, like the L1 holographic fan from LUMINA (2025a), where the base/stand, blades and motor/power housing are often assembled using these three parts and sold separately (section 2.1).
- PR14 Total weight per fan display: The target system weight of a single fan display, including the stand, is 2 kg or 3.89 lb, which is slightly more than the combined weight of the LUMINA L1 fan and tripod stand according to their technical specifications (LUMINA, 2025a, 2025d). This requirement is set to ensure that the system can be classified as portable if this weight target is achieved.
- PR16 System noise above the residual noise level: According to the definition for disturbing noises as set by the Province of the Western Cape (2013:2), the system may not exceed the residual noise threshold by more than 7 dB. The residual noise is specified as 25 dB, which is the lowest maximum equivalent continuous noise rating level as set in Table 1, Column 2, of the SANS 10103 (2008) standard for indoor occupancies. The target value of 3 dB was selected since

this is the average sound increase required to become noticeable to the human ear, independent of hearing ability (McShefferty, Whitmer & Akeroyd, 2015).

- PR17 Maximum fan noise level: The target value of 60 dB was set based on the maximum acceptable noise level of all the LUMINA 3D holographic fans, including the L1 fan from LUMINA (LUMINA, 2025a).
- PR18 Minimum lifetime of any individual part used: Target based on the warranty from LUMINA for the L1 holographic fans (LUMINA, 2025a).DotStars initial testing

Appendix F. DotStars Testing

The DotStars LED strip was connected to the Firebeetle ESP32-S3 microcontroller's SPI interface, running an Arduino control script. Testing scripts, data, and videos are available in the "Dotstars Testing" git repository with README.md files for static (test 6) and dynamic (test 4) tests (Botes, 2025a).

Both components were powered by a laboratory DC supply (Gwinstek GPS-3303), with current measurements taken from its display. The microcontroller drew approximately 0.03 A, included in all results. A single strip was used for efficiency, with testing data in Table 10. For example, test 6 set the first 30 LEDs to blue at 50% brightness, followed by 30 more at the same settings.

Theoretical current estimates were calculated beforehand to avoid exceeding the supply's 3 A limit. Each LED was estimated at 60 mA at full white brightness (Burgess, 2024:20). A conservative 1 mA per off LED was included based on prior tests to prevent overload of the DC power supply (Foss, 2018). From the datasheet, each LED is made up of 3 sub-LEDs (red, green and blue), each sub-LED's power consumption was estimated to be 20 mA at full brightness (iPixel LED, 2018). Mixed colours like purple were estimated at 40 mA using the additive colour model (Cloud, 2023).

For the dynamic tests, which involved cycling colours, only the number of white LEDs was used in the theoretical calculations. Static test measurements closely matched estimates (within ±0.088 mA) except for the 3rd static test conducted, where the theoretical approximation was much higher than the actual measured value. The difference indicates that the 60 mA assumption is more conservative for LEDs at 100% brightness compared to lower LED brightness. For the dynamic tests, all of the measured currents were higher than the expected theoretical calculations. This might be due to the microcontroller requiring more power due to the LEDs needing to be updated continuously instead of only once (as done in the static tests). The rapid switching of the LEDs on and off might also indicate that the LEDs form constant current spikes, which can result in slightly higher current readings compared to the static tests, which allowed the current spikes to settle once the LEDs have been set.

The tests conducted helped support the decision to only turn the LEDs on at 50% brightness, as they remained clearly visible under laboratory lighting while consuming half the current. The reduced brightness also helped keep the LEDs cooler, especially when compared to LEDs set to display 100% white in static tests, where the LEDs would become warm to the touch. The tests also concluded that a logic shifter would not be required, since all of the LEDs could be reliably controlled without any artefacts at 3.3 V levels, which the microcontroller outputs.

Table 10: DotStars static test data

	First LEDs			Subsequent LEDs			Calculations	
Test nr	**Number of LEDs**	**Brightness**	**Colour**	**Number of LEDs**	**Brightness**	**Colour**	**Theoretical [A]**	**Measured [A]**
1	36	50%	White	-	-	-	1.116	1.09
2	72	50%	White	-	-	-	2.16	1.96
3	30	50%	White	31	100%	White	2.771	2.39
4	30	50%	Green	30	100%	Green	0.912	0.99
5	30	50%	Red	30	100%	Red	0.912	1
6	30	50%	Blue	30	100%	Blue	0.912	0.97
7	30	50%	Purple	30	100%	Purple	1.812	1.72

Table 11: DotStars dynamic test data

Test nr	Trail length [Number]	Brightness	Colour order	Speed [ms]	Theoretical [A]	Measured [A]
1	10	100%	Green, Red, Blue	50	0.262	0.29
2	5	50%	White only	50	0.217	0.24
3	10	50%	White, Purple, Blue, Green, Yellow	50	0.362	0.37
4	36	50%	White, Purple, Blue, Green, Yellow	50	1.116	1.13
5	36	50%	White only	50	1.116	1.14
6	36	50%	White only	1	1.116	1.14

Appendix G. DC settling time and inertia calculations

To determine the settling time of the DC motor, the inertia of the rotating subassembly needed to be determined first. Since the true mass moment of inertia cannot be determined until the physical system is fully built and weighed, a conservative estimate was made as follows, using the dimensionally accurate CAD model (shown in Figure 15 in section 5.4) of the wireless rotating subassembly. Since the housing will be made of CR-PLA and the fan blades will be made of CR-PETG (reasons given in section 5.14, the densities of both materials (ρ_{PLA} and ρ_{PETG}) were assumed to be 1.24 g/cm3 and 1.23 g/cm3 based on data from the Wootware (2025) and Simplify3D (2025). From this, the model was simplified since a conservative estimate was made using the measuring tool in Inventor Professional 2025 on the CAD model. The central housing (drawn in blue in Figure 34) was assumed to be a solid cylinder (by neglecting the ball socket joints, which were considered to be part of the fan blade) with a diameter and height of 40 mm ($d_{Housing}$) and 38 mm ($H_{Housing}$), respectively. The fan blades were also assumed to be a solid cylinder with a diameter of 16.8 mm (d_{Blade}) and a length of 85 mm (H_{Blade}) (drawn in red in Figure 34). The centroids of the central housing and fan blades, which are given in the top view, are drawn in pink and marked with "G" in Figure 34, where "G" was assumed to be in the centre of the rigid body. The arrows given in Figure 34, indicates the axis about which the inertia was determined.

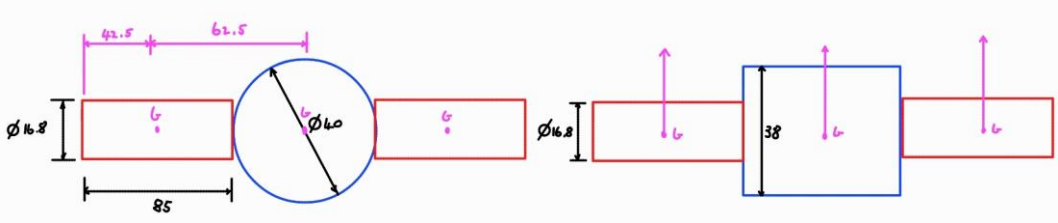

Figure 34: Hand drawn rotating subassembly top view (left), side view (right)

From these dimensions the volume of both the rotating subassembly housing and fan blades could be determined as 4.76 m^3 ($V_{Housing}$) and 1.88 m^3 (V_{Blade}) respectively. Using these volumes and multiplying them by their respective densities the mass of both the rotating subassembly housing and fan blade could be determined as 59.2 g ($m_{Housing}$) and 23.2 g (m_{Blade}) respectively. Using mass moment of inertia formula for a the axis through the centre of a solid cylinder, the mass moment of inertias for the rotating subassembly housing ($I_{Housing}$) and fan blades (I_{Blades}) were determined as 1.18 kgm^2 and 1.44 kgm^2,

respectively (Hibbeler, 2017). Then using the parallel axis theorem the inertia at the motor axis could be determined as 6.77 kgm^2 (Hibbeler, 2017).

From the information available on the HKD 795 motor from Communica, the rated power of the DC motor could be determined based on the rated voltage and current of the DC motor of 12 V and 2.05 A[24], respectively (Communica South Africa, 2025c). Using these values, the rated power (P_{Rated}) of the DC motor could be determined as 24.6 W, at its rated 12 V speed of 10 000 rpm (ω_{Rated}) (Chapman, 2012). Using the rated power and speed, the torque of the motor could be determined by dividing the rated power by its rated speed, which gave 0.235 Nm of torque (T) for the motor. With the target steady state speed of the motor set to 1 440 rpm based on the performance requirements set in Table 3, the time required for the fan to each its steady state speed was determined to be 0.43 s using the equation from Priya et al. (2020), which is less than the 14 s Priya et al. (2020) deemed acceptable. The calculations created using the free version of SMath Studio (version 1.1, build 8763) for all of the above values mentioned are shown below in Figure 35.

[24] Value of 2.05 A taken instead of the 3.34 A value rating used in section 0, since these calculations were conducted before the DC motor could be tested practically.

$\rho_{PLA} := 1.24 \frac{g}{cm^3}$ Density of CR-PLA

$\rho_{PETG} := 1.23 \frac{g}{cm^3}$ Density of CR-PETG

$d_{Housing} := 40\ mm$ Diameter of rotating subassembly housing

$H_{Housing} := 38\ mm$ Height of rotating subassembly housing

$d_{Blade} := 16.8\ mm$ Average diameter of fan blade ([6.1mm+27.5mm]/2)

$H_{Blade} := 85\ mm$ Length of fan blade

$P_{Rated} := 12\ V \cdot 2.05\ A = 24.6\ W$ Rated power of the HKD 795 DC motor (based listed on rated voltage and load amps from Communica)

$\omega_{Rated} := 10000\ rpm = 1047.1976 \frac{rad}{s}$ Rated rpm of the HKD 795 DC motor (based listed on rated voltage and load amps from Communica)

$T := \frac{P_{Rated}}{\omega_{Rated}} = 0.0235\ N\ m$ Rated torque of the HKD 795 DC motor

$v := 1440\ rpm = 48 \cdot \pi \frac{rad}{s}$ Target rpm of the fan required for 24 fps images

$V_{Housing} := \pi \cdot \left(\frac{d_{Housing}}{2}\right)^2 \cdot H_{Housing} = 4.775 \cdot 10^{-5}\ m^3$ (Volume of a cylinder)

$V_{Blade} := \pi \cdot \left(\frac{d_{Blade}}{2}\right)^2 \cdot H_{Blade} = 1.884 \cdot 10^{-5}\ m^3$ (Volume of a cylinder)

$m_{Housing} := V_{Housing} \cdot \rho_{PLA} = 0.0592\ kg$

$m_{Blade} := V_{Blade} \cdot \rho_{PETG} = 0.0232\ kg$

$I_{Housing} := 0.5 \cdot m_{Housing} \cdot \left(\frac{d_{Housing}}{2}\right)^2 = 1.1843 \cdot 10^{-5}\ kg\ m^2$ (Hibbeler, 2017, p. 793)

$I_{Blade} := \frac{1}{12} \cdot m_{Blade} \cdot \left(3 \cdot \left(\frac{d_{Blade}}{2}\right)^2 + H_{Blade}^2\right) = 1.4363 \cdot 10^{-5}\ kg\ m^2$ (Hibbeler, 2017, p. 793)

$I_{Total} := I_{Housing} + 2 \cdot \left(I_{Blade} + m_{Blade} \cdot \left(\frac{d_{Blade}}{4} + \frac{d_{Housing}}{2}\right)^2\right) = 6.7713 \cdot 10^{-5}\ kg\ m^2$

$t := \frac{I_{Total} \cdot v}{T} = 0.4347\ s$ Time to reach target rpm (Priya et al., 2023, p. 6)

Figure 35: Smath calculations for DC motor inertia and settling time

Appendix H. Low-pass filter simulation and testing

Before building the low-pass filter circuit, it was first simulated using NGSpice (version 34) using a resistor and capacitor value of 680 Ω and 1 µF, from which the following graphs in Figure 36 could be generated, to show how an analogue voltage could be generated based on a 3.3 V, 8 kHz PWM signal over a range of duty cycles. Some examples output figures are given for PWM duty cycles of 100% and 30%. The figures show the input PWM voltage [$v(in)$] in green and output analogue voltage [$v(out)$] in red for the duty cycles over time in milliseconds.

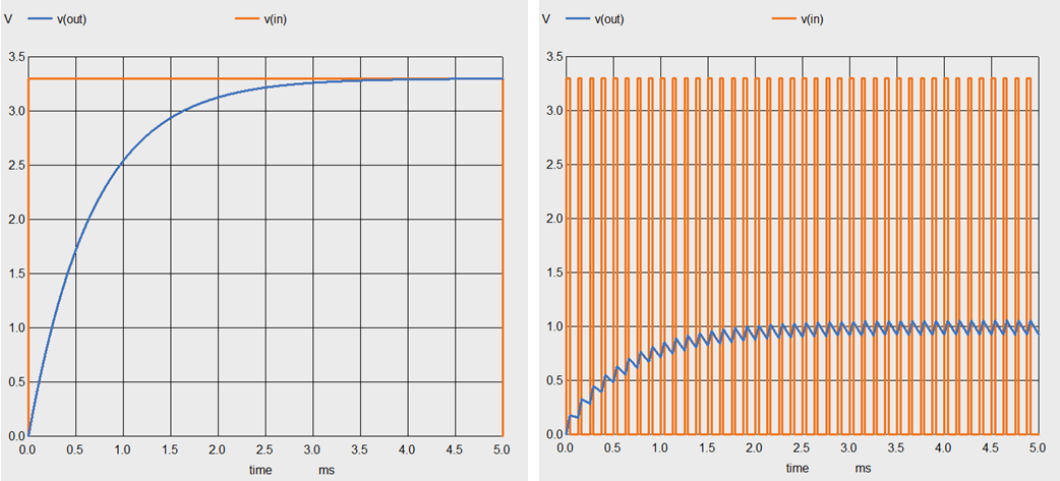

Figure 36: Low-pass filter simulations, 100% duty cycle (left), 30% duty cycle (right)

By using a RIGOL DG1022 signal generator from the laboratory, a 3.3 V, 8 kHz PWM could be simulated and used as an input to test the practical low-pass filter circuit. The order in which the practical tests were conducted (shown in Table 12), where random duty cycles were chosen between 20% and 80% duty cycles, limited by the signal generator model. To measure the results, a Tektroniks TDS 2001C oscilloscope and P6000 1X & 10X oscilloscope probes were used to measure both the PWM input signal from the signal generator and output analogue signals with both channels 1 and 2 configured to DC coupling with the probe voltage set to 10X. To capture the rise times, a manual ("normal" mode) trigger was set up and configured to use rising edge detection. After two subsequent peaks of the analogue signal had identical maximum and minimum values, the midpoint of the first peak was taken as the timestamp at which the analogue signal settles (t_2). From this, the settling time could be determined as the difference between the start of the PWM signal (t_1) and t_2 by using the

cursor function as shown in Figure 37 for a duty cycle of 80% where a settling time of 3.16 ms was determined. Graphs showing the general trend and comparison between the simulated and measured values are given in Figure 38 and Figure 39, respectively. From the trendline in the graphs, the circuit exhibits a stable average approximate -0.02 V output error with a settling time error averaging between -0.6 ms and 0.7 ms. This helped verify the low-pass circuits accuracy, which shows precise analogue voltage outputs can be achieved through a cost-effective low-pass filter circuit.

Table 12: Low-pass filter testing results

Duty Cycle	Theoretical output [V]	Measured Output [V]	Simulated settling time [ms]	Measured settling time [ms]	Output error [V]	Settling time difference [ms]
80%	2.64	2.56	2.61	3.16	-0.08	0.55
60%	1.98	1.96	2.78	2.66	-0.02	-0.12
20%	0.66	0.56	1.8	1.66	-0.1	-0.14
28%	0.924	0.92	2.2	1.92	-0.004	-0.28
34%	1.122	1.16	2.3	2.12	0.038	-0.18
50%	1.65	1.64	2.5	2.14	-0.01	-0.36
65%	2.145	2.12	2.8	2.5	-0.025	-0.3
35%	1.155	1.16	2.3	2.12	0.005	-0.18
25%	0.825	0.8	2	1.76	-0.025	-0.24
28%	0.924	0.92	2.2	1.76	-0.004	-0.44
73%	2.409	2.4	2.9	2.9	-0.009	0
80%	2.64	2.6	2.61	2.66	-0.04	0.05
20%	0.66	0.64	1.8	1.1	-0.02	-0.7
55%	1.815	1.8	2.6	2.5	-0.015	-0.1

Figure 37: Measurement of settling time difference at 80% duty cycle

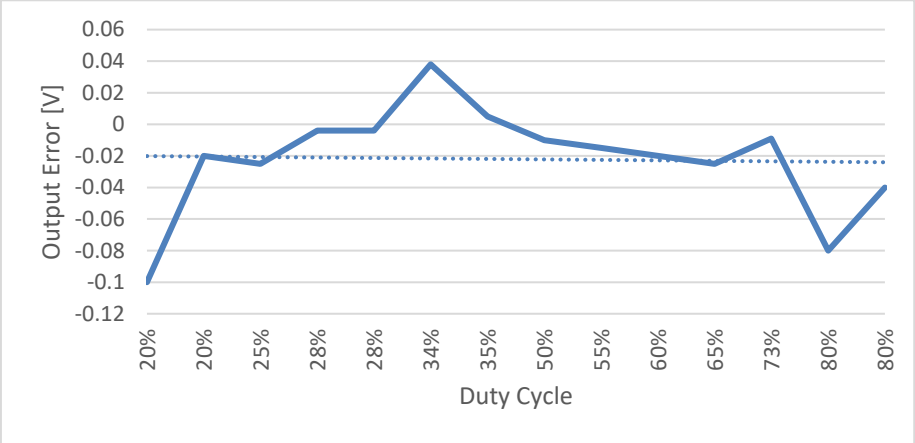

Figure 38: Voltage output error of the low-pass filter circuit

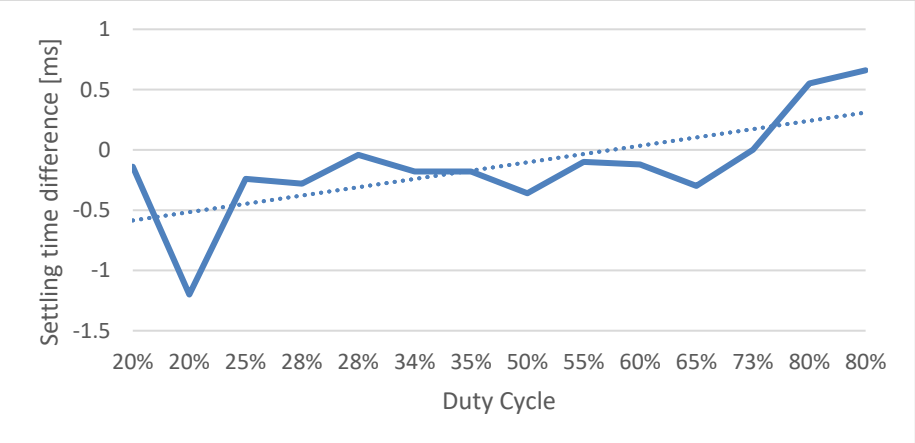

Figure 39: Settling time difference of low-pass filter circuit

Appendix I. Fan blade strength calculations

Below are the calculations performed using the free version of Smath version 1.1 (build 8763), shown in Figure 41. The yield strength of PETG was assumed to be 39 MPa based on the lowest yield strength value from section 5.14. The mass *m* of the fan blade was assumed to be 15.51 g based on data from the Creality Print 6.1 slicer software for the model without added supports, shown in Figure 40. An additional 3 g was included in the mass calculation to account for the a third of the DotStars LEDs, which the fan blade will need to support.

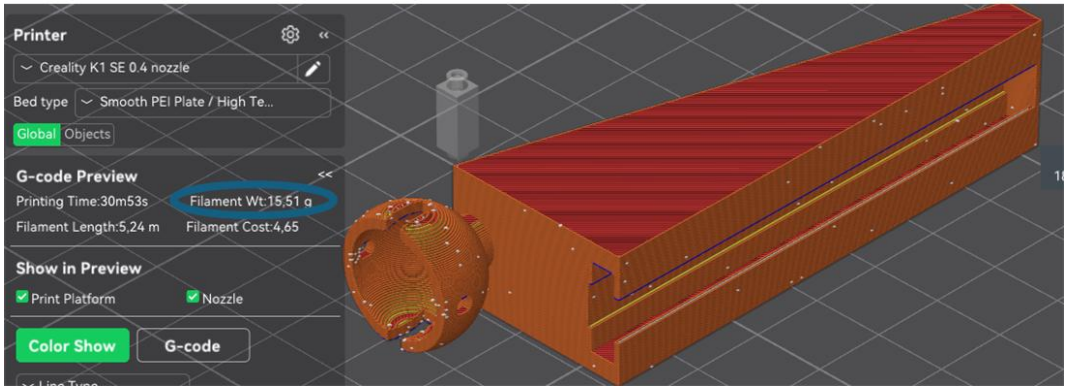

Figure 40: Weight of individual fan blade

The radius *r* was taken as 85 mm, which is the full length of the fan blade and with the centre of mass of the fan blade at the furthest edge to allow a conservative approach. Thereafter, the angular velocities of the fan blades were calculated for both low and high rpms of 320 and 1 440 rpm, respectively. The thickness of the ball-socket *h* was measured from the top of the fastener hole to the bottom as 1.5 mm (Figure 41). The length *L*, measured from the outer edge of the ball socket to the fastener hole, was 1.95 mm according to the fan blade CAD model as well, with a through-hole diameter (w_{Hole}) of 2.2 mm for the fastener. Using the respective angular velocities ($\omega_{Low/High}$) and mass *m* of the fan blade, the centrifugal force experienced by the fan blade F_c could be calculated (Hibbeler, 2017:672). By assuming the force F_c will be equally distributed at both contact points on the fastener, the reaction forces F_R could be calculated as half of F_c. From this, a thin wall section at one of the contact points was modelled as a cantilever beam with a width of w_{Hole}. By assuming a point load F_R acting at the centre of the cantilever beam, the reaction forces M_R and shear forces could be determined. By calculating inertia I and area A over which these reaction forces act with a width of *L* and height of *h*, the normal ($\sigma_{Low/High}$) and shear stresses ($\tau_{Low/High}$) could be calculated. Using these normal and shear stresses, the principal stresses ($\sigma`_{Low/High}$) were determined

as 1.25 MPa and 25.30 MPa for both low and high rpms, respectively. Using these values, the safety factors of 31.2 and 1.54 for both rpms were obtained by dividing the yield strength of PETG by the calculated principal stresses (Budynas, Nisbett & Shigley, 2020).

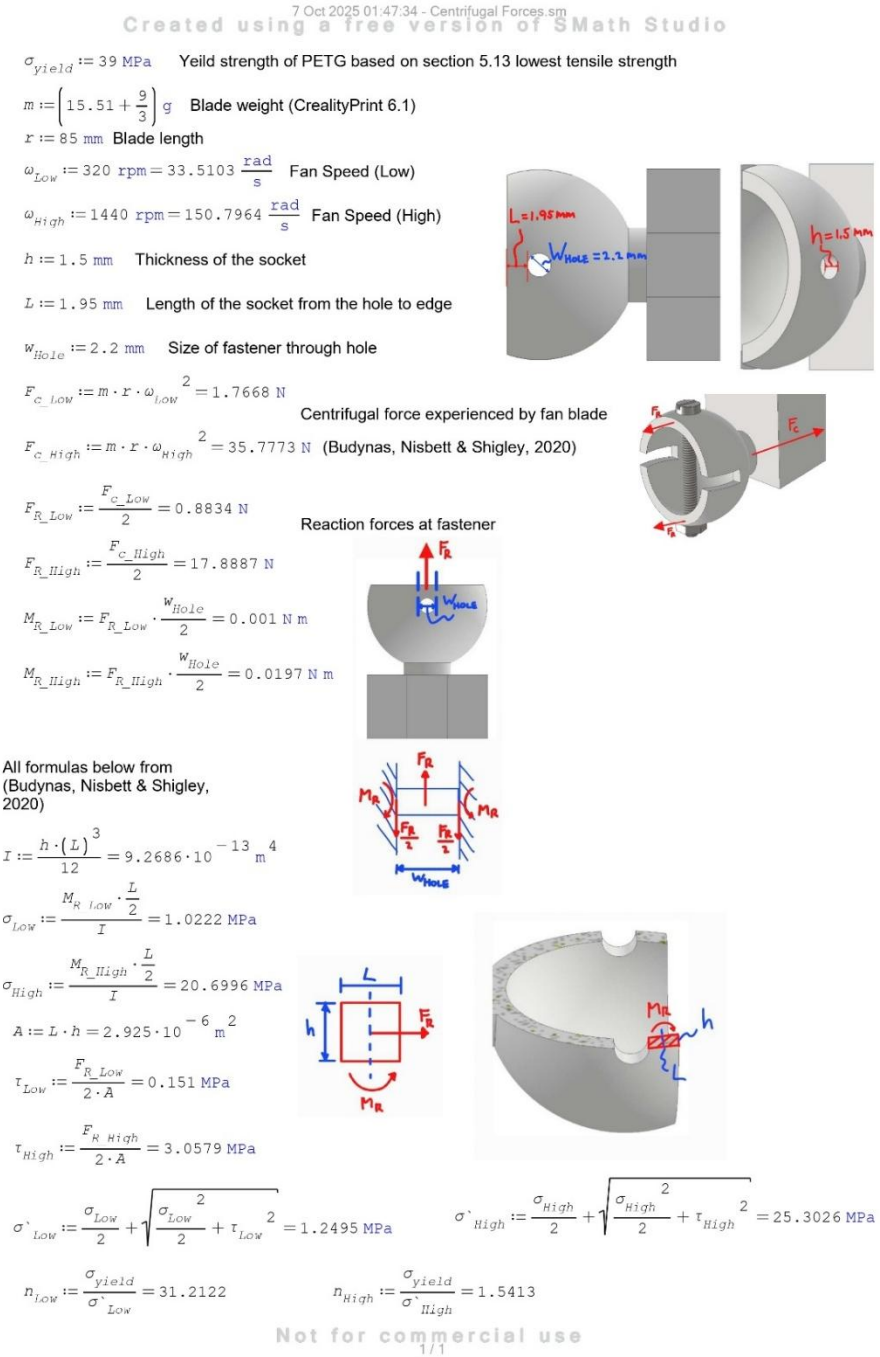

Figure 41: Fan blade centrifugal force calculations

References

3D HoloSPiN (2025) *3D HoloSPiN PRODUCT RANGE 3D Hologram fans are available for hire, rental, and purchase in South Africa*. [Online] Available: https://3dholospin.com/3d-led-hologram-fanproduct-range-available-in-south-africa-for-purchase-or-hire [31 July 2025].

Adobe (2025) 'Persistence of Vision (POV) Guide.' [Online] Available: https://www.adobe.com/uk/creativecloud/animation/discover/persistence-of-vision.html.

Ali, A.Z.M. & Ramlie, M.K. (2021) 'Examining the user experience of learning with a hologram tutor in the form of a 3D cartoon character'. Available: https://doi.org/10.1007.

Amador, A.M.G., Avendano, R.A.V., González, A.Q. & Fernández, L.P. (2025) 'Mechanical characterization and testing of multi-polymer combinations in 3D printing Mechanical characterization and testing of multi-polymer combinations in 3D printing', *Heliyon*,11(3):e42420-.

Ashby, M.F. (2023) *Materials and sustainable development*. Second edition. Oxford: Elsevier.

Barnes, A. (2024a) *How to Build a 3D Holographic LED Fan in 5 Easy Steps*. [Online] Available: https://luminafans.com/blogs/hologram-blog/how-to-make-3d-holographic-led-fan.

Barnes, A. (2024b) *How to Use a 3D Hologram Fan: 5 Steps That Guarantee Results*. [Online] Available: https://luminafans.com/blogs/hologram-blog/how-to-use-a-3d-hologram-fan?srsltid=AfmBOor5IwePhQWdLhE-WAxADjG5_GeF7J1Q2lsZkjaZOp4uYbwUjPeC.

Botes, S.P. (2025a) 'LxttleSplat42U/DotStars_Testing'. [Online] Available: https://github.com/LxttleSplat42U/DotStars_Testing [4 October 2025].

Botes, S.P. (2025b) 'LxttleSplat42U/Fan_Blade'. [Online] Available: https://github.com/LxttleSplat42U/Fan_Blade [7 October 2025].

Botes, S.P. (2025c) 'LxttleSplat42U/holo3d'. [Online] Available: https://github.com/LxttleSplat42U/holo3d [7 October 2025].

Botes, S.P. (2025d) 'LxttleSplat42U/Holo3D_Base'. [Online] Available: https://github.com/LxttleSplat42U/Holo3D_Base [7 October 2025].

Botes, S.P. (2025e) 'LxttleSplat42U/Holo3D_Base_Client'. [Online] Available: https://github.com/LxttleSplat42U/Holo3D_Base_Client [7 October 2025].

BUCO Hardware & Buildware (2025) *Carbon Brush Set Ryobi HG-650*. [Online] Available: https://www.buco.co.za/carbon-brush-set-ryobi-hg-650-1328668 [5 October 2025].

Budynas, R.G., Nisbett, J.K. & Shigley, J.E. (2020) *Shigley's mechanical engineering design*. Eleventh edition. New York, NY: McGraw-Hill Education.

Burgess, P. (2024) 'Adafruit DotStar LEDs'. [Online] Available: https://cdn-learn.adafruit.com/downloads/pdf/adafruit-dotstar-leds.pdf.

Chacón, J.M., Caminero, M.A., García-Plaza, E. & Núñez, P.J. (2017) 'Additive manufacturing of PLA structures using fused deposition modelling: Effect of process parameters on mechanical

properties and their optimal selection', *Materials & Design*,124. Available: https://doi.org/10.1016/j.matdes.2017.03.065.

Chapman, S.J. (2012) *Electric machinery fundamentals*. 5th ed. New York: McGraw-Hill.

Chen, J. & Huang, S. (2023) 'Analysis and Comparison of UART, SPI and I2C', in *2023 IEEE 2nd International Conference on Electrical Engineering, Big Data and Algorithms (EEBDA)*. *2023 IEEE 2nd International Conference on Electrical Engineering, Big Data and Algorithms (EEBDA)*,:272–276. Available: https://doi.org/10.1109/EEBDA56825.2023.10090677.

City of Cape Town (2025) *Gordon's Bay Drop-off*. [Online] Available: https://www.capetown.gov.za/Explore%20and%20enjoy/See-all-city-facilities/our-service-facilities/Drop-off%20facilities/gordons-bay-drop-off#section-docs [22 October 2025].

Cloud, N.L. (2023) 'What is RGB: Understanding the RGB Color Model and the Fundamentals of LED Color Reproduction', *NSELED*,28 November. [Online] Available: https://nseledcloud.com/what-is-rgb/ [4 October 2025].

Communica Online (2025) *Switch Mode Power Supply Unit [PSU SWMMC 5V 5A]*. [Online] Available: http://archive.communica.co.za/Catalog/Details/P0337376514?gad_source=1&gad_campaignid=22552818411&gbraid=0AAAADLTnIZKtt0NmoWtI7-5G_OReU9Cf&gclid=EAIaIQobChMI0vLp3uaMkAMVvYBQBh1zHRfZEAQYAyABEgLul_D_BwE [5 October 2025].

Communica South Africa (2025a) *BDD 2212 920KV B/LESS MOTOR CW*, *Communica South Africa*. [Online] Available: https://www.communica.co.za/products/bdd-2212-920kv-b-less-motor-cw [20 October 2025].

Communica South Africa (2025b) *BDD PWM DC MOTOR CONTR 10A 6-90V*, *Communica South Africa*. [Online] Available: https://www.communica.co.za/products/bdd-pwm-dc-motor-contr-10a-6-90v [5 October 2025].

Communica South Africa (2025c) *HKD 795 MOTOR 12-24V HI SPD/TORQ*, *Communica South Africa*. [Online] Available: https://www.communica.co.za/products/hkd-795-motor-12-24v-hi-spd-torq [17 September 2025].

Creality (2025) *HALOT-SKY 3D Printer*, *creality-ae*. [Online] Available: https://www.creality.com/ae/products/halot-sky-3d-printer [21 October 2025].

Dejan (2015) 'What is Schmitt Trigger | How It Works', *How To Mechatronics*,24 August. [Online] Available: https://howtomechatronics.com/how-it-works/electrical-engineering/schmitt-trigger/ [23 October 2025].

DIYElectronics (2025a) *FireBeetle 2 ESP32-C6 IoT Microcontroller | WiFi/BLE*, *DIYElectronics*. [Online] Available: https://www.diyelectronics.co.za/store/iot/5497-firebeetle-2-esp32-c6-iot-microcontroller-with-wifi-ble-zigbee.html [17 September 2025].

DIYElectronics (2025b) *Hall Effect Magnetic Sensor Module - Analog*, *DIYElectronics*. [Online] Available: https://www.diyelectronics.co.za/store/other/1508-hall-effect-magnetic-sensor-module-analog.html [6 October 2025].

DIYElectronics (2025c) *LM2587 DC-DC Boost 3A 30V V2 | Voltage Boost Converter*, *DIYElectronics*. [Online] Available: https://www.diyelectronics.co.za/store/switch-mode-modules/2511-dc-dc-boost-3a-30v-lm2587-v2.html [22 October 2025].

DIYElectronics (2025d) *Magnetic Hall Effect Sensor Module | Magnetic Sensor*. [Online] Available: https://www.diyelectronics.co.za/store/other/1509-hall-effect-magnetic-sensor-module-digital.html?srsltid=AfmBOopfT0yVbg3eVRz2LwBGN0OVRFpM2pREdqFZlipdqqVlFPrWMoQB [6 October 2025].

DIYElectronics (2025e) *Wireless Charging Module | 5V 2A - DIY Electronics*, *DIYElectronics*. [Online] Available: https://www.diyelectronics.co.za/store/battery-chargers/745-wireless-charging-module-5v-2a.html?utm_campaign=google_shopping&utm_source=cpc&utm_medium=evergreen&utm_content=20485427402&gad_source=1&gad_campaignid=20489613595&gbraid=0AAAADpm0l9W6BEFCn-mJiVfMpynk8dZP&gclid=EAIaIQobChMIouHZ1PvtjQMVqaRQBh0WNS0UEAQYAiABEgIQw_D_BwE [10 June 2025].

Dorsey, G. & Daun, C. (2018) *Data Reliability with Slip Rings in Construction Equipment*. White Paper MS3316L, rev. 1. Moog Inc. [Online] Available: https://www.moog.com/content/dam/moog/literature/MCG/Data%20Reliability%20with%20Slip%20Rings%20in%20Construction%20Equipment_WhitePaper.pdf [25 October 2025].

Espressif Systems (2023) *ESP32-C6 Series Datasheet*. Datasheet Version 1.0. 5 Espressif Systems (Shanghai) Co., Ltd,:72. [Online] Available: https://dfimg.dfrobot.com/5d57611a3416442fa39bffca/wiki/5eeffd974782b6cc442f7a2ee7f00577.pdf.

Espressif Systems (2025a) *ESP32-S3-WROOM-1 ESP32-S3-WROOM-1U Datasheet*. Datasheet Version 1.6. 5 Espressif Systems (Shanghai) Co., Ltd,:54. [Online] Available: https://www.espressif.com/sites/default/files/documentation/esp32-s3-wroom-1_wroom-1u_datasheet_en.pdf [10 May 2025].

Espressif Systems (2025b) *Pulse Counter (PCNT) - ESP32 - — v5.5.1 documentation*, *ESP-IDF Programming Guide*. [Online] Available: https://docs.espressif.com/projects/esp-idf/en/stable/esp32/api-reference/peripherals/pcnt.html [6 October 2025].

FastBitLab (2019) *STM32 SPI Lecture 6 : SPI bus configuration discussion: Full duplex, Half-duplex, and Simplex*. [Online] Available: https://fastbitlab.com/spi-bus-configuration-discussion-full-duplex-half-duplex-simplex/ [11 September 2025].

Fioretti, A., Di Maio, D., Ewins, D.J., Castellini, P. & Tomasini, E.P. (2010) 'Deflection Shape Reconstructions of a Rotating Five-blade Helicopter Rotor from TLDV Measurements', *AIP Conference Proceedings*,1253(1):17–28. Available: https://doi.org/10.1063/1.3455457.

Foss, R. (2018) *APA102 LED Current Usage*, *memcpy.io*. [Online] Available: https://memcpy.io/apa102-led-current-usage.html [3 October 2025].

GyokovSolutions (2025) *Stroboscope Engineer – Apps on Google Play*. [Online] Available: https://play.google.com/store/apps/details?id=com.gyokovsolutions.stroboscopeengineer&hl=en_ZA [24 October 2025].

Hibbeler, R.C. (2017) *Engineering mechanics - dynamics*. Fourtheenth edition in SI units, global edition. Hoboken: Pearson (Always learning).

Hypervision (2023) 'Hologram for education 3D Hologram in Education : A Transformation of Learning Experiences'. [Online] Available: https://medium.com/@Hypervision-Technologies/hologram-for-education-3d-hologram-in-education-a-transformation-of-learning-experiences-604c22777d26.

Insane Spinning LED Hologram Fan: Unboxing, Demo & Tear Down! (2022). [Online] Available: https://www.youtube.com/watch?v=bT716nyK0AY [20 October 2025].

iPixel LED (2018) 'APA102C Datasheet'. Shenzhen Shiji Lighting Co., Ltd. [Online] Available: https://www.alldatasheet.com/html-pdf/1245107/ETC1/APA102C/465/4/APA102C.html [10 February 2025].

Jones, G. (2023) 'Holograms 101 and Their Use in Today's Marketing'. [Online] Available: https://www.groovejones.com/holograms-101-marketing.

KendinYap (2024) *KV Comparison of Cheap & Popular A2212 Brushless Motors. Which KV For your Airplane.*, *YouTube*. [Online] Available: https://www.youtube.com/watch?v=g3ZRp6UCkp0 [17 September 2025].

Kitcasthq (2023) 'The rise of a concert hologram: 6 mind-blowing examples'. [Online] Available: https://blog.kitcast.tv/the-rise-of-a-concert-hologram-6-examples/.

KTW Apps (2025) *Sound meter : SPL & dB meter - Apps on Google Play*. [Online] Available: https://play.google.com/store/apps/details?id=com.ktwapps.soundmeter&hl=en_US [23 October 2025].

Lu, G., Qu, S. & Chen, Y. (2025) 'Understanding user experience for mobile applications: a systematic literature review', *Discover Applied Sciences*,7(6):587. Available: https://doi.org/10.1007/s42452-025-07170-3.

LUMINA (2025a) *L1 Holographic Fan 12.5"*, *LUMINA*. [Online] Available: https://luminafans.com/products/l1-holographic-fan-12-5 [12 September 2025].

LUMINA (2025b) *L1 Holographic Fan 12.5" Acrylic case (image)*, *LUMINA*. [Online] Available: https://luminafans.com/cdn/shop/files/PhotoAug142024_121049PM_2.jpg?v=1723667258&width=1800 [12 September 2025].

LUMINA (2025c) *L1 Holographic Fan 12.5" Logo Showcase*, *LUMINA*. [Online] Available: https://assets.replocdn.com/projects/c0c66674-316a-4fb1-8ace-379e21847dcb/e7770329-c30b-4281-8e05-27d35bc6f7df [12 September 2025].

LUMINA (2025d) *Tripod with Mount*, *LUMINA*. [Online] Available: https://luminafans.com/products/heavy-duty-extendable-tripod-with-mount [12 September 2025].

LxttleSplat42U (2025a) *Holo3D_Base/BUILD.md at main · LxttleSplat42U/Holo3D_Base*, *GitHub*. [Online] Available: https://github.com/LxttleSplat42U/Holo3D_Base/blob/main/BUILD.md [24 October 2025].

LxttleSplat42U (2025b) *holo3d/lib/main.dart at main · LxttleSplat42U/holo3d*, *GitHub*. [Online] Available: https://github.com/LxttleSplat42U/holo3d/blob/main/lib/main.dart [23 October 2025].

MakeItFrom.com (2025) *Polylactic Acid (PLA, Polylactide)*. [Online] Available: https://www.makeitfrom.com/material-properties/Polylactic-Acid-PLA-Polylactide [21 October 2025].

McShefferty, D., Whitmer, W.M. & Akeroyd, M.A. (2015) 'The Just-Noticeable Difference in Speech-to-Noise Ratio', *Trends in Hearing*,19:2331216515572316. Available: https://doi.org/10.1177/2331216515572316.

Micro Robotics (2025a) *Fuse 5A 20mm (4 Pack)*. [Online] Available: https://www.robotics.org.za/FUSE20-5A [5 October 2025].

Micro Robotics (2025b) *Slip Ring Flange 8 Way - 240V 2A*. [Online] Available: https://www.robotics.org.za/SLIP-FLA-08P-240-2A [17 September 2025].

Micro Robotics (2025c) *Step Down Regulator 5V 3.2A - VIN 5.3-50V*. [Online] Available: https://www.robotics.org.za/3782?search=5V%20converter [5 October 2025].

Micro Robotics (no date a) *AC Adapter 5V 8A - 2155 Standard*. [Online] Available: https://www.robotics.org.za/AC-5V8A-2155 [5 October 2025].

Micro Robotics (no date b) *Heatsink TO220 Aluminium (4 Pack)*. [Online] Available: https://www.robotics.org.za/TO220-ALU?search=heatsink [5 October 2025].

Microchip Technology Inc (2020a) *ATmega4808/4809 Data Sheet*. Datasheet DS40002173A,:551. [Online] Available: https://ww1.microchip.com/downloads/en/DeviceDoc/ATmega4808-4809-Data-Sheet-DS40002173A.pdf [10 May 2025].

Microchip Technology Inc (2020b) *Using PWM to Generate an Analog Output*. Datasheet DS90003250A,:17. [Online] Available: https://ww1.microchip.com/downloads/en/Appnotes/90003250A.pdf.

Mulindi, J. (2020) *Pulse Width Modulation (PWM) Speed Control of a DC motor*, *Electrical and Control Systems*. [Online] Available: https://www.electricalandcontrol.com/pulse-width-modulation-pwm-speed-control-of-a-dc-motor/ [12 September 2025].

NXP (2025) *i.MX RT1060 Processor Reference Manual*. Datasheet IMXRT1060RM Rev. 3,:3522. [Online] Available: http://pjrc.com/teensy/IMXRT1060RM_rev3_annotations.pdf [5 October 2025].

Patra, A. & Saini, L.M. (2024) 'Analysis of Serial Peripheral Interface', in. *2023 Second IEEE International Conference on Measurement, Instrumentation, Control and Automation (ICMICA)*, Kurukshetra, India: IEEE,:1–6. Available: https://doi.org/10.1109/ICMICA61068.2024.10732859.

Phipps Electronics (2025) '795 12V - 24V High Speed DC Motor', *Phipps Electronics*,12 September. [Online] Available: https://www.phippselectronics.com/product/795-12v-24v-high-speed-dc-motor/ [12 September 2025].

Plastics SA (2016) ‘Plastics Recyclers in South Africa - 2016’. [Online] Available: https://www.plasticsinfo.co.za/wp-content/uploads/2019/11/Plastics-Recyclers-2016.pdf [22 October 2025].

Priya, C., Chithra, V., Sanjay, B. & Aniruthan, M. (2020) ‘Design And Development Of Holographic Fan’, *Elementary Education Online*,19(2):1809–1816. Available: https://doi.org/10.17051/ilkonline.2020.02.696764.

Province of the Western Cape (2013) ‘Western Cape Noise Control Regulations’, *Provincial Gazette Extraordinary*,13 June. [Online] Available: https://resource.capetown.gov.za/documentcentre/Documents/Procedures,%20guidelines%20and%20regulations/Western_Cape_Noise_Control_Regulations.pdf.

Ramsden, E. (2006) ‘1. Hall-Effect Physics’, in *Hall-Effect Sensors - Theory and Application (2nd Edition)*. Elsevier. [Online] Available: https://app.knovel.com/hotlink/khtml/id:kt0047RSB3/hall-effect-sensors-theory/hall-effect-physics.

RC Ratings (2025) *What is an ESC(Electronic Speed Controller)?*, *RC Ratings*. [Online] Available: https://rcratings.com/what-is-an-esc/ [17 September 2025].

REPROC METALS (2024) *WE BUY*. [Online] Available: https://www.reprocmetals.co.za/services-9 [22 October 2025].

RS Components (2025) *2328 | ADAFRUIT INDUSTRIES 5V dc RGB LED Strip Light, 500mm Length | RS*, *RS Components*. [Online] Available: https://za.rs-online.com/web/p/led-strip-lights/1245482 [17 September 2025].

RS Components (no date) *Texas Instruments LM1084IT-5.0/NOPB, 1 Low Dropout Voltage, Voltage Regulator 5A, 5 V 3-Pin, TO-220*. [Online] Available: https://za.rs-online.com/web/p/voltage-regulators/5339331 [5 October 2025].

SANS (South African National Standards) (2008) *The measurement and rating of environmental noise with respect to annoyance and to speech communication*. SANS 10103. Edition 6. Pretoria: SABS Standards Division.

SEC Electronics inc. (2012) *SS49E PDF*. Datasheet V2.00. [Online] Available: http://www.alldatasheet.com/datasheet-pdf/view/473135/SECELECTRONICS/SS49E.html [13 October 2025].

Simplify3D (2025) ‘Ultimate 3D Printing Material Properties Table’. [Online] Available: https://www.simplify3d.com/resources/materials-guide/properties-table/ [6 October 2025].

Sinoseen (2024) *Can you see infrared light with phone camera?* [Online] Available: https://www.sinoseen.com/can-you-see-infrared-light-with-phone-camera [19 October 2025].

STMicroelectrics (2004) *L7800 Series*. Datasheet Rev. 12. STMicroelectrics. [Online] Available: http://www.alldatasheet.com/datasheet-pdf/view/22634/STMICROELECTRONICS/L7805CV.html [5 October 2025].

STMicroelectronics (2004) *L7800 Series*. Datasheet. [Online] Available: http://www.alldatasheet.com/datasheet-pdf/view/22634/STMICROELECTRONICS/L7805CV.html [21 October 2025].

STMicroelectronics (2009) *LM339N Datasheet*. Datasheet Rev 2. [Online] Available: http://www.alldatasheet.com/datasheet-pdf/view/556027/STMICROELECTRONICS/LM339N.html [23 October 2025].

SZLEDWORLD (2025) 'Disadvantages of Hologram 3D LED Fan',18 May. [Online] Available: https://szledworld.com/hologram-3d-led-fan-disadvantages.html [16 September 2025].

Takealot (2025a) *Koosda Tripod Stand For Camera and Phones, Bluetooth Remote, Phone holder - 140cm | Shop Today. Get it Tomorrow!* [Online] Available: https://www.takealot.com/koosda-tripod-stand-for-camera-and-phones-bluetooth-remote-phone/PLID96345290 [20 October 2025].

Takealot (2025b) 'USB Led Clock Electric Fan Led Lighting Fan USB Gifts For PC Mobile Power'. [Online] Available: https://www.takealot.com/usb-led-clock-electric-fan-led-lighting-fan-usb-gifts-for-pc-mob/PLID95918167?gad_campaignid=19740765778&gad_source=1&gbraid=0AAAADuiBEx_W1sGWMjZWh9h7reyuibYW&gclid=Cj0KCQjwhafEBhCcARIsAEGZEKKL8z_-8bDgytVrZYH0LV9jwHf4UjvKwkjRuRVvJbDr_GXMBZX3gAUaAs_2EALw_wcB&gclsrc=aw.ds.

Texas Instruments (2024) *LM1084 5A Low Dropout Positive Regulators*. Datasheet SNVS037H. Texas Instruments Incorporated,:33. [Online] Available: https://www.ti.com/lit/ds/symlink/lm1084.pdf.

Tidwell, T. (2025) *Wireless Power Transfer: What It Is, How It Works, and Why You Should Care*, *Nemko*. [Online] Available: https://www.nemko.com/blog/wireless-power-transfer [2 October 2025].

TomorrowDesk (2025) 'Holograms: Fascinating World of Three-Dimensional Imaging'. [Online] Available: https://tomorrowdesk.com/info/hologram.

Valvez, S., Silva, A.P. & Reis, P.N.B. (2022) 'Optimization of Printing Parameters to Maximize the Mechanical Properties of 3D-Printed PETG-Based Parts', *Polymers*,14(13). Available: https://doi.org/10.3390/polym14132564.

Voyage, A. (2022) 'ABBA Voyage, only at the ABBA Arena, London, UK | ABBA Voyage'. [Online] Available: https://youtu.be/JxWNxGymi4U.

VR Tech Art (2025) *A2212 1200KV BLDC Motor Testing‼*, *YouTube*. [Online] Available: https://www.youtube.com/watch?v=ED_flZGOlCQ [31 July 2025].

Walker, J., Resnick, R. & Halliday, D. (2014) *Fundamentals of physics*. Tenth edition, extended. Hoboken, NJ: John Wiley & Sons, Inc. [Online] Available: https://dl.icdst.org/pdfs/files4/39e1817b05cf155433309dbb2f3289fe.pdf.

Wang, V., Salim, F. & Moskovits, P. (2013) *The Definitive Guide to HTML5 WebSocket*. 1st edn. Berkeley, CA: Apress L. P (The expert's voice in Web development).

Wootware (2025) *Creality 3301010061 PLA 1KG Black Premium 3D Printer Filament*, *Wootware*. [Online] Available: https://www.wootware.co.za/creality-3301010061-cr-pla-black-premium-3d-printer-filament.html [21 October 2025].

World, E. (2025) ‘Hologram Etymology’. [Online] Available: https://etymologyworld.com/item/hologram.